AFRL-AFOSR-UK-TR-2013-0003

Waveform Diversity and Design for Interoperating Radar Systems

Dr. Maria S. Greco

University Di Pisa
Department Di Ingegneria Dell Informazione
Elettronica, Informatica, Telecomunicazioni
Via Girolamo Caruso 16
Pisa, Italy 56122

EOARD Grant 07-3096

Report Date: January 2013

Final Report from 01 October 2007 to 30 September 2012

Air Force Research Laboratory
Air Force Office of Scientific Research
European Office of Aerospace Research and Development
Unit 4515 Box 14, APO AE 09421

REPORT DOCUMENTATION PAGE

Form Approved OMB No. 0704-0188

1. REPORT DATE *(DD-MM-YYYY)*	2. REPORT TYPE	3. DATES COVERED *(From – To)*
15 January 2013	Final Report	1 October 2007 – 30 September 2012

4. TITLE AND SUBTITLE

Waveform Diversity and Design for Interoperating Radar Systems

5a. CONTRACT NUMBER

FA8655-07-1-3096

5b. GRANT NUMBER

Grant 07-3096

5c. PROGRAM ELEMENT NUMBER

61102F

6. AUTHOR(S)

Dr. Maria S. Greco

5d. PROJECT NUMBER

5d. TASK NUMBER

5e. WORK UNIT NUMBER

7. PERFORMING ORGANIZATION NAME(S) AND ADDRESS(ES)

University Di Pisa
Department Di Ingegneria Dell Informazione
Elettronica, Informatica, Telecomunicazioni
Via Girolamo Caruso 16
Pisa, Italy 56122

8. PERFORMING ORGANIZATION REPORT NUMBER

N/A

9. SPONSORING/MONITORING AGENCY NAME(S) AND ADDRESS(ES)

EOARD
Unit 4515 BOX 14
APO AE 09421

10. SPONSOR/MONITOR'S ACRONYM(S)

AFRL/AFOSR/IOE (EOARD)

11. SPONSOR/MONITOR'S REPORT NUMBER(S)

AFRL-AFOSR-UK-TR-2013-0003

12. DISTRIBUTION/AVAILABILITY STATEMENT

Approved for public release; distribution is unlimited.

13. SUPPLEMENTARY NOTES

Government Purpose Rights - University Di Pisa

14. ABSTRACT

For many years, conventional radars transmitted, received, and processed the same waveform on every pulse or burst within a coherent processing interval (CPI), independently of the environment. Now, modern radar systems have considerable flexibility in their modes of operation, both on receive and transmit. In particular, it is possible to modify the waveform on a pulse to pulse basis, and electronically steered phased arrays can quickly point the radar beam in any feasible direction. In the course of this research project, we introduced the Ambiguity Function, an analytical tool for waveform design and analysis that is useful for examining resolution, sidelobe behavior, and ambiguity in range and Doppler of a given signal waveform. Some techniques to design multiple access frequency hop codes with good auto and cross-ambiguity functions are characterized, focusing on the frequency hop patterns. We have shown that the performance of each channel of the multistatic system heavily depends on the transmitted waveform and on the geometry of the scenario, that is, the position of receivers and transmitters with respect to the position of the target. In particular, both geometry factors and transmitted waveforms play an important role in the shape of the Ambiguity Function and hence in the value of the Cramer-Rao Lower Bound (CRLB). We have calculated the bistatic CRLBs of target range and velocity of each transmit-receive pair as a function of the target kinematic parameters and to provide a local measure of the estimation accuracy of these parameters. Finally, in this work we have analyzed the problem of the optimum sensor selection along the trajectory of a tracked target in a multistatic radar systems. To this end we have evaluated the Posterior Cramer-Rao Lower Bound (PCRLB) of the sequential target state estimation and we will define an algorithm that exploits this mathematical tool to select the best channels for the tracking of the target.

15. SUBJECT TERMS

EOARD, Electromagnetics, radar, Antennas

16. SECURITY CLASSIFICATION OF:			17. LIMITATION OF ABSTRACT	18, NUMBER OF PAGES	19a. NAME OF RESPONSIBLE PERSON
a. REPORT	b. ABSTRACT	c. THIS PAGE			JAMES LAWTON Ph. D.
UNCLAS	UNCLAS	UNCLAS	SAR	91	**19b. TELEPHONE NUMBER** *(Include area code)* +44 (0)1895 616187

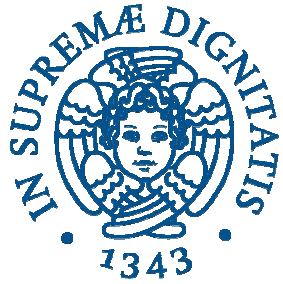

UNIVERSITÀ DI PISA

DIPARTIMENTO DI INGEGNERIA DELL'INFORMAZIONE

ELETTRONICA, INFORMATICA, TELECOMUNICAZIONI

WAVEFORM DIVERSITY AND DESIGN FOR INTEROPERATING RADAR SYSTEM

Pietro Stinco, Maria S. Greco, Fulvio Gini

and

Muralidhar Rangaswamy*

**collaborating engineer from the Air Force Research Laboratory*

Pisa, December 2012

This work has been funded by EOARD grant FA8655-07-1-3096 on "Waveform Diversity and Design for Interoperating Radar System".

Effort sponsored by the EOARD, European Office of Aerospace Research and Development, under grant number FA8655-07-1-3096. The U.S. Government is authorized to reproduce and distribute reprints for Government purpose notwithstanding any copyright notation thereon.

The authors certify that there were no subject inventions to declare during the performance of this grant.

Abstract

This report summarizes the research activity from 2008 to 2010 founded by EOARD grant FA8655-07-1-3096 on "Waveform Diversity and Design for Interoperating Radar System". The technical reports summarized in this work are:

[TR1] M. Greco, F. Gini, P. Stinco, M. Rangaswamy, "DOA Estimation and Multi-User Interference in a Two-Radar System", EOARD Grant FA8655-07-1-3096, University of Pisa, Italy, June 2008.

[TR2] M. Greco, F. Gini, P. Stinco, M. Rangaswamy, "DOA Estimation and Multi-Use Interference", EOARD Grant FA8655-07-1-3096, University of Pisa, Italy, December 2008.

[TR3] M. Greco, F. Gini, P. Stinco, Rangaswamy Muralidhar, "Ambiguity Function and Cramer-Rao Bounds for Multistatic Radar Networks", ", EOARD Grant FA8655-07-1-3096, University of Pisa, Italy, October 2009.

[TR4] P. Stinco, M. Greco, F. Gini, M. Rangaswamy, "Data Fusion and Optimizzation in a Multistatic Radar System", EOARD Grant FA8655-07-1-3096, University of Pisa, Italy, September 2010.

[TR5] P. Stinco, M. Greco, F. Gini, M. Rangaswamy, " Performance Analysis of Passive Radar System Exploiting the Downlink Signal Of a UMTS Base Station ", EOARD Grant FA8655-07-1-3096, University of Pisa, Italy, November 2011.

For more details on the research activity we refer the reader to these documents.

Summary

List of Figures

1 Introduction

For many years, conventional radars transmitted, received, and processed the same waveform on every pulse or burst within a coherent processing interval (CPI), independently of the environment. In the 70s, adaptive processing began to be developed and radars began to be more flexible on receive. For the first time, the processing of received signals changed depending on the environment (noise, clutter, interferences).

Now, modern radar systems have considerable flexibility in their modes of operation, both on receive and transmit. In particular, it is possible to modify the waveform on a pulse to pulse basis, and electronically steered phased arrays can quickly point the radar beam in any feasible direction. Such flexibility calls for new methods of designing and scheduling the waveforms to optimize the radar performance. Then, an agile and diverse waveform radar system should be able to change on the fly the transmitted waveform based on the information estimated or a priori known on the environment, on the targets and the jammers.

Moreover, in a radar network each sensor should also be able to operate and perform its task without negatively interfering with the other sensors and, possibly, to improve the performance of the whole network. Then, the waveforms used by the radars in a complex network should be designed and changed on the fly, based on the clutter, target and interference echoes; they should guarantee good target detection and parameter estimation in different scenarios and should allow an optimal access to the same transmit channel.

In the first report of the research activity [TR1] we introduced the Ambiguity Function, an analytical tool for waveform design and analysis that is useful for examining resolution, sidelobe behavior, and ambiguity in range and Doppler of a given signal waveform. As well known, to improve resolution without worsening detection performance, radars should use pulse compressed waveforms. These waveforms are obtained by adding frequency or phase modulation to a rectangular pulse. There are a vast number of pulse compressed waveforms in the literature; the most commonly used from the radar community are the Frequency Coded Waveforms (FCW), that has been analyzed in detail in [TR1]. These kind of waveform are often used in high resolution radar systems because they guarantee good target detection and estimation. FCW signals are characterized by an auto-ambiguity function that exhibits a narrow thumb tack shape with low sidelobes. In contrast, in applications like multi-access communications, attention is paid in designing a sequence of frequency coded waveforms with small cross-correlation functions. In multi-user radar system scenarios both objectives are desirable. Unfortunately, there is a tradeoff between these objectives. Frequency hop pulse

trains based on Costas codes, for instance, are known to have almost ideal auto-ambiguity function but not very good cross-ambiguity properties. On the contrary, frequency coded signals based on linear congruences have ideal cross-ambiguity properties but unattractive auto-ambiguity properties. Some techniques to design multiple access frequency hop codes with good auto and cross-ambiguity functions have been described in [TR1]; in our work we focused on the frequency hop patterns constructed upon an extension of the theory of quadratic congruences and we analyzed also a scenario composed of two radars transmitting in the same band, which can illuminate the same area looking for same target. In particular, these systems can use either the same or different transmitted FCW. In [TR1] we investigated the impact of the presence of the transmitted signal of the second radar (the interfering radar) on the first one (the reference radar) in the estimation of the target direction of arrival (DOA). The considered target DOA estimators were the Monopulse, the Pseudo Monopulse (PM), and the Maximum Likelihood (ML) techniques. The performances of these estimators have been numerically evaluated in terms of root mean square error (RMSE) and probability of loosing the target in different operational conditions. Clearly, the performances of the reference radar are strongly dependent on the codes used by the two radars; therefore, using proper coding the influence of the interfering radar can be significantly reduced. This was the main topic of [TR2] where we presented two modified version of the PM and ML estimators, the Modified Pseudo-Monopulse (MPM), the Modified Maximum Likelihood (MML), the Sub-sequent Pseudo-Monopulse (SPM) and the Sub-sequent Maximum Likelihood (SML). In this report we describe briefly only the MPM technique for the lack of space, for more details we refer the reader to [TR2]. In [TR1] and [TR2] we analyzed a netted system composed by monostatic radar system. In the most general case, in a multistatic radar system the receivers can also exploit the signal emitted by non colocated transmitters. To this end, it is very important to define and analyze bistatic radar system. This was the main topic of [TR3] and [TR4]. Bistatic radar may be defined as a radar in which the transmitter and receiver are at separate locations. In monostatic configuration, estimation of the time delay and Doppler shift directly provides information on range and velocity of the target. This is possible also in the case of bistatic radar configuration, even if the relation between measured or estimated time delay and Doppler frequency, and target distance and velocity is not linear. To measure the possible global resolution and large error properties of the target parameters estimates, the ambiguity function (AF) is often used both in mono and in multistatic scenarios.

We also exploit the relation between the AF and the Cramér-Rao lower bound (CRLB) to calculate the bistatic CRLBs of target range and velocity. The bistatic CRLBs provide a local measure of the estimation accuracy of these parameters. Moreover, we compare monostatic and bistatic CRLBs as a function of the number of integrated pulses, target direction of arrival (DOA), and bistatic baseline length. The information gained through the calculation of the bistatic CRLBs can be used in a multistatic radar system for the choice of the optimum transmit-receive pair. Multistatic radars utilize multiple transmitters and receivers. Such systems differ from typical modern active radars since they consist of several different monostatic and bistatic channels of observation. Due to this spatial diversity, these systems present challenges in managing their operation as well as in usefully combining the data from multiple sources of information on a particular area of surveillance. The information gain, obtained through this spatial diversity, combined with some level of data fusion, can give rise to a number of advantages over both the individual monostatic and bistatic cases for typical radar functions, such as detection, parameter estimation, tracking and identification. As showed in [TR3], the performance of each channel of the multistatic system heavily depends on the transmitted waveform and on the geometry of the scenario, that is, the position of receivers and transmitters with respect to the position of the target. In particular, both geometry factors and transmitted waveforms play an important role in the shape of the Ambiguity Function and hence in the value of the CRLBs. In [TR4], after we calculated the bistatic CRLBs of target range and velocity of each TX-RX pair as a function of the target kinematic parameters and to provide a local measure of the estimation accuracy of these parameters. In [TR4], we exploited the results obtained from this analysis to compute the rules for selecting the best weighting coefficients for fusing the signals from multiple receivers in order to improve the detection performance and the estimation accuracy of the kinematic parameters of the target. We also introduced an optimization methodology for selecting only some channels for the network, independent of the adopted fusion rule.

The results derived in [TR3] and [TR4] can also be used to analyzed the performance of a Passive Coherent Location (PCL) system, that is, bistatic radars that exploit the signal emitted by illuminators of opportunity, such as broadcast or communications signals. PCL systems have some significant attractions, in addition to those common to all bistatic radars: the PCL receivers do not need any transmitter hardware of their own, are completely passive, and hence undetectable. In [TR5] we calculated the monostatic and bistatic Ambiguity Function (AF) of a Quadrature Phase Shift Keying (QPSK) signal where the pulses are shaped with a

Root Raised Cosine (RRC) filter. The monostatic and bistatic modified Cramér-Rao lower bounds (MCRLBs) for the estimation of target range and velocity are also derived and analyzed. The QPSK modulation is used in the downlink of a Universal Mobile Telecommunications System (UMTS) base station, hence the results of our analysis provide a useful tool to asses the performance of a Passive Coherent Location (PCL) system where the non co-operative transmitter of opportunity is a UMTS-base station. The actual growing coverage of UMTS signals on the international territory makes multistatic radar configuration feasible, therefore these results can also be exploited for the dynamical selection of the transmitter in a multistatic radar system where multiple UMTS base stations are used.

All the obtained results are briefly summarized in this report, for more details we refer the reader to in [TR1],[TR2],[TR3],[TR4] and [TR5].

In addition to previous reports, in this work we also analyze the problem of the optimum sensor selection along the trajectory of a tracked target in a multistatic radar systems. To this end we will evaluate the Posterior Cramér-Rao Lower Bound (PCRLB) of the sequential target state estimation and we will define an algorithm that exploits this mathematical tool to select the best channels for the tracking of the target.

2 The Ambiguity Function

Classically, the properties of radar waveforms are analyzed and presented in terms of the Complex Ambiguity Function, originated by Woodward in the 1950s [Wod80].

The Complex Ambiguity Function (CAF) is well known in the context of radar as a key tool for determining target resolution capability, and is a consequence of the nature of the optimal detector, which involves decision-making based on the output of a matched filter determined from the transmitted waveform [Tsa97]. As a matter of fact, the CAF is the auto-correlation of the complex envelope of the waveform with a copy shifted in time and frequency, and presents the point target response of the waveform as a two-dimensional function of range and Doppler, showing the resolution, sidelobe structure and ambiguities in the delay and Doppler domains. The CAF is intuitively appealing and has been very widely used – indeed, it is no exaggeration to say that every serious radar engineer on the planet will have encountered and used the Woodward ambiguity function.

The mathematical definition of the Complex Ambiguity Function is [Tsa97]:

$$X\left(\tau_H,\tau_a,\nu_H,\nu_a\right)=\int_{-\infty}^{+\infty}u(t-\tau_a)u^*\left(t-\tau_H\right)e^{-j2\pi(\nu_H-\nu_a)t}dt \qquad (1)$$

where $u(t)$ is the complex envelope of the transmitted signal, τ_a and v_a are the actual delay and Doppler frequency of the radar target respectively and τ_H and v_H are the hypothesized delay and frequency. The Ambiguity Function (AF) is defined as the absolute value of the Complex Ambiguity Function and is clearly maximum for $\tau_H = \tau_a$ and $v_H = v_a$. The CAF in (1) and the AF can can be also expressed as a function of τ and v, where $\tau = \tau_H - \tau_a$ and $v = v_H - v_a$. In this case the definition of the Ambiguity Function is:

$$\left|X\left(\tau,\nu\right)\right|=\left|\int_{-\infty}^{+\infty}u(t)u^*\left(t-\tau\right)\exp\left(-j2\pi\nu t\right)dt\right| \qquad (2)$$

Three properties of the AF are of particular interest [Van71].

If the waveform has energy E, then

$$\left|X(\tau,\nu)\right|\le\left|X(0,0)\right|=E \qquad (3)$$

Thus, when the filter is matched both in delay and Doppler the response attains the maximum. If the filter is not matched then the response assumes a value lower than the maximum.

The second property states that the total area under any ambiguity function is constant and it is given by

$$\int_{-\infty}^{+\infty}\int_{-\infty}^{+\infty} \left|X(\tau,\nu)\right|^2 d\tau d\nu = E^2 \qquad (4)$$

This conservation of energy statement implies that, in the design of waveforms, one cannot remove energy from one portion of the ambiguity surface without placing it somewhere else; it can only be moved around on the ambiguity surface.

The third property is a symmetry relation

$$X(\tau,\nu) = X(-\tau,-\nu) \qquad (5)$$

Moreover, if we consider the CAF for ν=0, we obtain the autocorrelation function of $u(t)$, similarly, if we consider the CAF for τ=0, we obtain the Fourier transform of $|u(t)|^2$.

It is reasonable to ask how an ideal ambiguity function should be. The answer varies depending on the aim of the system design, but a common goal is the thumbtack shape, which features a single central peak, with the remaining energy spread uniformly throughout the delay-Doppler plane. The lack of any secondary peak implies that there will be no delay or Doppler ambiguities. The uniform plateau suggests low and uniform side lobes, minimizing target masking effects. All of these features are beneficial for a system designed to make high resolution measurement of targets in delay and Doppler, or to perform radar imaging.

In our work we evaluated the CAF of several pulse. In particular we calculated in closed form the CAF of the rectangular pulse [TR1], the burst of pulses [TR1], the frequency/phase coded waveform [TR1], the Linear Frequency Modulated (LFM) pulse [TR3] and the Sinusoidal Frequency Modulated (SFM) pulse. For more detail we refer the reader to these technical reports.

3 Frequency Coded Waveforms

As known, in order to have an auto-ambiguity function that exhibits a narrow thumbtack shape with low sidelobes, it is necessary to perform a pulse compression through an angle modulation. In this Section we briefly describe the *Frequency-Coded Waveforms* (FCW), where the transmitted signal is frequency modulated through a code sequence, for more details we refer the reader to [TR1]. The complex envelope of the transmitted signal $u(t)$ is composed of N pulses $p(t)$ with a pulse repetition interval T_r and it can be written in the form:

$$u(t) = \sum_{l=0}^{N-1} p(t - lT_r) \cdot e^{-j2\pi\Omega_l t} \tag{6}$$

Where $\Omega_l = d_l/\tau_c$ and $\{\underline{d}_N\} = \{d_0, d_1, ..., d_l, ..., d_{N-1}\}$ is a sequence of integer numbers which belong to the set $J_N=\{0,1,2,\ldots,N\text{-}1\}$; this sequence is commonly a permutation of the integer $0,1,2,\ldots,N\text{-}1$ and, in this case, the code sequence is a *full code*. The pulses $p(t)$ are often rectangular pulses with time duration τ_c and pulse repetition interval T_r equal to τ_c. In this case, the transmitted signal $u(t)$ is a pulse with time duration $\tau_s = N\tau_c$ composed of N subpulses (or *chips*) with time duration τ_c. It is clear that an FCW signal is closely related to the code sequence (or *placement operators*) $\{\underline{d}_N\}$. The code sequence is commonly described through the *geometric array*, that is a matrix whose columns represent N continuous time slices and the rows represent N distinct frequencies. Through the *geometric array* it is possible to calculate the *sidelobes matrix*, or *hits matrix*, by considering the *geometric array* as a bidimensional signal and calculating its autocorrelation function [TR1]. Clearly, the AF of an FCW signal is closely related to the sidelobe matrix of the code, in fact the sidelobe matrix describe how the sidelobe peaks are distributed in the delay-Doppler plane. In [TR1] we described the techniques commonly used to construct a code sequence that generates a good auto-ambiguity function, in particular we analyzed the *Costas-Sequences*, the *Pushing-Sequences*, the *Lee-Sequences*, the *Linear Congruence Codes*, the *Quadratic Congruence Codes*, the *Cubic Congruence Codes* and the *Hyperbolic Congruence Codes*. Anyway, particular attention has been devoted to the analysis of the techniques to construct a set of code sequence that generate a set of FCW signals for netted radar system application, that is a set of signals that exhibit a good auto-ambiguity function and a small cross-correlation function between each pair of signals of the set. In particular we analyzed the Simulated-Annealing technique and the *Extended Quadratic Congruences* (EQC) technique, that will be briefly described in next subSection. For more detail we refer the reader to [TR1].

3.1 Frequency Coded Waveforms for Netted Radar Systems

With the ongoing rapid development in *sensor fusion technology*, netting multiple radar systems through fast communication links is becoming a trend in the high-performance radar design. Via information fusion, radar performance in target search, tracking and recognition can be significantly improved. However, the waveforms used by the netted radar systems must be carefully designed to avoid the self-interference and detection confusion. Then, the waveforms used by the radars in a complex network should guarantee an auto-ambiguity function that exhibits a narrow thumb tack shape with low sidelobes and, in contrast, with small cross-ambiguity functions. In this Section we describe an algebraic technique to construct a set of FCW code sequences which is best described as a compromise between ease of design and good auto- and cross-ambiguity properties. The set of sequences $\{d_n\}_{n=0}^{N-1}$ are constructed upon an extension of the theory of quadratic congruences (*Extended Quadratic Conguences* EQC) [Bel88], [Bel90], [Bel91a], [Bel91b], [Tit81a], [Tit81b], [Tit91], [Tit93], [Xia98]. The class of extended quadratic congruence placement operators regroups all the operators given by [TR1]

$$d_k = \begin{cases} \left| a\dfrac{k(k+1)}{2} \right|_N & 0 \le k \le \dfrac{N-1}{2} \\ \left| b\dfrac{k(k+1)}{2} + (a-b)\dfrac{N^2-1}{8} \right|_N & \dfrac{N-1}{2} \le k \le N-1 \end{cases} \tag{7}$$

where N is an odd prime number and a and b are integers. Note also that the identity $|N^2|_8=1$ holds for any odd integer, so that $(N^2\text{-}1)/8$ is always an integer. In [TR1] we showed that the sequence of integers $\{d_n\}_{n=1}^{N-1}$ is a permutation of the set $\{1,2,\ldots,N\text{-}1\}$ if and only if a and b are not both *quadratic residues* (*QR*) or *quadratic nonresidues* (*QNR*) of the odd prime N. Each of these permutations is uniquely defined by the ordered pair (a, b).

The number λ is a *QR* or a *QNR* if

$$\left|\lambda^{(N-1)/2}\right|_N = (\lambda \mid N) = \begin{cases} 1 & QR \\ -1 & QNR \end{cases} \tag{8}$$

where $(\lambda|N)$ is the so-called Legendre symbol.

By definition, the class of EQC codes regroups all code words parameterized by ordered pairs (a, b) with a and b not both *QR* or *QNR*.

As there are $(N\text{-}1)/2$ *QR*s and $(N\text{-}1)/2$ *QNR*s, there are exactly $(N\text{-}1)^2/2$ EQC code words.

As showed in [TR1], it is useful to organize these EQC code words in (N-1)/2 sets containing N-1 code arrays each, with the property that each unequal pair of code words among the N-1 code arrays of each set has one, and only one, intersection modulo N (at k=0 by construction). In general, each set contains the ordered pairs $(a_1,b_1),(b_1,a_2),(a_2,b_2),(b_2,a_3),\ldots,(a_{(N-1)/2},b_{(N-1)/2}),(b_{(N-1)/2},a_1)$ for some sequences of all distinct *QR* or *QNR* a_i, and all distinct *QNR* or *QR* b_i ; in addition, when (N-1)/2 is odd, one set can be formed with the ordered pairs $(a_1,N-a_1),(N-a_1,a_1),\ldots,(a_{(N-1)/2},N-a_{(N-1)/2}),(N-a_{(N-1)/2},\ a_{(N-1)/2})$. As an example, let us consider the case N = 5. There is a total of eight possible EQC code words that can be generated for N = 5, which are grouped in two sets containing four code arrays each. The first set is shown in Figure 1.a; it corresponds to the sequence of pairs (1,2), (2,4), (4,3), and (3,l), respectively. Note that there is only one intersection (at k = 0) between any two code words of the set. Figure 1.b displays the second set of four code arrays; it is associated with the pairs (1,3), (3,4), (4,2), and (2,l), respectively.

In this elementary example, the only alternative sequence is obtained by simply changing the pair ordering. Again, there is only one intersection between any two code words of this set. Any set different from those of Figure 1 would not possess this property.

To show the FCW-EQC signals guarantee good auto- and cross-ambiguity properties, Figure 2-4 show the auto and cross ambiguity functions of the FCW-EQC signals for N=23 generated with the ordered pair (18,14) and (2,11), namely $\tilde{d}_k$ ={0, 18, 8, 16, 19, 17, 10, 21, 4, 5, 1, 15, 22, 20, 9, 12, 6, 14, 13, 3, 7, 2, 11} e d_k ={0, 2, 6, 12, 20, 7, 19, 10, 3, 21, 18, 17, 11, 16, 9, 13, 5, 8, 22, 1, 14, 15, 4}.

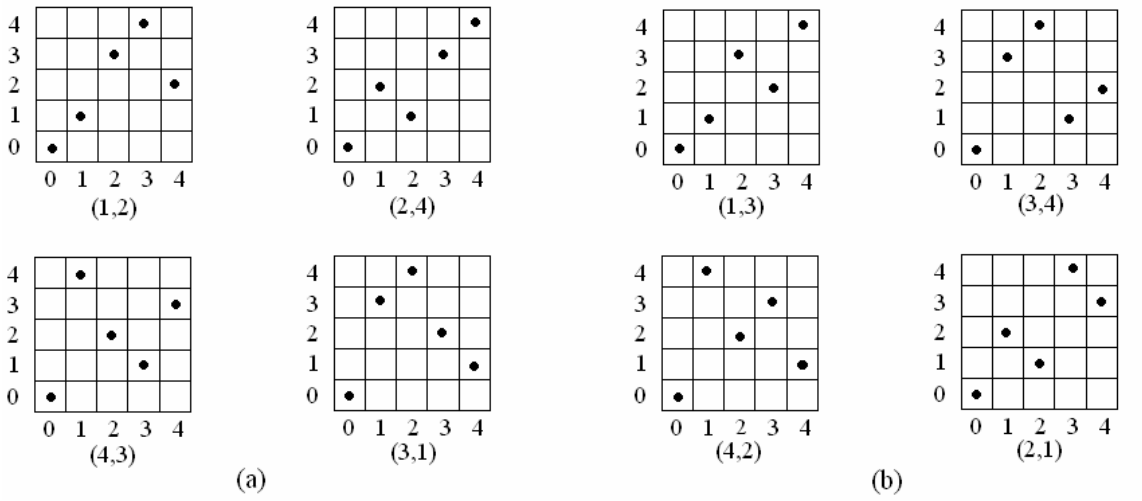

Figure 1- EQC geometric array with *N=5*.

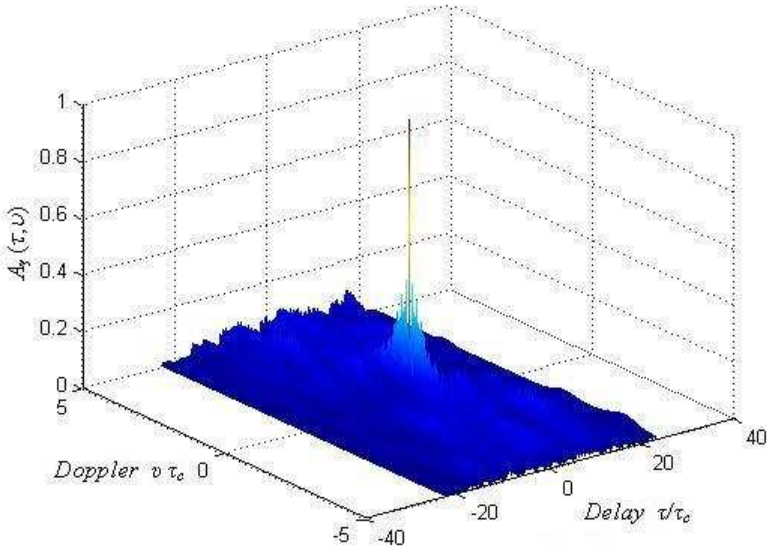

Figure 2 - Ambiguity Function of sequence $\tilde{d}_k$.

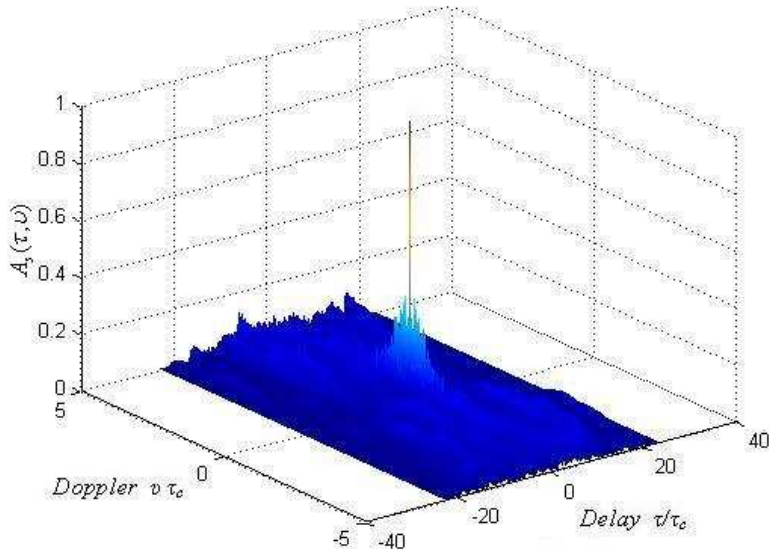

Figure 3 - Ambiguity Function of sequence d_k.

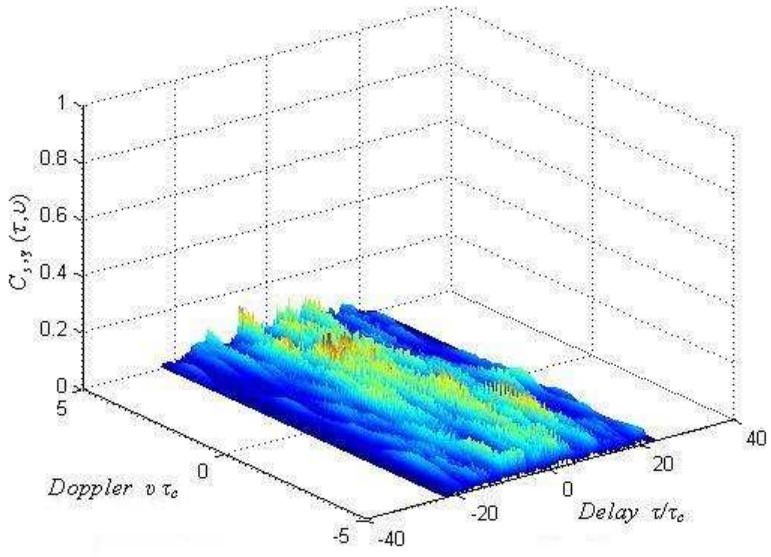

Figure 4 - Cross-Ambiguity Function of sequences d_k and $\tilde{d}_k$.

4 Adaptive waveform diversity for cross-channel interference mitigation

In previous Section we showed that the waveforms used by the radars in a complex network should guarantee good target detection and parameter estimation in different scenarios and should allow an optimal access to the same transmit channel. We also showed that FCW-EQC waveforms are characterized by an auto-ambiguity function that exhibits a narrow thumb tack shape with low sidelobes and a good cross-ambiguity function, almost null in the delay-Doppler plane.

In this Section we analyze a scenario composed of two radars transmitting in the same frequency band, which can illuminate the same area looking for same target. These two radars can use either the same or different codes. In particular, we investigate the impact of the presence of the transmitted signal of the second radar (the interfering radar) on the first one (the reference radar) in the estimation of the target Direction Of Arrival (DOA). The analyzed scenario is pictorially showed in Figure 5, for more details on the impact of the intergfering signal on target DOA estimate we refer the reader to [TR1] where we also described a phased-array FCW receiver and we evaluated the Cramér-Rao Lower Bounds (CRLBs) of target DOA estimate.

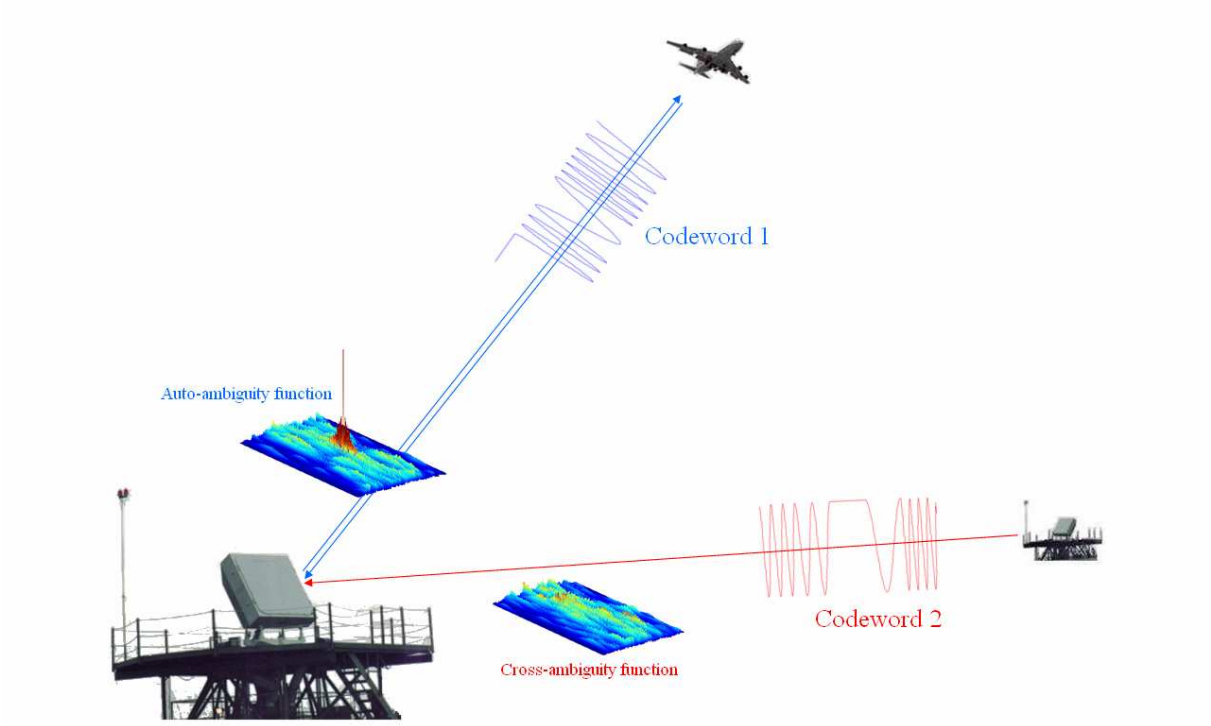

Figure 5 – Impact of the interfering radar on the reference radar.

In a typical phased array radar, a single beam is formed on transmission and two or more beams are formed on reception. We assume here that the system is a linear array radar that estimates the target DOA by using the sum channel Σ on transmission and two matched channels, the sum Σ and the difference Δ on reception. The two channels $f_\Sigma(\theta_T)$ and $f_\Delta(\theta_T)$, or antenna patterns, are defined as the complex amplitude profiles versus target azimuth angle θ_T (for more detail we refer the reader to [TR1] and [TR2]). We assume that the sum channel has a HPBW of 3° and that the reference system is a tracking system, then the target and the radar are static during the Time on Target (ToT). If the radar use a Pseudo-Monopulse (PM) estimator as in [TR1], it transmits a sequence of K pulses used for DOA estimation.

The performance of PM-DOA estimator in presence of an interfering radar has been analyzed in detail in [TR1], where we also analyzed the performance of the ML (Maximum Likelihood) estimator, not reported here for the lack of space.

As showed in [TR1], the interfering radar introduces on the DOA estimation a strong bias that depends on the angular position of the interference and, particularly, on the ratio $|C/A|$, where C is the complex value of Cross-Ambiguity Function at the sampling instant while A is the complex value of Auto-Ambiguity Function at the sampling instant.

In [TR2] we proposed a technique for mitigating the effect of the interfering radar that will be briefly described in this Section. For more details we refer the reader to [TR2].

The proposed idea is simple, that is if the target is still during the ToT, and there is not interference, the difference between two subsequent DOA estimates is related only to the power of disturbance (noise and clutter) contribution and for high signal–to-disturbance power ratio tends to zero. If there is an interference and the contribution of the interfering signal has a different weight on each estimate the difference between the two subsequent DOA estimates depends also on the interference.

Then the difference between two estimates can be used as key statistic to detect the presence of the interference and waveform diversity in transmission should be applied for having different contributions of the interfering signal on each estimate. For this purpose, during the ToT the radar transmits two bursts of N frequency hop coded pulses. The frequency hop signals used in the two bursts are generated with different codes. The receiver is initially matched to the first frequency hop pulse used in the first burst and, in a second time, it is matched to the second frequency hop pulse used in the second burst. Based on this, it is possible to write the expression of the two pairs of signals received on the sum and on the difference channels. Let's suppose that the Doppler frequencies of the target and of the

interference radar are the same with respect to the reference radar. In this case, the reference radar cannot distinguish between the two signals by means of Doppler processing.

Without lack of generality, we assume that both Doppler frequencies are zero; then the received signals can be written as:

$$y_{1,\Sigma}(n) = \alpha \cdot A \cdot f_{\Sigma}^{2}(\vartheta_T) + \beta \cdot C_1 \cdot f_{\Sigma}(\vartheta_I) + d_{1,\Sigma}(n), \quad (9)$$

$$y_{1,\Delta}(n) = \alpha \cdot A \cdot f_{\Sigma}(\vartheta_T) \cdot f_{\Delta}(\vartheta_T) + \beta \cdot C_1 \cdot f_{\Delta}(\vartheta_I) + d_{1,\Delta}(n), \quad (10)$$

$$y_{2,\Sigma}(n) = \alpha \cdot A \cdot f_{\Sigma}^{2}(\vartheta_T) + \beta \cdot C_2 \cdot f_{\Sigma}(\vartheta_I) + d_{2,\Sigma}(n) \quad (11)$$

$$y_{2,\Delta}(n) = \alpha \cdot A \cdot f_{\Sigma}(\vartheta_T) \cdot f_{\Delta}(\vartheta_T) + \beta \cdot C_2 \cdot f_{\Delta}(\vartheta_I) + d_{2,\Delta}(n) \quad (12)$$

Subscripts “1” and “2” refer to the first and the second burst, which are received in series, and n=0,1,…,N-1. The first term in $y_{i,\Sigma}$ and $y_{i,\Delta}$ (i=1,2) is due to the target signal; it depends on the target DOA θ_T through $f^2_{\Sigma}(\theta_T)$ in sum channel and through $f_{\Sigma}(\theta_T)f_{\Delta}(\theta_T)$ in the difference channel. This is due to the two-way antenna gain. The second term is due to the signal transmitted by the second radar, which has DOA θ_I, and it depends on the one-way gain of the antenna patterns, i.e. $f_{\Sigma}(\theta_I)$ and $f_{\Delta}(\theta_I)$ $f_{\Delta}(\vartheta_I)$. $d_{i,\Sigma}$ and $d_{i,\Delta}$ are the noises on the two channels, modeled as mutually independent complex white Gaussian processes. A is the complex value of the Auto-Ambiguity Function of the transmitted signal, C_1 is the complex value of the Cross-Ambiguity Function between the first frequency hop pulse and the interfering signal and C_2 is the complex value of the Cross-Ambiguity Function between the second frequency hop pulse and the interfering signal. If the reference radar is synchronized in reception and transmission and the receiver is tuned on the Doppler of the target, then A is the energy of the transmitted pulse; α is the complex amplitude of the received echo and β is the complex amplitude of the interfering signal. They are modeled as complex Gaussian mutually independent random variables; in short $\alpha \sim CN(0,\sigma^2_{\alpha})$ and $\beta \sim CN(0,\sigma^2_{\beta})$. The signal-to-noise power ratio is defined as $SNR=|A|^2\sigma^2_{\alpha}/\sigma^2_{d}$ and the signal-to-interference ratio as $SIR=\sigma^2_{\alpha}/\sigma^2_{\beta}$.

Then, using the N samples received on each of the two channels Σ and Δ from the first burst, the signal processor performs a first target DOA estimation $\hat{\vartheta}_1$ through the Pseudo-Monopulse (PM) technique. In particular, the signal processor forms the monopulse ratio defined by $r_1(n)=Re\{y_{1,\Delta}(n)/y_{1,\Sigma}(n)\}$ for each pulse, where $Re\{\}$ denotes the real part. In absence of disturbance and in the presence of only one target, the monopulse ratio reduces to

$r_1(n)=Re\{f_\Delta(\theta_T)/f_\Sigma(\theta_T)\}$ from which the angular location of the target for each pulse can be determined. Finally, we obtain $\hat{\vartheta}_1 = \sum_{n=0}^{N-1} \hat{\vartheta}_{T,1}^{(n)} \big/ N$, where $\hat{\vartheta}_{T,1}^{(n)}$ is the target DOA estimate for each pulse. Similarly, the signal processor performs a second target DOA estimation $\hat{\vartheta}_2$ using the N samples in Eqs. (11)-(12) received on the two channels from the second burst. The proposed Modified Pseudo-Monopulse (MPM) estimate is obtained from these two PM estimates as described in the following (see [TR2] for more details). First the difference $\Delta\vartheta = \left|\hat{\vartheta}_1 - \hat{\vartheta}_2\right|$ is calculated and then compared with a threshold λ. If $\Delta\theta \leq \lambda$, the MPM estimate is calculated as the average of the two PM estimates, $\hat{\vartheta}_1$ and $\hat{\vartheta}_2$, that is $\hat{\vartheta}_T = \left(\hat{\vartheta}_1 + \hat{\vartheta}_2\right)\big/ 2$.

On the contrary, if $\Delta\theta > \lambda$, a third PM estimate $\hat{\vartheta}_3$ is calculated by using the samples received on the two channel Σ and Δ from a third burst of N frequency hop pulses, coded whit a third code sequence. Then, the signal processor calculates $\Delta\vartheta_1 = \left|\hat{\vartheta}_1 - \hat{\vartheta}_3\right|$ and $\Delta\vartheta_2 = \left|\hat{\vartheta}_2 - \hat{\vartheta}_3\right|$. If the lowest between these two quantities is less than λ, then the MPM estimation of the target DOA is calculated as

$$\hat{\vartheta}_T = \begin{cases} \dfrac{\hat{\vartheta}_1 + \hat{\vartheta}_3}{2} & \Delta\vartheta_1 < \Delta\vartheta_2 \\ \dfrac{\hat{\vartheta}_2 + \hat{\vartheta}_3}{2} & \Delta\vartheta_1 \geq \Delta\vartheta_2 \end{cases} \tag{13}$$

If both $\Delta\theta_1$ and $\Delta\theta_2$ are greater than λ, the MPM estimation of the target DOA is calculated as the average of the three PM estimates, that is $\hat{\vartheta}_T = \left(\hat{\vartheta}_1 + \hat{\vartheta}_2 + \hat{\vartheta}_3\right)\big/ 3$.

In this last case, the target DOA can be also calculated as the value closest to $\hat{\vartheta}_p$ among the three PM estimates, where $\hat{\vartheta}_p$ is the MPM estimation of the target DOA performed in the previous tracking time lag. However, it is important to consider that the value of $\hat{\vartheta}_p$ is not always available and it is often difficult to perform the initialization of $\hat{\vartheta}_p$.

To evaluate the impact of the presence of the interfering radar, the RMSE of the DOA estimator has been derived by running 10^4 Monte Carlo simulations. In our simulations, we set θ_T=0°, N=8, SIR=0dB and SNR=20dB. With this value of SNR the probability of detection of the filter matched to the transmitted signal is almost unitary, even for $P_{FA}=10^{-6}$. Due to the high value of SNR, the performance of the DOA estimator are mainly affected by the presence

of the interfering radar. Let's first show, as comparison for the MPM estimator, some results relating to the PM estimator in presence of interference. In the case of PM estimation the received signals are [TR2]:

$$y_{\Sigma}(n) = \alpha A\, f_{\Sigma}^{2}(\vartheta_T) + \beta C\, f_{\Sigma}(\vartheta_I) + d_{\Sigma}(n) \tag{14}$$

$$y_{\Delta}(n) = \alpha A\, f_{\Sigma}(\vartheta_T)\, f_{\Delta}(\vartheta_T) + \beta C\, f_{\Delta}(\vartheta_I) + d_{\Delta}(n) \tag{15}$$

In our analysis, we considered $0 \le |C/A| \le 1$. The worst case is when $|C/A|=1$; this value characterizes two synchronized radars using the same code. The best case is when $|C/A|=0$; this value characterizes the case of synchronized radars using two orthogonal codes. In Figure 6 we plotted the RMSE of the PM estimator as a function of the interfering DOA. We suppose that the PM estimator performs the estimation of the target DOA using a burst of 24 frequency hop pulses (that corresponds to three bursts of $N=8$ pulses). The RMSE has been calculated for $|C/A|=1$ and $|C/A| \sim U(0,1)$, that is when $|C/A|$ is an uniformly distributed random variable in the interval [0,1]. As apparent in Figure 6, the performances of the PM estimator are strongly dependent on the interfering signal.

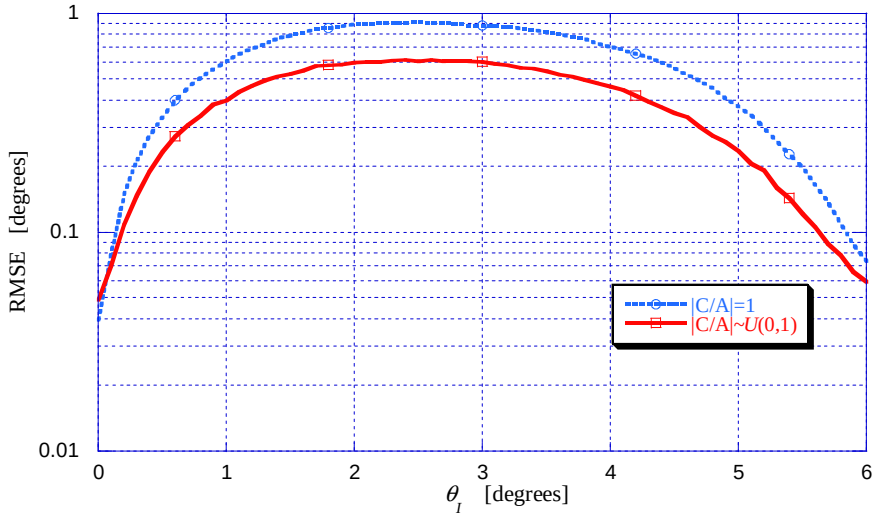

Figure 6 - RMSE of the PM estimator as a function of the interfering DOA.

In Figure 7 we reported the RMSE of the MPM estimator as a function of the interfering DOA for different values of the threshold λ. In this simulation, when both $\Delta\theta_1$ and $\Delta\theta_2$ are greater than λ, the MPM estimation of the target DOA has been calculated as the value closest to $\hat{\vartheta}_p$ among the three PM estimates. The value of $\hat{\vartheta}_p$ has been modeled as a Gaussian random variables with mean equal to the target DOA and variance equal to the Cramér-Rao Lower Bound (CRLB) of the target DOA estimation performed using a burst of 2*N* pulses (for more details see [TR2]). In this simulation we also set $|C_1/A|=1$, $|C_2/A|=0$ and $|C_3/A|=0$. That is, we supposed that the codes transmitted in the first burst by the reference radar and the interfering radar are the same, but the codes transmitted in the second and in the third burst are orthogonal to the interfering signal. As apparent in Figure 7, when the threshold λ is large (i.e. $\lambda\geq 2$) the performance of the MPM estimator is almost the same as the PM estimator. This is due to the fact that in this case the probability that Δθ is lower than λ $\Pr\{\Delta\theta\leq\lambda\}$ is almost unitary and the MPM estimator works as a PM estimator which performs the target DOA estimation using a burst of 2*N* pulses. The only difference is that the MPM estimator uses two bursts of *N* frequency hop pulses coded with two different code sequences instead of a burst of 2*N* frequency hop pulses coded with the same sequence.

On the other hand, when the threshold λ decreases, the probability $\Pr\{\Delta\theta\leq\lambda\}$ decreases and the MPM estimator calculates the target DOA using two or three bursts of *N* pulses. It is apparent from Figure 7 that the lower is λ, the lower is the dependence of the estimation accuracy on the interfering DOA. When the threshold λ tends to zero, also the probability $\Pr\{\Delta\theta\leq\lambda\}$ tends to zero, and the MPM estimator always processes three different PM DOA estimates. It is clear from Figure 7 that this algorithm minimizes the RMSE, that is, when the estimate $\hat{\vartheta}_p$ is available, the optimum value of λ is 0. However, the value of $\hat{\vartheta}_p$ is not always available, then, in the more general case, when both $\Delta\theta_1$ and $\Delta\theta_2$ are greater than λ, the MPM estimation of the target DOA must be calculated using the three PM estimates.

In Figure 8 we report the RMSE of the MPM estimator as a function of the interfering DOA for different values of the threshold λ. In this simulation, when both $\Delta\theta_1$ and $\Delta\theta_2$ are greater than λ, the MPM estimation of the target DOA has been calculated as the average of the three PM estimates, that is $\hat{\vartheta}_T=\left(\hat{\vartheta}_1+\hat{\vartheta}_2+\hat{\vartheta}_3\right)\Big/3$. Also in this simulation we set $|C_1/A|=1$, $|C_2/A|=0$ and $|C_3/A|=0$. In this case, when $\lambda=0$, the performance of the MPM estimator is strongly dependent on the interfering signal. Through simulations, it is possible to find the value of λ that minimizes the RMSE, in our case, as apparent from Figure 8, this value is $\lambda=0.3$.

Then, using the MPM estimator with a proper threshold, it is possible to improve greatly the performance of the radar with respect to the PM DOA estimator.

The case of $|C_2/A|=0$ and $|C_3/A|=0$ is the best for the second and third bursts. In Figure 9 we show some results with more general cases. In this Figure the RMSE of the MPM estimator has been calculated by assuming $|C_1/A|=1$, $|C_2/A| \sim U(0,1-\gamma)$ and $|C_3/A| \sim U(0,1-\gamma)$. The results are reported as a function of the interfering DOA, for different values of the parameter γ and for $\lambda=0.3$. Also in this simulation, when both $\Delta\theta_1$ and $\Delta\theta_2$ are greater than λ, the MPM estimation of the target DOA has been calculated as the average of the three PM estimates.

It is apparent that, for high values of γ the MPM estimator allows again an improvement with respect to the MP estimator. It is important to notice that, using proper frequency hop codes, the values of $|C/A|$ tends to zero for every Doppler-delay shift between the reference and the interfering signals. Then the value of γ commonly tends to one and the results obtained for low values of γ have to be considered the worst cases.

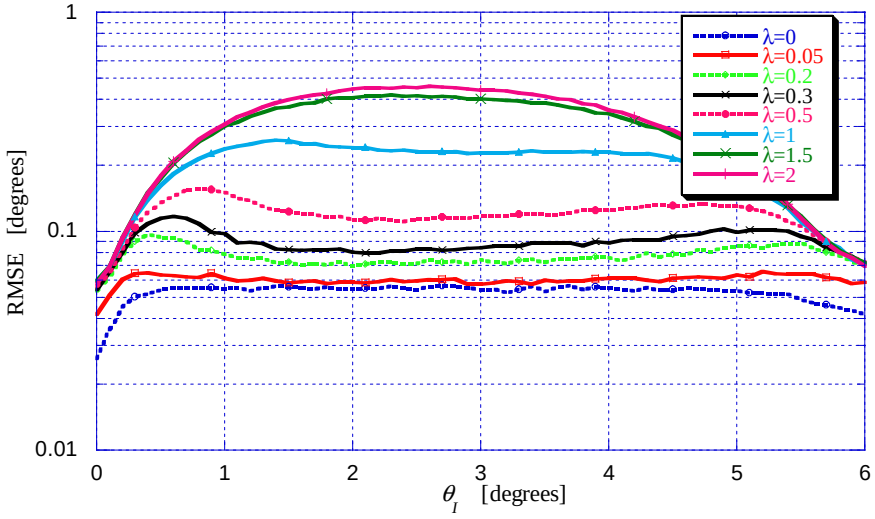

Figure 7 - RMSE of the MPM estimator as function of θ_I for different value of λ.

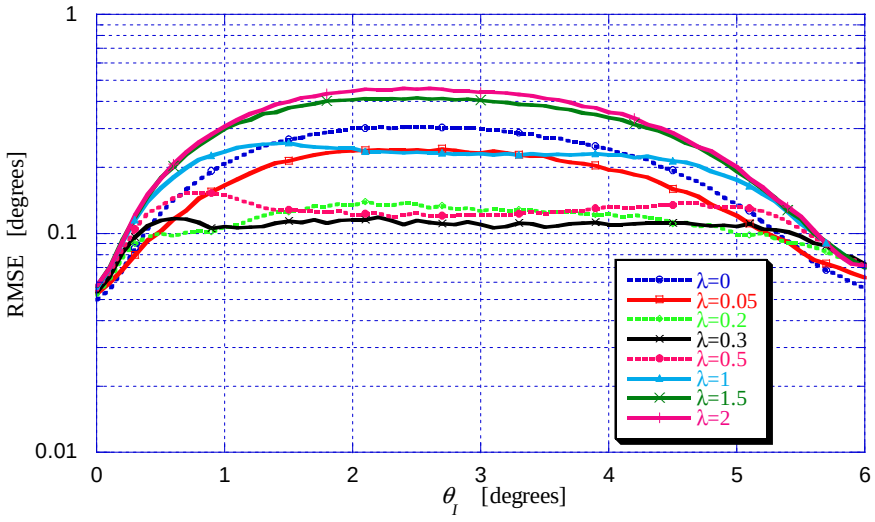

Figure 8 - RMSE of the MPM estimator as function of θ_I for different value of λ.

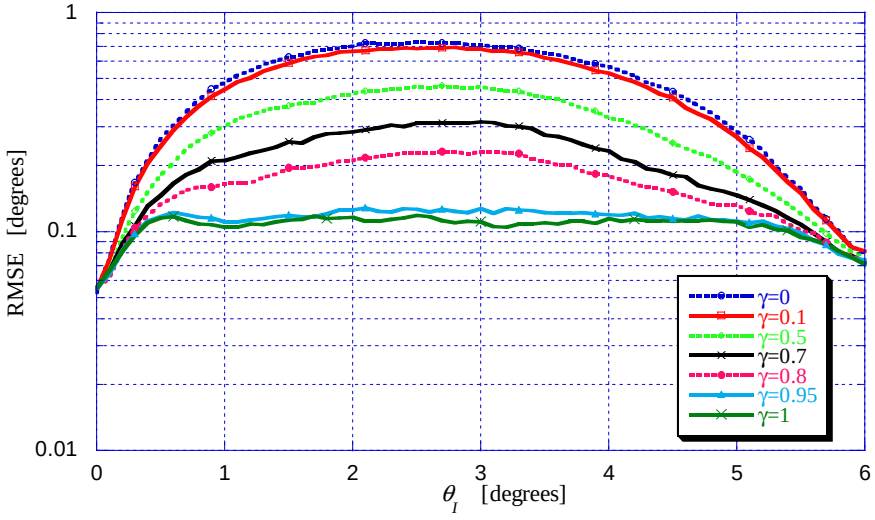

Figure 9 - RMSE of the MPM estimator as function of θ_I for different value of γ.

5 Bistatic Radar Systems and Bistatic Ambiguity Function

In previous Section we analyzed a netted system composed by monostatic radar system. In the most general case, in a multistatic radar system the receivers can also exploit the signal emitted by non colocated transmitters. To this end, it is very important to define and analyze bistatic radar system. This was the main topic of [TR3] and [TR4] summarized hereafter.

Bistatic radar may be defined as a radar in which the transmitter and receiver are at separate locations. The very first radars were bistatic, until pulsed waveforms and T/R switches were developed. Since then interest has varied up and down, but is demonstrably now at a high level, with numerous experimental systems being built and the results reported in the literature. Rather fewer operational systems, though, have been deployed.

Bistatic radars can operate with their own dedicated transmitters, which are specially designed for bistatic operation, or with transmitters of opportunity, which are designed for other purposes but found suitable for bistatic operation. When the transmitter of opportunity is from a monostatic radar the bistatic radar is often called a hitchhiker. When the transmitter of opportunity is from a non-radar transmission, such as broadcast, communications or radionavigation signal, the bistatic radar is called Passive Coherent Location (PCL).

Finally, transmitters of opportunity in military scenarios can be designated either cooperative or non-cooperative, where cooperative denotes an allied or friendly transmitter and non-cooperative denotes a hostile or neutral transmitter. Passive bistatic radar operations are more restricted when using the latter. In this Section we first define the bistatic parameters and the bistatic coordinate system and then we analyze the Bistatic Ambiguity Function.

5.1 Bistatic Geometry

Before starting, it is necessary to describe the coordinate system used to represent a bistatic radar geometry. Figure 10 shows the coordinate system and its parameters. The positions of the TX, RX and of the target are generic. Considering an ordinary Cartesian grid, the TX is located at point T, whose coordinates are (x_T, y_T), the RX is located at point R in (x_R, y_R) and the target is located at point B, whose coordinates are (x, y). The triangle formed by the transmitter, the receiver and the target is called the bistatic triangle.

As shown in Figure 10, the sides of the bistatic triangle are R_T, R_R and L, where R_T is the range from transmitter to target, R_R is the range from receiver to target and L is the baseline

between the transmitter and the receiver. The internal angles of the bistatic triangle, that, without lack of generality, are assumed to be positive, are α, β and γ. In particular, the bistatic angle β is the angle at the apex of the bistatic triangle, at the vertex which represents the target. Assuming that the coordinates of the transmitter, the receiver and the target are known, it is possible to calculate all the parameters of the bistatic triangle. θ_T and θ_R are the look angle of the transmitter and the look angle of the receiver, respectively, they are measured positive clockwise from the vector normal to the baseline pointing towards the target.

From Figure 9.1, we have that $\theta_T = 90°-\alpha$, $\theta_R = \gamma-90°$, $\beta = 180°-\alpha-\gamma=\theta_T-\theta_R$, and from the cosine law we obtain: $R_T^2=R_R^2+L^2+2R_RL\sin\theta_R$, which gives the range from transmitter to target R_T, as a function of the range from receiver to target R_R and the look angle of the receiver θ_R. Figure 9.1 also shows the target velocity vector $\vec{V}$; ϕ is the angle between the target velocity vector and the bistatic bisector, which is measured in a positive clockwise direction from the bisector. In particular the bistatic bisector is represented by the vector $\overrightarrow{BI}$, where I is the incenter of the bistatic triangle, whose coordinates are (x_I, y_I).

The coordinates of the incenter can be easily obtained as

$$(x_I, y_I) = \frac{L}{L+R_R+R_T}(x, y) + \frac{R_R}{L+R_R+R_T}(x_T, y_T) + \frac{R_T}{L+R_R+R_T}(x_R, y_R) \qquad (16)$$

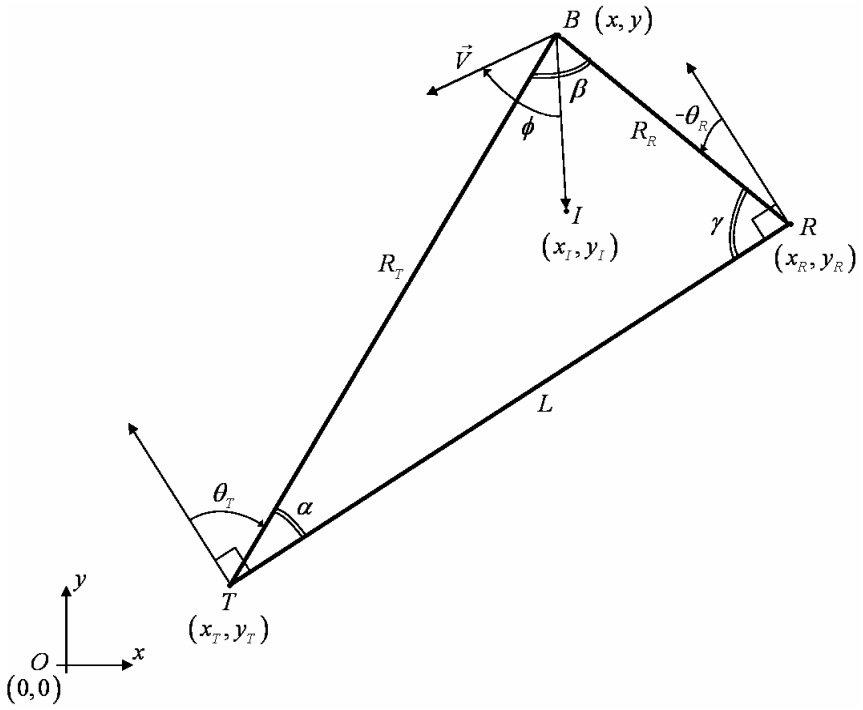

Figure 10 - Bistatic geometry.

In the bistatic geometry, an important parameter is the radial velocity V_a, which is the target velocity component along the bistatic bisector. From the observation of Figure 9.1, we obtain $V_a = \vec{V} \cdot \overrightarrow{BI} \Big/ \left|\overrightarrow{BI}\right| = \left|\vec{V}\right| \cos\phi$. Using the notation $\vec{V} = V_x \cdot \vec{x} + V_y \cdot \vec{y}$, it is easy to verify that:

$$V_a = \frac{(x_I - x)V_x + (y_I - y)V_y}{\sqrt{(x_I - x)^2 + (y_I - y)^2}} \tag{17}$$

The bistatic radar geometry can be completely specified in terms of any three of the five parameters, θ_T, θ_R, L, R_R and R_T. In this Section we will use θ_R, L, and R_R that can be obtained using the following equations:

$$L = \sqrt{(x_T - x_R)^2 + (y_T - y_R)^2} \tag{18}$$

$$R_R = \sqrt{(x - x_R)^2 + (y - y_R)^2} \tag{19}$$

$$R_T = \sqrt{(x - x_T)^2 + (y - y_T)^2} \tag{20}$$

$$\vartheta_R = \cos^{-1}\left(\frac{R_R^2 + L^2 - R_T^2}{2R_R L}\right) - \frac{\pi}{2} \tag{21}$$

5.2 Bistatic Ambiguity Function

As showed in Section 1, the mathematical definition of the Ambiguity Function is:

$$\left|X\left(\tau_H, \tau_a, \nu_H, \nu_a\right)\right| = \left|\int_{-\infty}^{+\infty} u(t-\tau_a) u^*\left(t-\tau_H\right) \exp\left(-j2\pi\left(\nu_H - \nu_a\right)t\right) dt\right| \tag{22}$$

where $u(t)$ is the complex envelope of the transmitted signal, τ_a and v_a are the actual delay and Doppler frequency of the radar target respectively and τ_H and v_H are the hypothesized delay and frequency. The AF in (22) can be also expressed as a function of τ and v, where $\tau = \tau_H - \tau_a$ and $v = v_H - v_a$. As known, in the monostatic case there is a linear relationship between τ_a and v_a, and the range position R_a and radial velocity V_a of the target, more specifically $\tau_a = 2R_a/c$ and $\nu_a = -2V_a f_C/c$. Similar relations hold for τ_H and v_H. Due to this linear relationship, the AF in the range – velocity plane has the same behavior of the one expressed as a function of τ and v, except for a scale factor. Therefore, in the monostatic configuration,

the information about the target delay and the target Doppler shift directly provides information about the target range and the target velocity. This is different in the bistatic case, where the relation between time delay and Doppler frequency, and target distance and velocity is not linear. Referring to the bistatic geometry of Figure 10, for obtain the expression of the bistatic ambiguity function, we must replace in (22) the relations [Tsa97]:

$$\tau_H(R_R,\theta_R,L)=\frac{R_R+\sqrt{R_R^2+L^2+2R_RL\sin\theta_R}}{c} \tag{23}$$

$$\nu_H(R_R,V_B,\theta_R,L)=2\frac{f_c}{c}V_B\sqrt{\frac{1}{2}+\frac{R_R+L\sin\theta_R}{2\sqrt{R_R^2+L^2+2R_RL\sin\theta_R}}} \tag{24}$$

Similar relations hold for τ_H and ν_H[1]. It is clearly apparent from equations (23) and (24) that in the bistatic case, the Doppler shift and the delay depends on the geometry of the bistatic triangle and the relation between time delay and Doppler frequency, and target distance and velocity is not linear. Due to these non linear equations, it is apparent that the Bistatic Ambiguity Function depends also on the bistatic geometry parameters, i.e. the target direction of arrival, the bistatic baseline length and the distance between the target and the receiver. This dependence is very strong and can be appreciated later with an illustrative example. considering the case of a target close to the baseline joining the transmitter and receiver.

In [TR3] we analyzed the performance when the transmitted waveform is a burst of *Linear Frequency Modulated* (LFM) pulses, while in [TR4] we also analyzed the performance when the transmitted waveform is a *Sinusoidal Frequency Modulated* (SFM) pulse. Hereafter we will consider the case of a burst of LFM pulses, for the SFM case we refer the reader to [TR4]. As calculated in [TR3], the *Complex Ambiguity Function* (CAF) of a burst of LFM pulses can be expressed as:

$$X(\tau,\nu)=\frac{1}{N}\sum_{n=-(N-1)}^{N-1}\exp\left(j\pi\nu(N-1+n)T_R\right)\frac{\sin\left(\pi\nu\left(N-|n|\right)T_R\right)}{\sin\left(\pi\nu T_R\right)}X_1(\tau-nT,\nu) \tag{25}$$

where

$$X_1(\tau,\nu)=\frac{\sin\left(\pi T(\nu-k\tau)\left(1-|\tau|/T\right)\right)}{\pi T(\nu-k\tau)}rect\left(\frac{\tau}{2T}\right) \tag{26}$$

is the Complex Ambiguity Function of a single LFM pulse.

[1] Note that R_a and V_a are the actual range and bistatic velocity, while R_T and V_B=Vcosφ are the hypothesized range and bistatic velocity

Moreover, if we limit the delay to the mainlobe area, namely to $|\tau| \le T$, the AF reduces to:

$$\left|X(\tau,\nu)\right| = \left|\frac{\sin\left(\pi T(\nu - k\tau)\left(1-|\tau|/T\right)\right)}{\pi T(\nu - k\tau)}\right| \left|\frac{\sin(\pi\nu N T_R)}{N\sin(\pi\nu T_R)}\right| \quad \text{for } |\tau| < T \qquad (27)$$

To link this equation to the bistatic geometry of Figure 10 and to obtain the expression of the Bistatic AF (BAF), we must replace in (27) the relations $\tau = \tau_H - \tau_a$ and $\nu = \nu_H - \nu_a$ calculated using (23) and (24). The contour plot of the BAF is illustrated in Figure 11 in the plane R_R-V_B with V_B=Vcosφ, V_a=600m/s and R_a=20Km and L=50Km. The presence of discrete peaks (nails) is evident even in the bistatic plane, even if they are not symmetrically distributed.

The main peak corresponds to V_a=600m/s and R_a=20Km. The shape of the bistatic function strongly depends on the target angle θ_R, particularly for high values of BT. To highlight this phenomenon, in Figures 12-15 we show the zero-delay and zero-Doppler slices of the ambiguity function for different values of θ_R and BT. Both cuts are maximum for values of range and target velocity corresponding to the true values V_a=600m/s and R_a=20Km.

For values of θ_R close to $-\pi/2$ the bistatic AF presents multiple peaks. The worst case is for θ_R=$-\pi/2$, that is, when the target is on the baseline. If the target is between the transmitter and the receiver, the AF is flat and the range and velocity resolutions are completely lost. For values of θ_R far from $-\pi/2$ the shape of the bistatic ambiguity function is practically the same (see, for instance, $\theta_R = -\pi$, and $\theta_R = \pi/6$ in Figs. 12-15). For increasing values of N the range resolution improves, but many peaks appear in the bistatic AF shape.

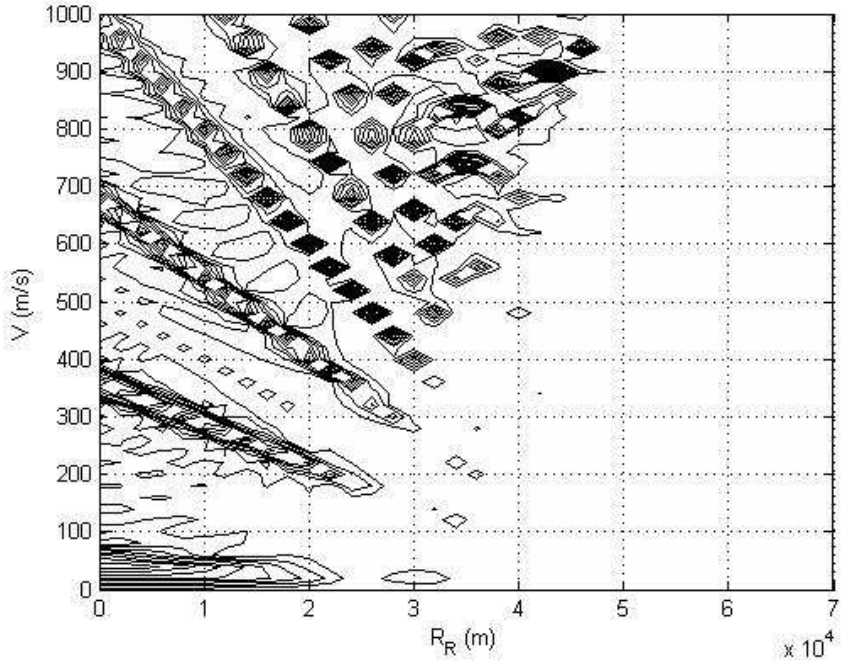

Figure 11 - BAF of a burst of Linear Frequency Modulated pulses, BT=250, T_R=1ms, T=250μs, N=8, θ_R=-0.47π , L=50Km, V_a=600m/s, R_a=20Km.

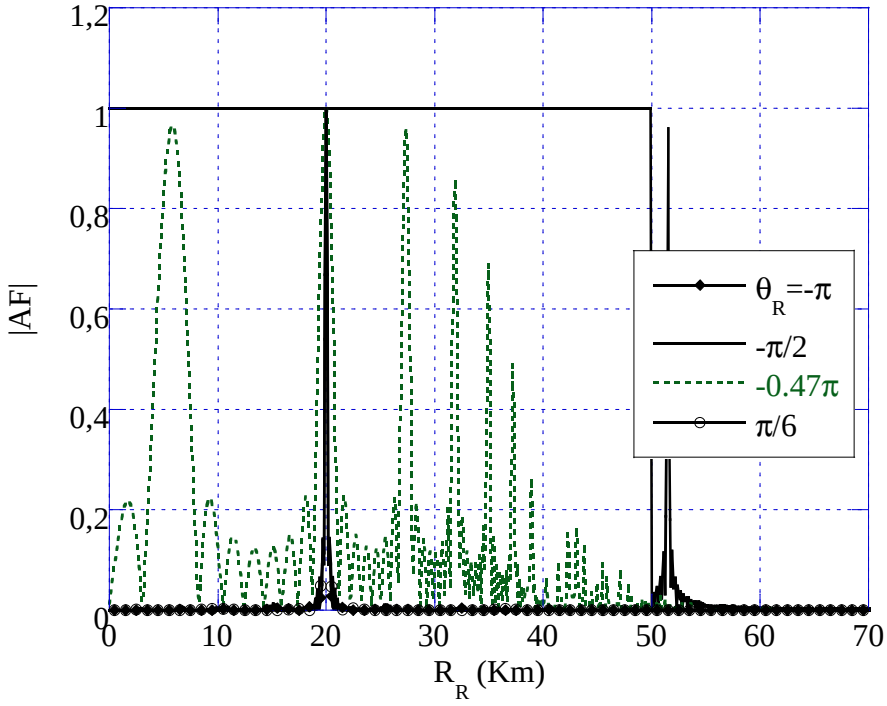

Figure 12 - BAF of a burst of Linear Frequency Modulated pulses; Zero-Doppler cut, BT=20, T_R=1ms, T=250μs, N=8, L=50Km, V_a=600m/s, R_a=20Km.

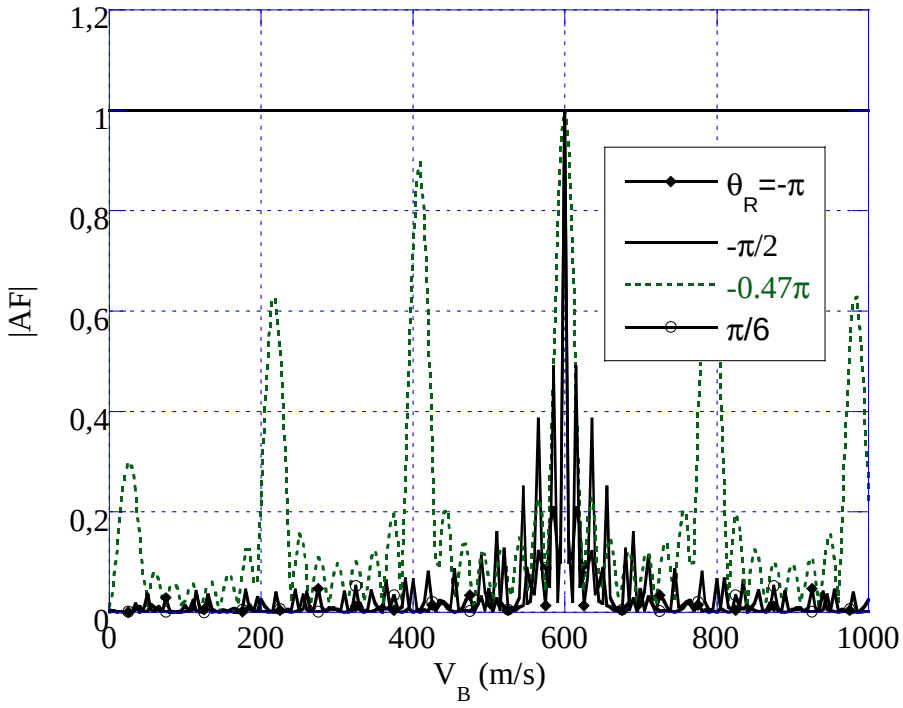

Figure 13 - BAF of a burst of Linear Frequency Modulated pulses; Zero-delay cut, *BT*=20, T_R=1ms, *T*=250μs, *N*=8, L=50Km, V_a=600m/s, R_a=20Km.

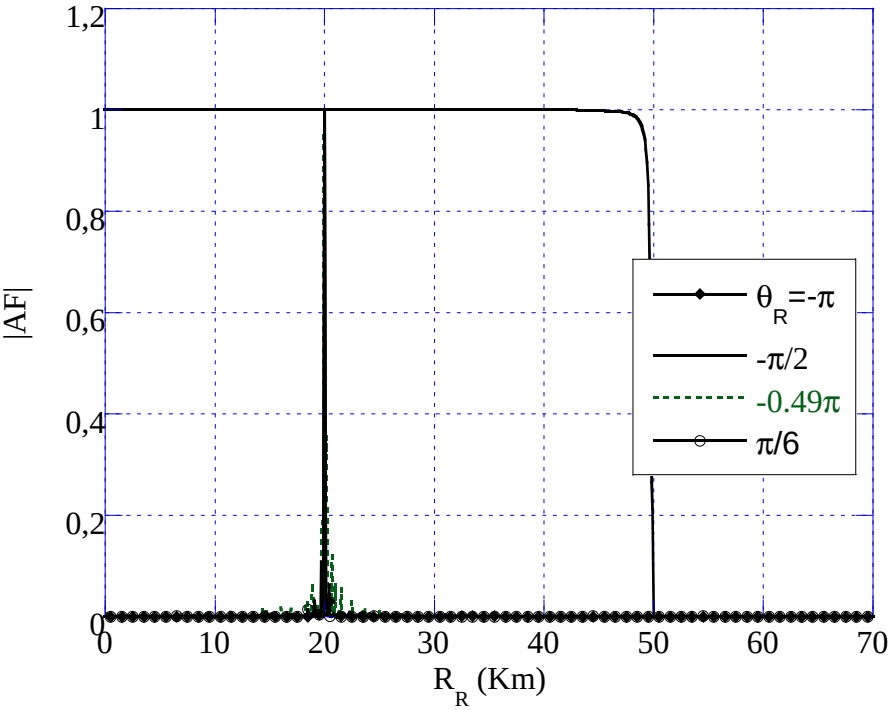

Figure 14 - BAF of a burst of Linear Frequency Modulated pulses; Zero-Doppler cut, *BT*=250, T_R=1ms, *T*=250μs, *N*=8, *L*=50Km, V_a=600m/s, R_a=20Km.

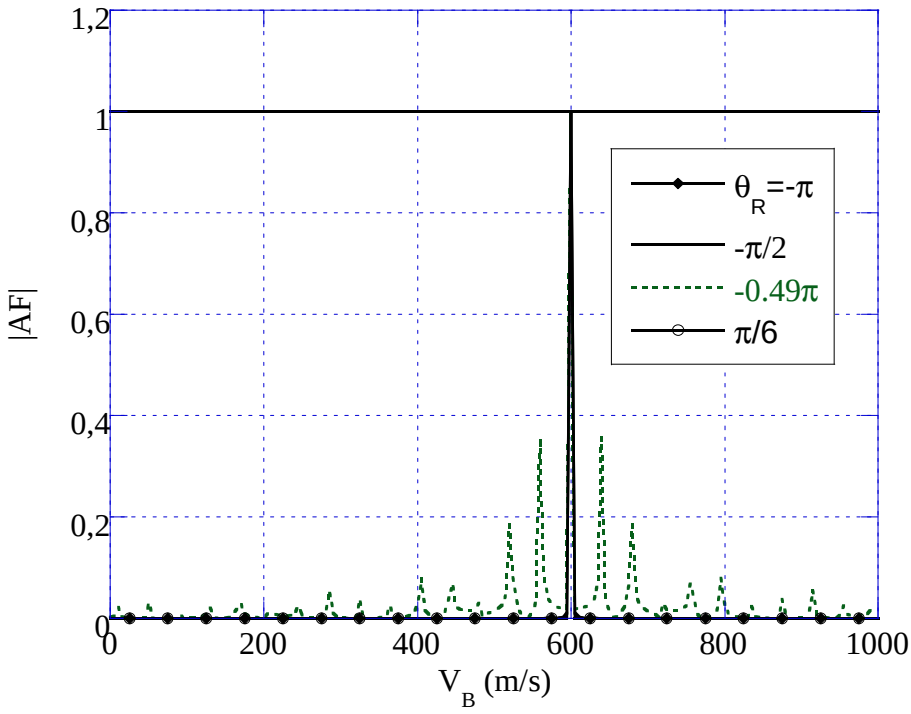

Figure 15 - BAF of a burst of Linear Frequency Modulated pulses; Zero-delay cut, *BT*=250, T_R=1ms, *T*=250μs, *N*=8, L=50Km, V_a=600m/s, R_a=20Km.

6 Channel Performance Evaluation in a Bistatic Radar System

6.1 Bistatic Cramér-Rao Lower Bounds

The AF directly determines the capability of a system to resolve two targets that exist at different ranges from the radar and have different radial velocities. When the receiver signals from the target have similar energy, the resolution is equal to the half power width of the AF mainlobe. The AF is also related to the accuracy with which the range and the velocity of a given target can be estimated. When the Signal to Noise power Ratio (*SNR*) is high, the CRLBs on estimation accuracy are dependent on both the *SNR* and the second derivatives of the AF, that is, the sharpness of the AF mainlobe. Unlike the ambiguity function which provides information on the global resolution, the CRLBs are a local measure of estimation accuracy. Anyway, both can be used to asses the error properties of the estimates of the signal parameters. In [Van71] the author derived a relationship between CRLB and ambiguity function, which has been successfully used in the analysis of passive and active arrays [Dog01]. In the monostatic configuration, [Van71] claims that for the Fisher Information Matrix (FIM) the following relationship holds (for more details see [TR3]):

$$\mathbf{J}_M(\tau,\nu) = -2SNR\left[\begin{array}{cc} \dfrac{\partial^2\Theta(\tau,\nu)}{\partial\tau^2} & \dfrac{\partial^2\Theta(\tau,\nu)}{\partial\tau\partial\nu} \\ \dfrac{\partial^2\Theta(\tau,\nu)}{\partial\nu\partial\tau} & \dfrac{\partial^2\Theta(\tau,\nu)}{\partial\nu^2} \end{array}\right]_{\tau=0,\nu=0} = -2SNR\mathbf{J}_{M_n} \qquad (28)$$

where $\Theta(\tau,\nu) = \left|X(\tau,\nu)\right|^2$ and *SNR* is the signal-to-noise power ratio at the receiver. The AF is the heart of this expression since it is the log-likelihood function excluding the effect of signal attenuation and clutter. In [TR3] we report the proof of relation (28). The property in (28) does not depend on the choice of the parameters of the ambiguity function, then it holds for both monostatic and bistatic case. From (28) the CRLBs follow: $\mathrm{CRLB}(\tau_a) = \left[\mathbf{J}_M(\tau_a,\nu_a)\right]^{-1}_{1,1}$ and $\mathrm{CRLB}(\nu_a) = \left[\mathbf{J}_M(\tau_a,\nu_a)\right]^{-1}_{2,2}$. In the bistatic configuration we should write the ambiguity function in terms of the bistatic $\tau(R_R,\theta_R,L)$ and $\nu(R_R, V_B,\theta_R,L)$ and derive it with respect to the useful parameters R_R and V_B. Then

$$\mathbf{J}_B\left(R_R,V_B\right)=-2SNR\left[\begin{array}{cc}\dfrac{\partial^2\Theta\left(R_R,V_B\right)}{\partial {R_R}^2} & \dfrac{\partial^2\Theta\left(R_R,V_B\right)}{\partial R_R\partial V_B}\\ \dfrac{\partial^2\Theta\left(R_R,V_B\right)}{\partial V_B\partial R_R} & \dfrac{\partial^2\Theta\left(R_R,V_B\right)}{\partial {V_B}^2}\end{array}\right]\Bigg|_{R_R=R_a,V_B=V_a} \tag{29}$$

For the calculation of the CRLBs in the bistatic domain we can partially use the results of the monostatic domain. Following the "chain rule" (see [TR3] for details) of the derivative we can prove that:

$$\mathbf{J}_B\left(R_R,V_B\right)=\mathbf{P}\mathbf{J}_M\left(\tau,\nu\right)\mathbf{P}^T \tag{30}$$

where

$$\mathbf{P}=\left[\begin{array}{cc}\dfrac{\partial\tau}{\partial R_R} & \dfrac{\partial\nu}{\partial R_R}\\ \dfrac{\partial\tau}{\partial V_B} & \dfrac{\partial\nu}{\partial V_B}\end{array}\right] \tag{31}$$

and

$$\frac{\partial\nu}{\partial R_R}=\frac{f_c}{2c}V_B\frac{L^2\cos^2\theta_R}{\left(R_R^2+L^2+2R_RL\sin\theta_R\right)^{3/2}\sqrt{\dfrac{1}{2}+\dfrac{R_R+L\sin\theta_R}{2\sqrt{R_R^2+L^2+2R_RL\sin\theta_R}}}} \tag{32}$$

$$\frac{\partial\nu}{\partial V_B}=\frac{2f_c}{c}\sqrt{\frac{1}{2}+\frac{R_R+L\sin\theta_R}{2\sqrt{R_R^2+L^2+2R_RL\sin\theta_R}}} \tag{33}$$

$$\frac{\partial\tau}{\partial R_R}=\frac{1}{c}\left(1+\frac{R_R+L\sin\theta_R}{\sqrt{R_R^2+L^2+2R_RL\sin\theta_R}}\right) \tag{34}$$

$$\frac{\partial\tau}{\partial V_B}=0 \tag{35}$$

The relationship showed in (30) is very interesting because the two effects that describe the Bistatic FIM are separated. In particular, matrix **P** takes into account only the effect of the bistatic geometry while $\mathbf{J}_M(\tau,\nu)$ takes into account only the effect of the transmitted waveform. The Cramér-Rao lower bounds are given by the inverse of the Fisher Information Matrix, therefore

$$\mathrm{CRLB}(R_R)=\frac{\left[\mathbf{J}_B\right]_{2,2}}{\left[\mathbf{J}_B\right]_{1,1}\left[\mathbf{J}_B\right]_{2,2}-\left[\mathbf{J}_B\right]_{1,2}^2} \tag{36}$$

$$\mathrm{CRLB}(V_B) = \frac{[\mathbf{J}_B]_{1,1}}{[\mathbf{J}_B]_{1,1}[\mathbf{J}_B]_{2,2} - [\mathbf{J}_B]_{1,2}^2} \tag{37}$$

From the last equation it is clearly apparent that the local accuracy in the bistatic case depends not only on the transmitted waveform but also on the bistatic geometry [Rih69], [Tsa97].

It is important to observe that the *SNR* at the receiver takes into account the energy loss due to propagation:

$$SNR \propto \frac{1}{R_R^2 R_T^2} \tag{38}$$

where $R_T = \sqrt{R_R^2 + L^2 + 2R_R L \sin\theta_R}$ is the range from transmitter to target.

It is clear that for L=0 the transmitter and the receiver are co-located and, from the last equations, it is clear that in this case the bistatic FIM coincides with the monostatic FIM.

The results derived in this Section can be used for defining a tool for evaluate the performance of a given monostatic or bistatic channel of the multistatic system and for design multistatic weighting coefficients for the detection process that will be described in the next Section.

6.2 Bistatic Cramér-Rao Lower Bounds for a burst of LFM pulses

Using the results showed in previous Section, after some algebra, it is possible to verify that, in the monostatic configuration, the FIM of a burst of LFM pulses is given by [Far09]

$$\mathbf{J}_M(\tau,\nu) = -2SNR\begin{bmatrix} -\frac{k^2\pi^2T^2}{3} & \frac{k\pi^2T^2}{3} \\ \frac{k\pi^2T^2}{3} & -\frac{\pi^2T^2}{3} + \frac{\pi^2T_R^2(1-N^2)}{3} \end{bmatrix} \tag{39}$$

Inverting (39), the monostatic CRLBs for the delay and the Doppler are given by:

$$\mathrm{CRLB}(\tau) = \frac{3}{2\pi^2T^2k^2SNR}\left[1 + \left(\frac{T}{T_R}\right)^2 \frac{1}{N^2-1}\right] \tag{40}$$

and

$$\mathrm{CRLB}(\nu) = \frac{3}{2\pi^2T_R^2SNR\left(N^2-1\right)} \tag{41}$$

These results are in agreement with those obtained in [Dog01].

Using this result, combined with (30), it is possible to compare the monostatic and the bistatic Root Cramér-Rao Lower Bounds (RCRLBs). Figures 16-18 show the RCRLBs of range and velocity, both in the monostatic and bistatic case, obtained selecting T=250μsec, T_R= 1msec, B= 1MHz, f_C=10GHz and N = 8. In particular, Figure 16 shows the RCRLBs as a function of the receiver to target range R_R when θ_R =0. While Figure 17 shows the results obtained choosing θ_R = -0.49π. Figure 18 shows the RCRLBs as a function of the receiver look angle θ_R , both in the case of $R_R<L$ and $R_R>L$. All these figures have been obtained choosing V_B=250 m/sec, L=50km and holding constant the *SNR* to 0dB. It is evident that, for all the parameter values we tested, the bistatic RCRLBs are always higher than the monostatic RCRLBs. Anyway when the distance from receiver to the target increases, the bistatic system behaves more and more as the monostatic one. As apparent from Figure 17, the effects of geometry are prominent where the target approaches the baseline, that is when $R_R \leq L$ and θ_R approaches $-\pi/2$. When the target is on the baseline, the RCRLBs tend to infinity.

In this case, the resulting delay is L/c and the radial velocity is zero, therefore resolution is totally lost and the RCRLBs tend to infinity. This can be appreciated by realizing that the echo arrives at the receiver at the same instant as the direct signal, independent of the target location, and the Doppler shift of a target crossing the bistatic baseline must be zero, because the transmitter-to-target range changes in an equal and opposite way to the target-to-receiver range, independent of the magnitude and direction of the target velocity. However, the effects of the bistatic geometry are less prominent when the distance to the target increases; in this case the bistatic system behaves more and more as a monostatic system. In [TR4] we also calculated in closed form the RCRLB obtained transmitting a Sinusoidal Frequency Modulated pulse. This signal model the waveform transmitted by a FM commercial radio station that is often the non co-operative transmitter of opportunity exploited by a Passive Coherent Location (PCL) system. The obtained results are pretty similar to those showed in this Section and are not reported here for the lack of space, for more details we refer the reader to [TR4].

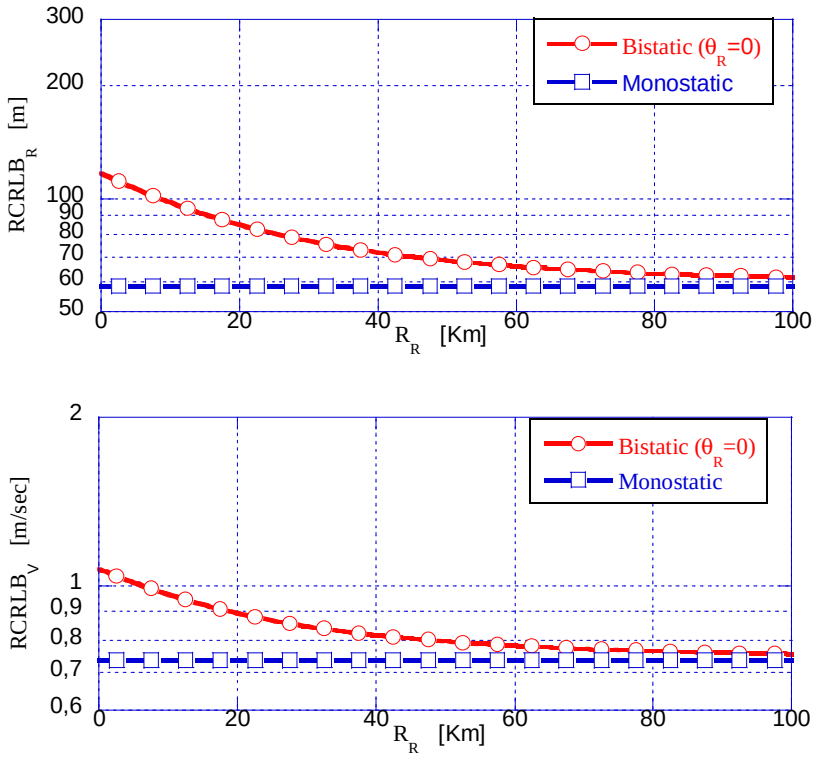

Figure 16 - RCRLB of Range and Velocity as a function of receiver to target range R_R, θ_R=0; L=50km, SNR=0dB. The transmitted signal is a burst of LFM pulses.

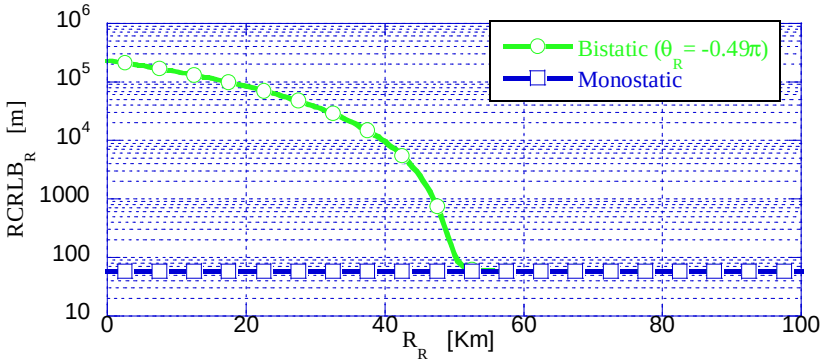

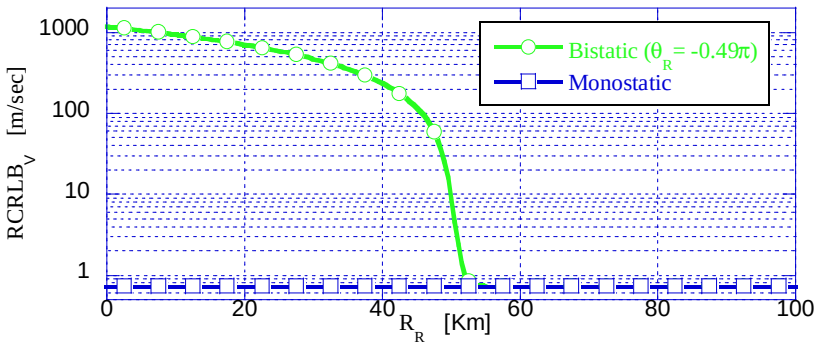

Figure 17 - RCRLB of Range and Velocity as a function of receiver to target range R_R, θ_R= -0.49π; L=50km, SNR=0dB. The transmitted signal is a burst of LFM pulses.

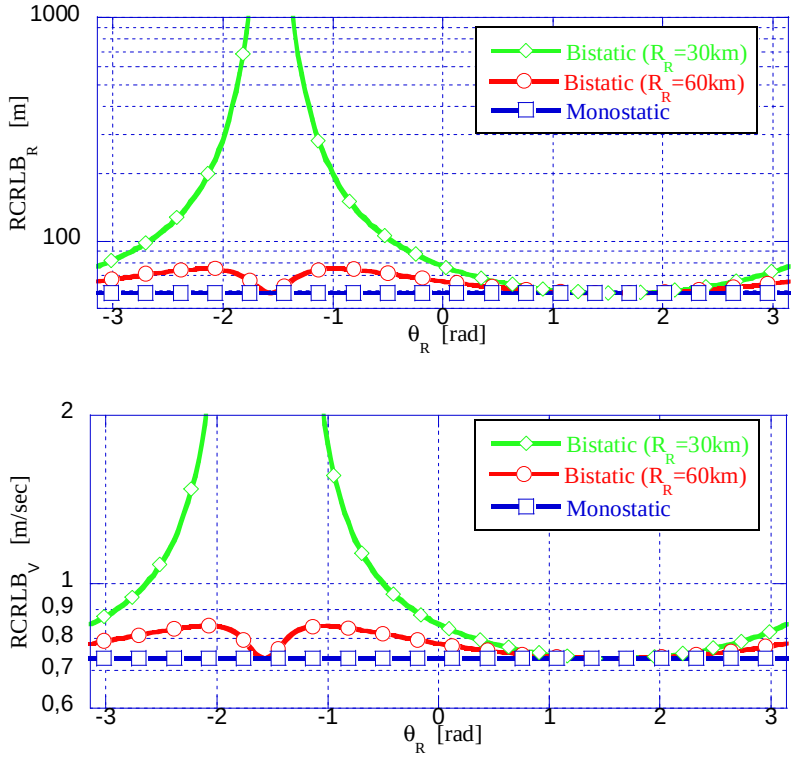

Figure 18 - RCRLB of Range and Velocity as a function of receiver look angle θ_R; L=50km, SNR=0dB. The transmitted signal is a burst of LFM pulses.

7 Multistatic Radar Systems

Multistatic radars utilize multiple transmitters and receivers. Such systems differ from typical modern active radars since they consist of several different monostatic and bistatic channels of observation. Due to this spatial diversity, these systems present challenges in managing their operation as well as in usefully combining the data from multiple sources of information on a particular area of surveillance. The information gain, obtained through this spatial diversity, combined with some level of data fusion, can give rise to a number of advantages over both the individual monostatic and bistatic cases for typical radar functions, such as detection, parameter estimation, tracking and identification. As showed in the previous Sections, the performance of each channel of the multistatic system heavily depends on the transmitted waveform and on the geometry of the scenario, that is, the position of receivers and transmitters with respect to the position of the target.

Exploiting the Monostatic and the Bistatic Cramér-Rao Lower Bounds, it is possible to calculate the channel performance of each TX-RX pair as a function of the target kinematic parameters. In particular, in this Section we summarize the results described in [TR4] where we presented some algorithms to select the best channels of the multistatic system and to compute the rules for selecting the best weighting coefficients for fusing the signals from multiple receivers in order to improve the detection performance and the estimation accuracy of the kinematic parameters of the target. In [TR4] we also introduced an optimization methodology for selecting only some channels for the network, independent of the adopted fusion rule. All the techniques described in this Section depend on the Fisher Information Matrix (FIM) which is itself dependent on the *SNR*, the AF and therefore on the geometry and the transmitted waveform.

7.1 Optimal channel selection in a multistatic radar system

The CRLB study carried out on the bistatic geometry can be applied for the selection of the transmitter-receiver (TX-RX) pair in a multistatic radar system. We have seen that the performance of each bistatic channel heavily depends upon the geometry of the scenario and the position of the target with respect to each receiver and transmitter. In this Section we investigate the problem of optimally selecting the TX-RX pair, based on the information provided by the CRLB for the bistatic geometry of each bistatic channel. The best pair is

defined as that exhibiting the lowest bistatic CRLB for the target velocity or range (or a combination of the two). These results can be used for the dynamical selection of the TX-RX signals for the tracking of a radar target moving along a trajectory in a multistatic scenario.

The optimal approach for a multistatic radar system would be central-level track processing, that is, to send all observations from the sensors to a fusion centre, where the observations are jointly processed.

This approach has two major disadvantages:

1) the amount of input measurement data to the fusion centre may be very high;
2) the observations from the sensors with the worst accuracy and resolution can significantly degrade the resolution of the whole systems.

This second problem is maybe the most important. There are studies that show that the best performance of the fused estimate in a multisensor system occurs when the sensors have similar accuracy and resolution [Azi07].

If accuracy and resolution vary widely, there is a risk that the fused track performs only marginally better, or even worse, than the track with the best quality estimate.

As an example, let consider the case of a target which is close to the baseline joining one of the transmitter and one of the receiver of the multistatic system.

In this case the range and Doppler resolution can be badly degraded, no matter what the radar waveform is. This can be appreciated by realising that the echo arrives at the receiver at the same instant as the direct signal, independent of the target location, and the Doppler shift of a target crossing the bistatic baseline must be zero, because the transmitter-to-target range changes in an equal and opposite way to the target-to-receiver range, independent of the magnitude and direction of the target velocity. In this case, resolution is totally lost and therefore the observation from this transmitter-receiver pair could hardly degrade the resolution of the whole multistatic radar system [Azi07], [Gre10],[Gre11].

This Section proposes an optimization algorithm that, in a generic multistatic scenario and independent of the adopted fusion technique, specifies what channels should be discarded and what channels should be considered during the fusion process.

Using this algorithm, only a subset of data are communicated to the fusion centre, more specifically only from those sensors exhibiting the best performance in terms of estimation accuracy of the target parameters.

In the most general case, the multistatic scenario is the one pictorially depicted in Figure 19, where there are M transmitter and N receivers, co-located or not, surveying a common

coverage area. It is supposed that a set of orthogonal waveform is transmitted, where orthogonality is assumed to be maintained for any Doppler-delay shift. With proper design, transmit-receive paths can be separated, so that each sensor can receive echoes due the signals generated by all the transmitters and can select the transmitted signal of interest. In this way, the multistatic system can be considered as consisting of *NM* different monostatic and bistatic channels of observation. The proposed optimization algorithm exploits the results obtained in the previous Sections to approach the problem of optimally selecting the channels to be used by the fusion process. This algorithm is divided in two steps. In the first step, each of the *N* receivers of the network selects one of the *M* transmitters in order to obtain the best performances in terms of estimation accuracy of the target range and/or velocity. While, in the second step, after ranking the so obtained *N* channels from the worst to the best, where the best is the one that exhibits the lowest bistatic CRLB, only the first $N' \leq N$ are selected for the fusion process. In the following, with the help of an illustrative example, we describe in detail how the optimization algorithm works. In the first step of the optimization process, each receiver selects the best transmitter on its own. In a multistatic network consisting of *M* transmitters and *N* receivers for each receiver there are *M* different channels. In the case that the considered receiver is colocated with one of the transmitter, there are *M*-1 bistatic channels and 1 monostatic channel.

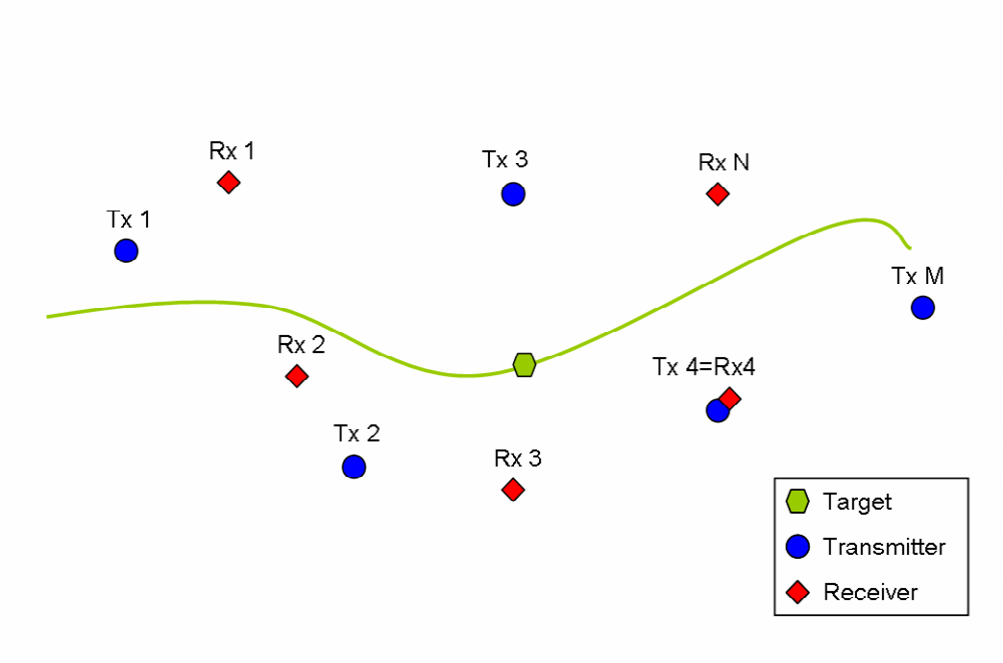

Figure 19 - Generic Multistatic Scenario.

As an example, let consider a surveillance map of dimension L_x=20km and L_y=20km where there are seven transmitters placed at coordinates $T^{(1)}$=(13.9 km,15.9 km), $T^{(2)}$=(6.3 km, 3.7 km), $T^{(3)}$=(19 km,9.8 km), $T^{(4)}$=(0.7 km,8.9 km), $T^{(5)}$=(8.8 km, 12.9 km), $T^{(6)}$=(7.6 km, 14.2 km), $T^{(7)}$=(15.3 km, 15.1 km) and the receiver is co-located with the first transmitter. In this example it is supposed that the transmitters send orthogonal signals with the same power and characterized by the same AF. Therefore, the different performances among the channels depend only on the propagation path loss and the configuration of the bistatic geometry. For each point of the analysed area, evaluating the performance of each bistatic channel, it is possible to select the transmitter with the best performance, that is, the one with the lowest CRLB on the target range and velocity estimation accuracy.

Figures 20 (a) and (b) show, in a colour coded map, the transmitter to be selected in order to provide the minimum CRLB for each point of the analysed area for range and velocity estimation, respectively. The color-map of these figures is clustered into 7 colours, each of which is associated with one of the 7 transmitters. It is apparent, that the results are very similar, but it is also possible to build a cost function using a weighted combination of the two CRLB. Figures 21 (a) and (b) show the minimum Root of the CRLB (RCRLB) of the target range and the target velocity, respectively, that is the value of the RCRLB which is provided by the transmitter-receiver pair which has the minimum RCRLB.

From this example, it is apparent that each receiver knows, for each point of the surveillance map, which is the transmitter to be selected in order to meet the best performance. Therefore, as pictorially shown in Figure 22, based upon the actual estimate of the target position, each receiver can dynamically select the signal of the best transmitter and discard the signals transmitted by the other sensors. Doing so, only *N* of the *MN* possible channels are selected for the fusion process.

Even so, from Figures 21 (a) and (b) it is apparent that, for same points of the surveillance map, the best performance that a receiver can achieve could be poor. This is only due to the geographical distribution of the sensors in the multistatic system but, for the reasons previously described, this could be a problem for the fusion process.

This problem can be solved by selecting a subset of channels among the N previously obtained. In particular, in the second step of the optimization algorithm, the *N* channels are ranked from the worst to the best and only the first *N'* are selected for the fusion process. The number *N'* could be also dynamically changed by the fusion process in order to meet pre-specified performance goals.

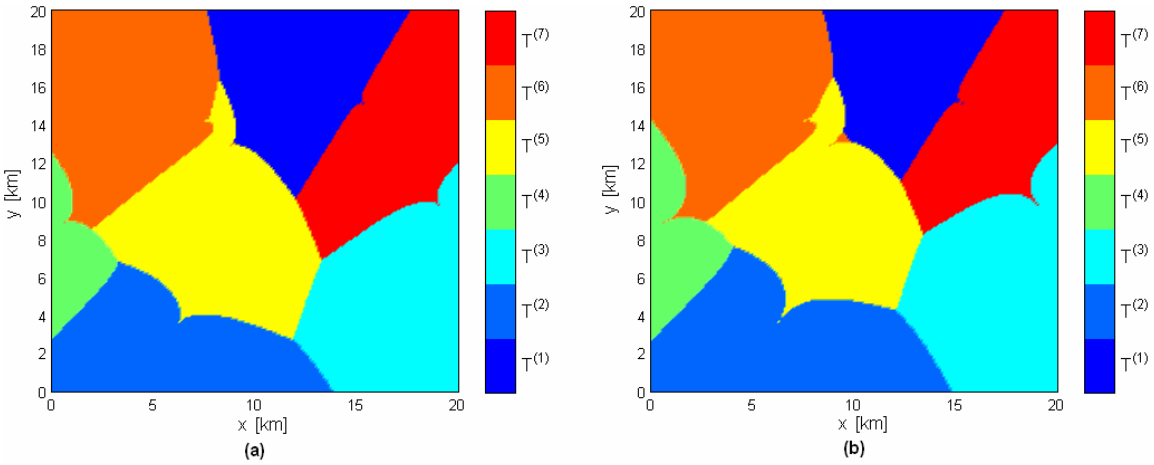

Figure 20 - (a) Optimum Transmitter for target range estimation; (b) Optimum Transmitter for target velocity estimation. The receiver is co-located with $T^{(1)}$.

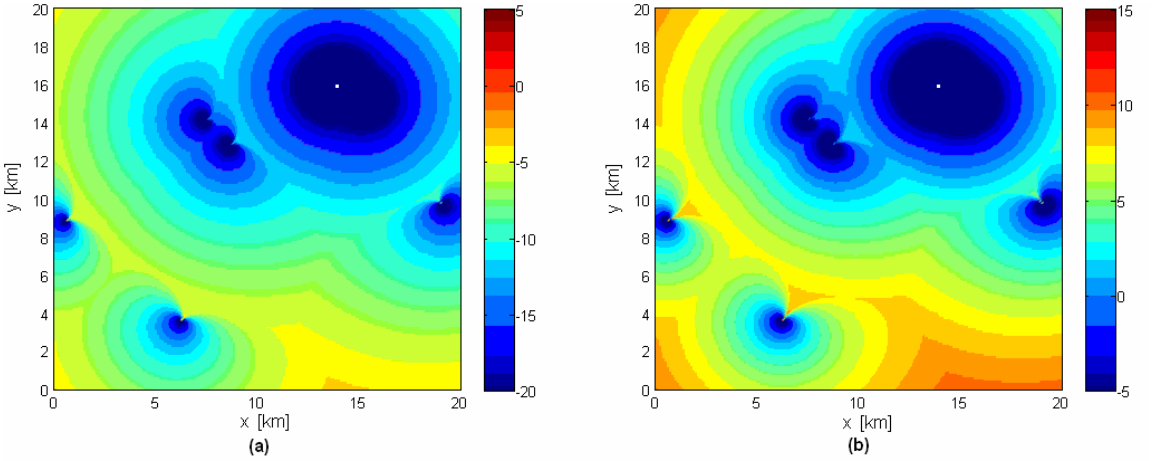

Figure 21 - (a) Minimum RCRLB of the target range [dBm]; (b) Minimum RCRLB of the target velocity estimation [dBm/sec].

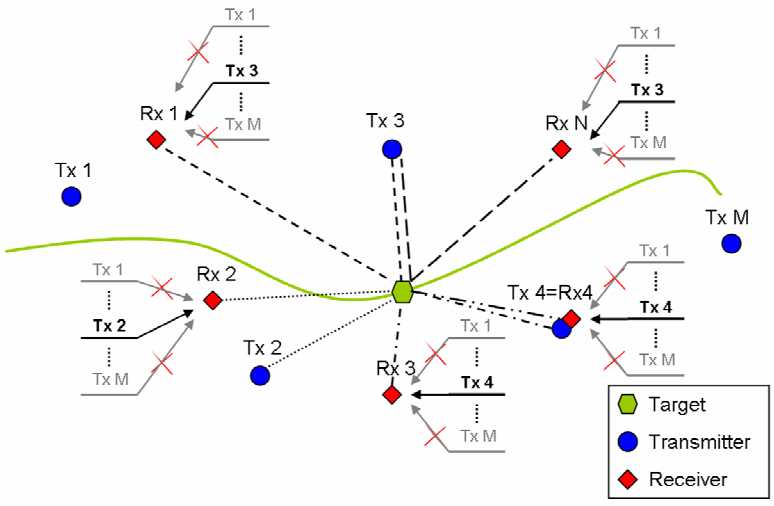

Figure 22 - Optimum transmitter selection.

7.2 Optimum weighting rule for multistatic detection

This Section deals with the description of a coherent multistatic system where the rule for selecting the weighting coefficients is computed exploiting the results obtained in previous Sections. For ease of notation, the described system is composed of one transmitter and N receivers. In the case of multiple transmitters, it is supposed that it is possible to separate each transmitter-receiver path so that each receiver can select the transmitted signal of interest. In this way, the multistatic system is composed by MN channels of observation, where M is the number of transmitters. The only difference with the case of a single transmitter is only on the number of channels, but the algorithm remains the same. The multistatic receiver that will be implemented refers to a centralized nomenclature where the data at each receiver are first collected by a central processor and then jointly combined for the detection.

In particular, the central processing of the analyzed system will exploit part of the results described in Section 7.1. In particular, the optimization algorithm described in Section 7.1 can be viewed as a fusion algorithm that uses hard weighting coefficients, that is, weights that can assume only two values: zero in the case of a bad channel and 1 in the other case. On the other hand, the weighting coefficients of the central processor described in this Section are soft, that is they can assume values that belongs to the range [0,1] depending on the information gained by the Fisher Information Matrix.

Figures 23 and 24 show the block diagram of the multistatic receiver that will be described in this Section. From Figure 23, it is apparent how the detection processing is divided in two parts: the local processing at each receiver and the central processing at the central processor. Figure 24 shows the flow diagram of the signal processing at the central processor.

As showed in Figure 23, the flow diagram of each receiver of the multistatic network is the most adopted in modern coherent radar system where, after the classical processing to down-shift the received signal to the base band, the receiver performs a range – Doppler matched filtering. In the case of multiple transmitters, the range – Doppler matched filtering consists in a bank of filters, each of which is matched to the waveform emitted by each transmitter. As previously discussed, the performance of each receiver depends on the transmitted waveform but unfortunately is also heavily sensitive to the geometry, that is, the position of the receiver and the transmitter with respect to the position of the target.

For a fixed geometry of the simulated scenario, it is possible to derive easily the CRLBs of each channel and therefore its performance.

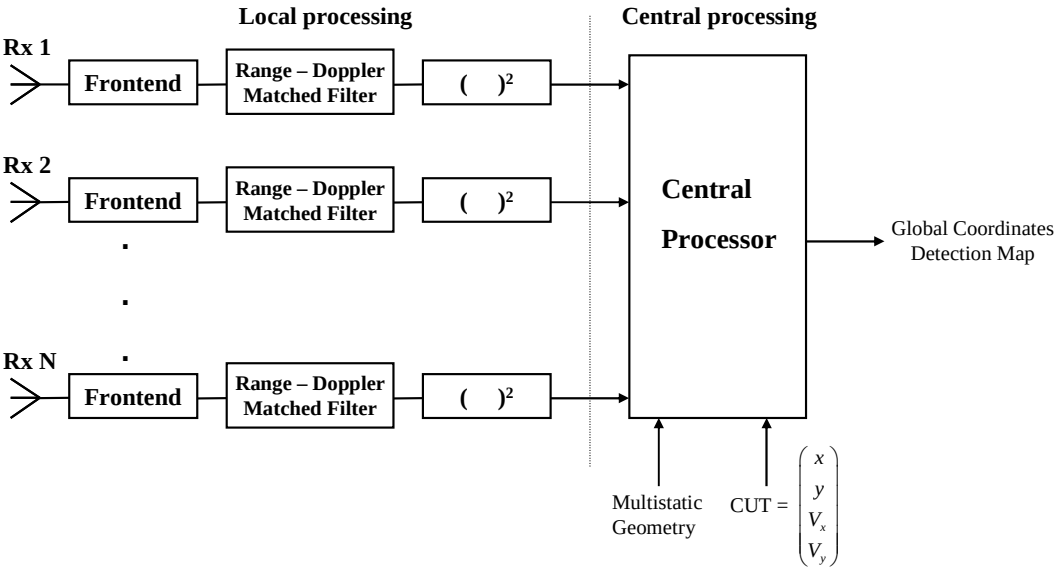

Figure 23 - Flow Diagram of the multistatic detector [TR4].

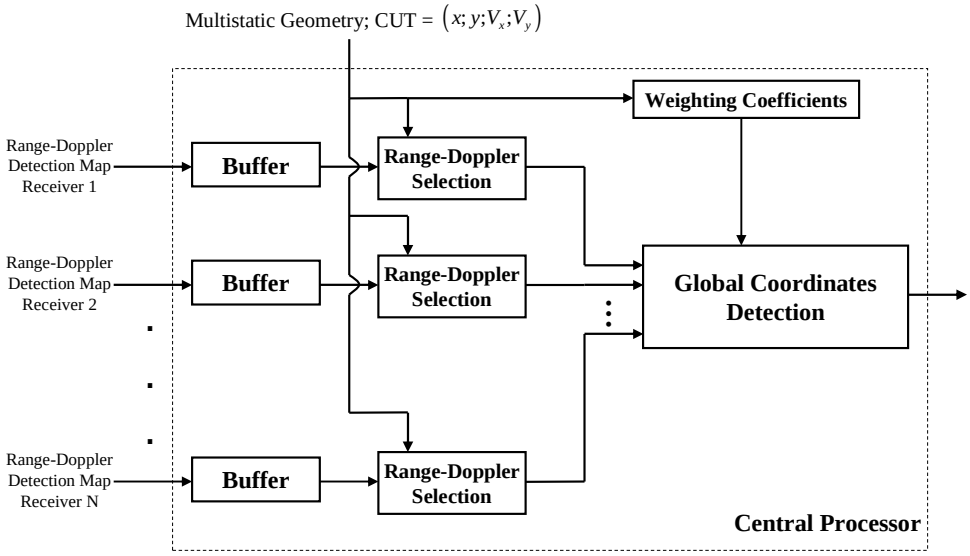

Figure 24 - Flow Diagram of the Central Processor.

Moreover, it is clear that, each receiver of the multistatic system has its own local geometry, that is, each receiver knows at what range from its location there is a target and the target speed straight towards or away from the receiver.

The role of the central processor is therefore to exploit the information gained by the knowledge of the geometry of the network (the position of each transmitter and each receiver) to convert the local coordinates of the receivers into global coordinates.

The information about range and radial velocity from each receiver are therefore converted into information about the target state, that is, the real position of the target and the velocity components along the axes of the reference coordinates system. Moreover, another important role of the central processor is to evaluate for each point of the global surveillance map, that is for each cell (x,y,V_x,V_y), the performance that can be gained for each path of the multistatic system. Therefore the role of the central processor is to generate a global coordinates detection map exploiting the information about the geometry of the multistatic network.

Let's describe now each block of the flow diagram of Figure 24. The block buffer indicates that, for each scan, the central processor stores the local range-Doppler maps of each receiver. In particular, each local map can be viewed as a two dimensional matrix whose elements are the samples at the output of the matched filter of each receiver.

The central processor scans each point of the global surveillance area described by the vector (x,y,V_x,V_y), that is the Cell Under Test (CUT). Once fixed the CUT and knowing the geometry of the multistatic system, the role of the block range-Doppler selection is to selects the corresponding range-Doppler cell of each receiver.

Thus, the problem of detecting a target signal in a fixed resolution cell of the surveillance map can be posed in terms of the following binary hypotheses test:

$$\begin{cases} r_i = \alpha_i c_i + n_i & H_1 \\ r_i = n_i & H_0 \end{cases} \quad i=1,\ldots,N \tag{42}$$

where the sample r_i is the output of the filter matched to the normalized transmitted signal for the i-th receiver in the range-velocity cell corresponding to the point (x,y,V_x,V_y). Note that if the transmitted signal is a burst of pulses, the sample r_i is the output of the filter matched to the entire burst. In the signal model in eq. (42), n_i is the additive noise at the i-th sensor; it is modelled as a zero-mean complex Gaussian variable, in short $n_i \sim CN(0, \sigma^2)$. The samples n_i are assumed to be independent from channel to channel and identically distributed. The parameter α_i accounts for the channel propagation effect and the target radar cross Section. We considered the case in which the amplitude α_i is a random variable. It depends on the target bistatic RCS of the i-th bistatic angle. This, together with the mentioned features of the multistatic geometry, justifies the assumption that the α_is are mutually independent random quantities. With regard to the marginal PDFs, α_i is a zero-mean complex Gaussian variable whit variance σ_i^2 varying from path to path $\alpha_i \sim CN(0, \sigma_i^2)$. In particular the Signal to Noise power Ratio at the input of the i-th channel is defined as $SNR_i = \sigma_i^2 / \sigma^2 = Const/(R_T^{(i)} R_R^{(i)})^2$ and, as previously mentioned, is inversely proportional to the energy path loss factor $(R_T^{(i)} R_R^{(i)})^2$

due to propagation where, $R_T^{(i)}$ and $R_R^{(i)}$ are the range from transmitter to target and the range from receiver to target for the *i*-th channel, respectively. The parameter c_i. that appears in eq. (42) is a complex number whit absolute value lower than or equal to one which accounts for the other effects of propagation and scattering along the *i*-th path. The meaning of c_i will be discussed later on, for the moment let consider the case in which c_i=1. Under this assumption and considering that the amplitude α_i and the noise n_i are independent, the observation r_i is a zero-mean complex Gaussian variable under both hypotheses. Therefore, it is possible to write:

$$\begin{cases} r_i \sim CN\left(0, \sigma_i^2 + \sigma^2\right) & H_1 \\ r_i \sim CN\left(0, \sigma^2\right) & H_0 \end{cases} \quad i=1,\ldots,N \tag{43}$$

Hence, by exploiting the independence of individual likelihoods in each channel, it is possible to verify that the Neyman-Pearson decision test develops into the following form [Dad86],[Con83]:

$$\sum_{i=1}^{N} p_i \left|r_i\right|^2 \underset{H_1}{\overset{H_0}{\lessgtr}} \lambda \tag{44}$$

where

$$p_i = \frac{SNR_i}{1+SNR_i} \tag{45}$$

Note that the weight p_i are non negative and are an increasing function of SNR_i, therefore the central processor emphasizes those channels along which the *SNR*s are the highest. Note that the receiver to implement the given test, depending on cell under test of the surveillance map, needs to continually update the weights, which are themselves dependent, through SNR_i, on the distances from the transmitter to the target and from the target to the receiver.

Consider now the case in which, under the H_1 hypothesis, c_i in eq. (42) is a complex random variable. This simple assumption has been done in order to model the effects of the bistatic geometry along the *i*-th path. In particular we generated c_i as

$$c_i = X\left(\tau_i, \nu_i\right) \tag{46}$$

where $\tau_i = \tau_{Hi} - \tau_a$ and $v_i = v_{Hi} - v_a$ are the delay and Doppler shift for the *i*-th path obtained using equations (23) and (24) and by random generating the estimates of the range and velocity as

$$\hat{R}_R^{(i)} \sim N(\, R_R^{(i)}\,,\ \mathrm{CRLB}_R^{(i)}\,) \tag{47}$$

$$\hat{V}_B^{(i)} \sim N(V_B^{(i)},\ \mathrm{CRLB}_V^{(i)}) \tag{48}$$

where $R_R^{(i)}$ and $\hat{V}_B^{(i)}$ are the actual range and bistatic velocity of the target, while $\mathrm{CRLB}_R^{(i)}$ and $\mathrm{CRLB}_V^{(i)}$ are the Cramér-Rao lower bounds of range and velocity in the *i*-th path.

By random generating $R_R^{(i)}$ and $\hat{V}_B^{(i)}$, the value of c_i takes into account the miss-matching at the *i*-th receiver, moreover, due the geometry dependent non linear transformation of equations (23) and (24), that gives the delay and the Doppler as a function of the range and the bistatic velocity, the value of c_i takes also into account the effects of the distortion of the Ambiguity Function due to the bistatic geometry.

As an example, let consider the case in which $\mathrm{CRLB}_R^{(i)}$ and $\mathrm{CRLB}_V^{(i)}$ are low, in this case the values assumed by $R_R^{(i)}$ and $\hat{V}_B^{(i)}$ are near the actual range and velocity, therefore the values assumed by τ_i and v_i are almost zero, and hence the value assumed by c_i is near the maximum that is 1. On the other hand, for a bad bistatic geometry, the values assumed by $\mathrm{CRLB}_R^{(i)}$ and $\mathrm{CRLB}_V^{(i)}$ are very high, therefore there is a high probability that also τ_i and v_i are high and hence the value assumed by them is almost zero and the observed signal is only noise.

In other words, by generating in this way the value of c_i, the signal model in eq (42) is now dependent on the sharpness of the CAF around its maximum and to the distortion of its behaviour due to the bistatic geometry. It is clearly apparent that it is very difficult to derive the PDF of c_i and hence it is difficult to derive the Neyman-Pearson decision test. By the way, our approach is to use the same receiver of eq. (44) but choosing the weights p_i in a different manner. In fact, the weights in eq. (45) depends only on the energy path loss and they do not take into account the other effects due to the bistatic geometry. As an example, let consider the case of a target is in the baseline between the transmitter and the *i*-th receiver. When the distance between the transmitter and *i*-th receiver is low, the expected signal to noise ratio is high and therefore the central processor using the weights in (45) tends to emphasize this path during the detection process. As showed, in this case the resolution is totally lost and therefore the observations from this path can significantly degrade the performance of the whole system. Therefore, the rule for selecting the weighting coefficients should be different. In particular, the weights should be highlight those channels that exhibit the best performance in terms of estimation accuracy of the target parameters instead of emphasizes those along which the *SNR*s are the highest. In this work we propose the following weighting rule

$$p_i = \frac{Trace\left\{\mathbf{J}_B^{-1}\left(R_R^{(i)}, V_B^{(i)}\right)\right\}^{-1}}{\gamma + Trace\left\{\mathbf{J}_B^{-1}\left(R_R^{(i)}, V_B^{(i)}\right)\right\}^{-1}} \tag{49}$$

where *Trace*{.} is the trace operator and γ is a constant that we fixed equal to the inverse of the sum of the CRLBs of range and velocity in the monostatic case when *SNR*=0dB. In this way the weighting coefficients depend on the *SNR* and the normalization constraint can be viewed as a terms of comparison of the performance of the bistatic channel. That is, a channel can be considered a good channel if trace{$\mathbf{J}_B^{-1}$} is lower than γ^{-1}, while a channel is bad if trace{$\mathbf{J}_B^{-1}$} is greater than γ^{-1}. It is important to recall that $R_R^{(i)}$ and $V_B^{(i)}$ are the actual range and velocity of the target. Therefore, depending on the cell (x,y,V_x,V_y) under test, the central processor can easily calculate these two values for each channel knowing the position of each sensor of the multistatic system.

As apparent in eq. (49), the weights p_i depend on the inverse of the bistatic Fisher Information Matrix which is dependent on the energy path loss through SNR_i, on the geometry and also on the transmitted waveform. This is also important in the case of a multistatic system where multiple transmitters are used. Using the weights in (49) the central processor emphasizes those channels that exhibit the best performance in terms of estimation accuracy and is also able to discard those channels where the resolution is totally lost. In this case the trace of the inverse of the bistatic FIM tends to infinity and the therefore the weight p_i tends to zero.

Note that the value of γ can be fixed to the inverse of the sum of the CRLBs of range and velocity in the monostatic case when *SNR*=0dB. In this way the weighting coefficients depend on the *SNR* and the normalization constraint can be viewed as a terms of comparison of the performance of the bistatic channel. That is, a channel can be considered a good channel if trace{$\mathbf{J}_B^{-1}$} is lower than γ^{-1}, while a channel is bad if trace{$\mathbf{J}_B^{-1}$} is greater than γ^{-1}.

Note that the receiver to implement the given test for both the weighting rules, depending on cell under test of the surveillance map, needs to continually update the weights. Moreover, note that the matrix in eq. (49) is 2×2 and therefore the inversion is straightforward.

7.3 Performance of the optimum multistatic detector

Figure 25 shows the multistatic scenario analyzed in our simulations. The multistatic system is composed by one transmitter and three receivers. The distance between the transmitter and each receiver is the same and equal to 30km. The transmitted signal is a burst of Linear Frequency Modulated pulses where T=250μsec, T_R= 1msec, B= 1MHz, f_C=10GHz and N = 8 (Number of coherent pulses).

As showed in Figure 25, in our simulation we considered three cases. In the first one we considered a target in the middle of the first baseline, that is between the transmitter and the first receiver. In this case the target is moving with a speed of 250 m/sec and direction of 135° with respect to the horizontal axis. In the second case the target is in the second baseline, 10 km far from the transmitter, moving with a speed of 250 m/sec and direction of 150°. While in the third case, the target is 15 km far from the third baseline and 20 km far from the second baseline, and it is moving with a speed of 250 m/sec and direction of 180° whit respect to the horizontal axis. Table 1 shows the weighting coefficients obtained with both the methods, that is the "*SNR*" rule in eq. (45) and the "*Trace*" rule in eq. (49). Note that the coefficients have been normalized in order to satisfy the relationship Σp_i=1.

As apparent from Figure 25, in Case 1 the target is in the first baseline, therefore the resolution of the first receiver is totally lost also if the *SNR* for this path is the highest.

As apparent from Table 1, the coefficient corresponding to the first receiver is null using the Trace rule while it is the highest using the *SNR* rule. Similar considerations can be drawn for Case 2. In the third case the target is in an optimal position for all the receiver, the main difference from one receiver to the other is related only to the energy path loss, therefore the weighting coefficients obtained with both the rule are almost the same. Figure 26 shows the Receiver Operating Characteristic (ROC) of the multistatic detector in (44) for all the three analyzed cases. We also plotted the ROC obtained by forcing all the coefficients to 1/N.

As apparent from the results the ROC obtained in Case 3 (dash-dotted lines) are almost the same for the three weighting rules, while in Case 1 (solid lines) and Case 2 (dashed-lines) the performances obtained whit the Trace rule are the best. Moreover, in Case 1, the performance obtained with the *SNR* rule is lower than that obtained with all the weights equal to 1/N. In this case, the *SNR* for the first receiver is the highest but, due to bad geometry, the resolution is totally lost. Using the *SNR* rule, the central processor emphasizes the observations from the first sensors and this strongly degrades the performance of the multistatic detector.

	SNR	TRACE
Case 1	**p**=[0.3495; 0.3328; 0.3177]	**p**=[0.0000; 0.4984; 0.5016]
Case 2	**p**=[0.3317; 0.3366; 0.3317]	**p**=[0.5000; 0.0000; 0.5000]
Case 3	**p**=[0.2735; 0.3553; 0.3712]	**p**=[0.2939; 0.3449; 0.3612]

Table 1- Weigting Coefficients.

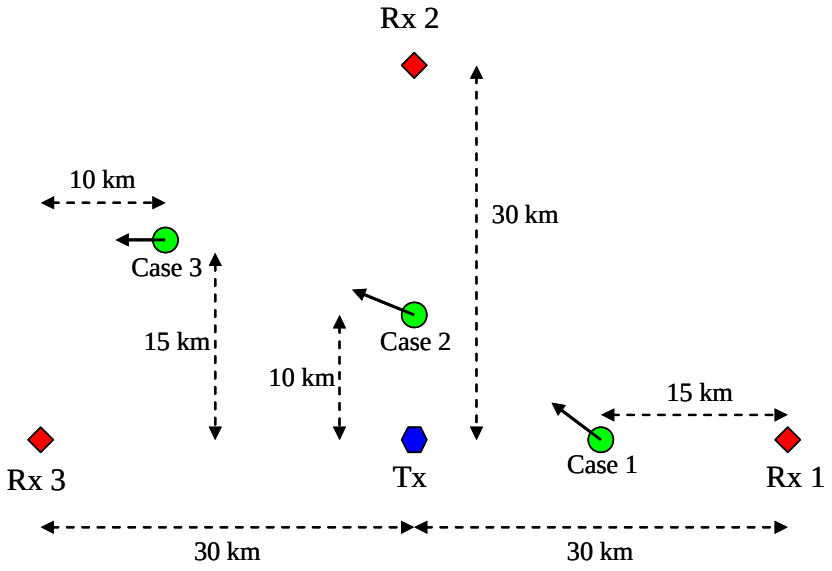

Figure 25 - Simulated scenario.

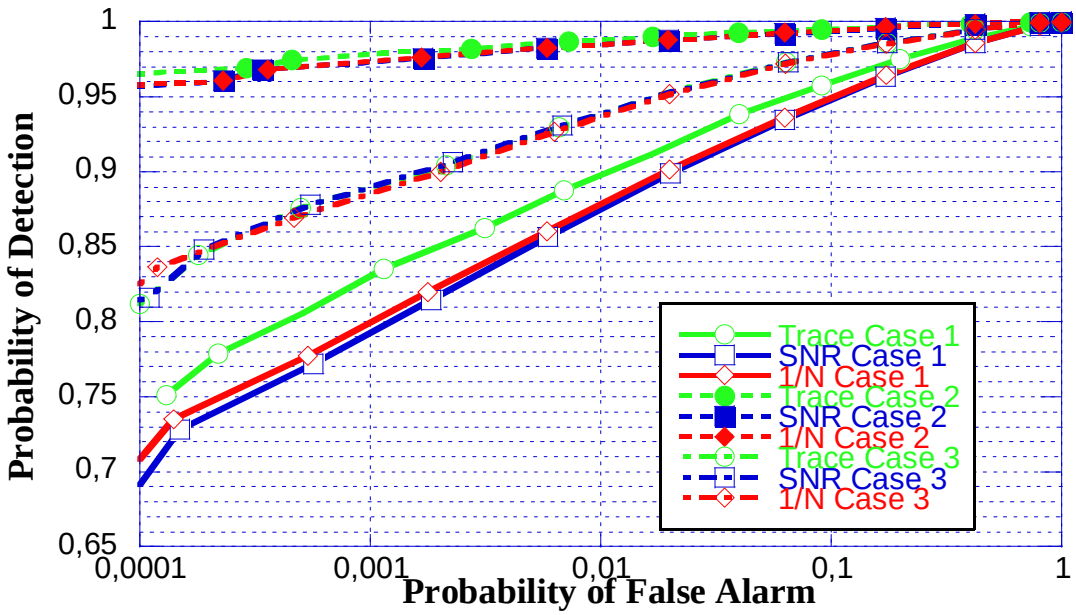

Figure 26 - Receiver Operating Characteristic of the Multistatic Detector.

8 Passive Coherent Location (PCL) Systems

Recently, great interest has been devoted to Passive Coherent Location (PCL) systems, that is, bistatic radars that exploit the signal emitted by illuminators of opportunity, such as broadcast or communications signals. PCL systems have some significant attractions, in addition to those common to all bistatic radars: the PCL receivers do not need any transmitter hardware of their own, are completely passive, and hence undetectable. Among all the potential signals of opportunity we can mention FM radio and Digital Audio Broadcast (DAB) [DiL08], [Mal07], [How05], [Gre10], analogue TV and Digital Video Broadcast (DVB) [And05] [Gri86], [How99], Wi-Fi [Guo08] or cell phone network signals [Sti12], [Sun08], [DeM08], [Men06], [Pet09].

Cellular phone networks are now ubiquitous in most countries and the implementation and application of PCL systems that exploit these signals is an active research area. Over the last few years there has been an evolution of mobile networks towards the third generation radio wireless communications (3G) such as UMTS (Universal Mobile Telecommunications System). The UMTS is the European standard for 3G wireless communication and it has been developed by 3GPP (3rd Generation Partnership Project) [TS06]. The downlink signal transmitted from the UMTS base-station presents interesting properties that suggest the usability of the UMTS signal as opportunity signal for passive radar systems. These properties are: the large bandwidth, that implies a high range resolution; the use of orthogonal codes, that guarantees low sidelobes of the Ambiguity Function; and the growing coverage of UMTS signals on the international territory, which renders a multistatic radar configuration feasible. Moreover, the UMTS system uses a band that spans from 2110-2170 MHz, that makes easy to work with directive antennas.

In particular, the UMTS signal has the following characteristics [TS06], [Wal98], [Wal03]. There are two forms, Frequency Division Duplex (FDD) and Time Division Duplex (TDD), each of which has a bandwidth of 5 MHz. FDD requires two frequency bands, one for the up-link and one for the down link, while the TDD requires a single band. The transmission is Wideband CDMA (WCDMA) using Walsh-Hadamard coding with a transmission rate of 3.84 Mchips/s. The modulation used is QPSK (Quadrature Phase Shift Keying) where the pulses are shaped with a Root Raised Cosine (RRC) filter with roll-off factor of 0.22. The study of PCL systems that exploits the downlink signal of a UMTS base station is of great interest, anyway the performance of such systems has been evaluated only with some experimental systems [Pet09], [Gri03], [Gri05].

In this Section we evaluate the performance of these systems by calculating the Ambiguity Function (AF) of a QPSK signal and the modified Cramér-Rao lower bounds (MCRLBs) on the estimation accuracy of target range and velocity, for both monostatic and bistatic configurations. These results provide a useful tool for the evaluation of the performance of a PCL system that exploits the downlink signal of a UMTS base station and they can also be used to design an algorithm for the dynamical selection of the transmitter in a multistatic network where the receiver can exploit the signals emitted from several base stations.

8.1 The UMTS downlink transmitted signal

The downlink signal transmitted by a UMTS base station is a QPSK signal where the pulses are shaped with a RRC filter [Wal98], [Wal03], [TS06].

The unit energy complex envelope of the QPSK signal is given by:

$$u(t) = \frac{1}{\sqrt{N}} \sum_{n=0}^{N-1} c_n g(t - nT), \tag{50}$$

where c_n are the transmitted symbols, N is the number of transmitted symbols, and T is the inverse of the symbol rate (or chip rate). In the QPSK modulation, symbols c_n belong to the set $\{ e^{j(2n+1)\pi/4}, n=1,2,3,4\}$ and they are assumed to be independent and identically distributed (IID):

$$E\left\{c_n c_k^*\right\} = \begin{cases} 1 & n = k, \\ 0 & n \neq k. \end{cases} \tag{51}$$

The pulse $g(t)$ is a delayed RRC pulse, in particular:

$$g(t) = h\left(t - \frac{D}{2}\right), \tag{52}$$

where the delay D is chosen such that

$$\int_{-D/2}^{D/2} h^2(t)dt = 0.95 \tag{53}$$

and

$$h(t) = \frac{\sin\left(\frac{\pi t}{T}(1-\alpha)\right) + \frac{4\alpha t}{T}\cos\left(\frac{\pi t}{T}(1+\alpha)\right)}{\frac{\pi t}{\sqrt{T}}\left[1 - \left(\frac{4\alpha t}{T}\right)^2\right]} \tag{54}$$

$$h(t=0)=\frac{1}{\sqrt{T}}\left(1-\alpha+\frac{4\alpha}{\pi}\right)$$

$$h\left(t=\pm\frac{T}{4\alpha}\right)=\frac{\alpha}{\sqrt{2T}}\left[\left(1+\frac{2}{\pi}\right)\sin\left(\frac{\pi}{4\alpha}\right)+\left(1-\frac{2}{\pi}\right)\cos\left(\frac{\pi}{4\alpha}\right)\right]$$

is a centered RRC. The parameter α is the roll-off factor, with $0\leq\alpha\leq1$. The Fourier Transform (FT) of the pulse $h(t)$ is equal to:

$$H(f)=\sqrt{C(f)} \tag{55}$$

where $C(f)$ is the FT of a Raised Cosine (RC) pulse $c(t)$. $C(f)$ and $c(t)$ are defined as:

$$C(f)=H(f)^2=\begin{cases} T & |f|\leq\frac{1-\alpha}{2T}, \\ \frac{T}{2}\left[1+\cos\left(\frac{\pi T}{\alpha}\left(|f|-\frac{1-\alpha}{2T}\right)\right)\right] & \frac{1-\alpha}{2T}\leq|f|\leq\frac{1+\alpha}{2T}, \\ 0 & \textit{elsewhere,} \end{cases} \tag{56}$$

$$c(t)=IFT\{C(f)\}=\operatorname{sinc}\left(\frac{t}{T}\right)\frac{\cos\left(\frac{\alpha\pi t}{T}\right)}{1-\left(\frac{2\alpha t}{T}\right)^2} \tag{57}$$

where $IFT\{\cdot\}$ is the Inverse Fourier Transform (IFT) operator. In Figs. 27 and 28, $h(t)$ and $H(f)$ are plotted for different values of the roll-off factor α. It is easy to verify that:

$$\int_{-\infty}^{\infty}h^2(t)dt=\int_{-\infty}^{\infty}H^2(f)df=\int_{-\infty}^{\infty}C(f)df=1 \tag{58}$$

In the following sections we evaluate the AF and the MCRLBs of the QPSK signal. These quantities are then used to measure the performance of a PCL system that exploits a UMTS base station as a transmitter of opportunity. In particular, for this kind of system the value of the roll-off factor is equal to 0.22 while the inverse of the symbol rate T is equal to 0.26 μs [Wal98], [Wal03], [TS06].

In order to achieve a fine Doppler resolution, PCL radar systems have long observation time, typically of the order of 0.1 s. Hereafter, without loss of generality, we will fix the observation time NT to 0.1 s, in this case the corresponding number of integrated pulses is N=384615.

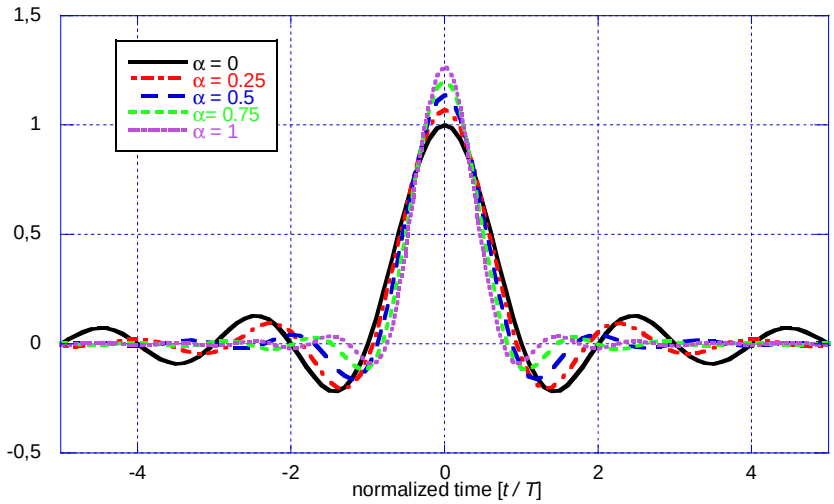

Figure 27 - Impulse response of a RRC for different values of the roll-off factor *α*.

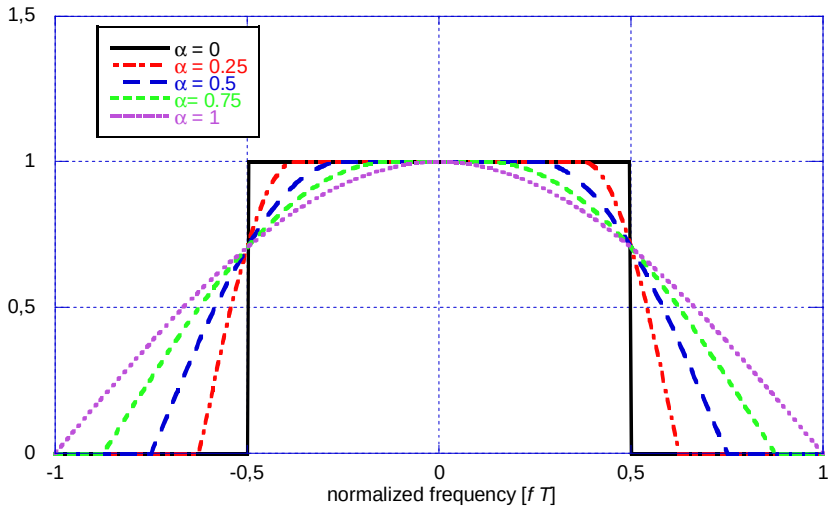

Figure 28 - Frequency response of a RRC for different values of the roll-off factor α.

8.2 Monostatic and Bistatic Ambiguity Function of the UMTS signal

Referring to the definition of CAF in eq. (1), and reported in (59) for convenience, we have that, for a fixed sequence of symbols $\{c_n,\ n=0,1,\ldots,N-1\}$, the CAF of the transmitted pulse in (1) is defined by [Tsa97]:

$$\chi_c(\tau,\nu)=\int_{-\infty}^{+\infty} u(t)u^*(t-\tau)e^{-j2\pi\nu t}dt\,, \tag{59}$$

where $\tau=\tau_H-\tau_a$ is the difference between the hypothesized delay and the actual delay, while $\nu=\nu_H-\nu_a$ is the difference between the hypothesized Doppler shift and the actual Doppler shift. The CAF in (59) describes the properties of the signal for a fixed sequence of symbols. To evaluate the target resolution of the transmitted waveform independently of the particular sequence of transmitted symbols, we can evaluate the average CAF (ACAF) defined as:

$$\chi(\tau,\nu)=E\{\chi_c(\tau,\nu)\}, \tag{60}$$

where the expectation $E\{\bullet\}$ is with respect to the vector of symbols $\boldsymbol{c}=[c_1,\ \ldots,\ c_N]$.
By these considerations, the CAF of the transmitted signal is given by

$$\begin{aligned}
\chi(\tau,\nu) &= E\left\{\frac{1}{N}\int_{-\infty}^{+\infty}\sum_{n=0}^{N-1}c_n g(t-nT)\sum_{k=0}^{N-1}c_k^* g^*(t-nT-\tau)e^{-j2\pi\nu t}dt\right\}= \\
&= \frac{1}{N}\sum_{n=0}^{N-1}\int_{-\infty}^{+\infty} g(t-nT)g^*(t-nT-\tau)e^{-j2\pi\nu t}dt= \\
&= \frac{1}{N}\sum_{n=0}^{N-1}\int_{-\infty}^{+\infty} g(t)g^*(t-\tau)e^{j2\pi\nu nT}e^{-j2\pi\nu t}dt= \\
&= \frac{1}{N}\sum_{n=0}^{N-1}\chi_g(\tau,\nu)e^{j2\pi\nu nT}= \\
&= \frac{1}{N}\frac{\sin(\pi NT\nu)}{\sin(\pi T\nu)}e^{j\pi\nu T(N-1)}\chi_g(\tau,\nu)
\end{aligned} \tag{61}$$

where we used the IID assumption for the symbols in eq. (51) and $\chi_g(\tau,\nu)$ is the CAF of $g(t)$ given by:

$$\chi_g(\tau,\nu)=e^{j\pi D\nu}\chi_h(\tau,\nu), \tag{62}$$

with

$$\chi_h(\tau,\nu)=\int_{-\infty}^{+\infty}h(t)h^*(t-\tau)e^{-j2\pi\nu t}dt=FT\{h(t)h^*(t-\tau)\}=H(\nu)\otimes H(\nu)e^{j2\pi\nu\tau} \tag{63}$$

where $\otimes$ is the convolution along the v axis while $FT\{\bullet\}$ the Fourier Transform operator. The average AF (AAF) is defined as the absolute value of the average CAF. Hence, the AAF of the transmitted pulse is given by:

$$\left|\chi(\tau,v)\right| = \left|\frac{1}{N}\frac{\sin(\pi NTv)}{\sin(\pi Tv)}\right|\left|\chi_h(\tau,v)\right| \tag{64}$$

and exhibits the maximum in (τ, v) = (0, 0). The AAF is plotted in Fig. 29 for NT=0.1 s, T=0.26 μs, and α=0.22.

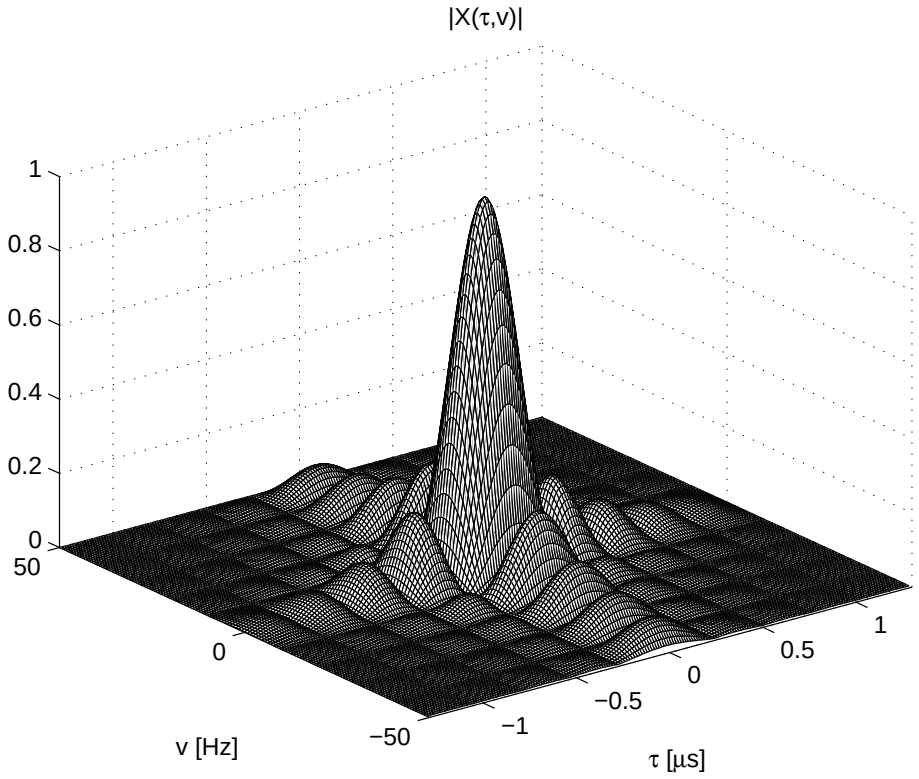

Figure 29 - AAF of a QPSK signal with NT=0.1 s, T=0.26 μs, and α=0.22.

To evaluate the delay and Doppler resolution of the transmitted pulse, the zero-Doppler and zero-delay cuts of the AAF are often analyzed. The zero-Doppler cut is the AAF at v=0, that is the autocorrelation function of the transmitted pulse. It represents the matched filter output when there is no Doppler mismatch. Using (64) and the definition of the RRC pulse, it is easy to verify that:

$$\left|\chi(\tau,0)\right| = \left|\chi_h(\tau,0)\right| = \left|h(\tau)\otimes h(\tau)\right| = \left|IFT\left\{C(v)\right\}\right| = \left|\operatorname{sinc}\left(\frac{\tau}{T}\right)\frac{\cos\left(\frac{\alpha\pi\tau}{T}\right)}{1-\left(\frac{2\alpha\tau}{T}\right)^2}\right|. \qquad (65)$$

On the other hand, the zero-delay cut is the AAF for τ =0 and represents the output of the matched filter at the expected peak time. Setting τ=0 in (63) and (64) we get:

$$\left|\chi(0,v)\right| = \left|\frac{1}{N}\frac{\sin(\pi NTv)}{\sin(\pi Tv)}\right|\left|\chi_h(0,v)\right| = \left|\frac{1}{N}\frac{\sin(\pi NTv)}{\sin(\pi Tv)}\right|\left|H(v)\otimes H(v)\right|. \qquad (66)$$

After some manipulations, it is possible to verify that:

$$\left|\chi_h(0,v)\right| = \begin{cases} \left(1-\alpha-T|v|\right)-\left(T|v|-\alpha\right)\cos\left(\frac{\pi T}{2\alpha}|v|\right)+\frac{4\alpha}{\pi}\sin\left(\frac{\pi T}{2\alpha}|v|\right), & 0\le|v|<\frac{\alpha}{T}, \\ -\left(T|v|-1+\alpha\right)+\frac{4\alpha}{\pi}, & \frac{\alpha}{T}\le|v|<\frac{1-\alpha}{T}, \\ \frac{4\alpha}{\pi}-\frac{4\alpha}{\pi}\sin\left(\frac{\pi}{2\alpha}\left(T|v|-1+\alpha\right)\right)+\frac{\alpha}{\pi}\cos\left(\frac{\pi}{2\alpha}\left(T|v|-1\right)\right) & \\ -\frac{T|v|-1+\alpha}{2}\sin\left(\frac{\pi}{2\alpha}\left(T|v|-1\right)\right), & \frac{1-\alpha}{T}\le|v|<\frac{1}{T}, \\ \frac{\alpha}{\pi}\cos\left(\frac{\pi}{2\alpha}\left(T|v|-1\right)\right)+\frac{T|v|-1-\alpha}{2}\sin\left(\frac{\pi}{2\alpha}\left(T|v|-1\right)\right), & \frac{1}{T}\le|v|<\frac{1+\alpha}{T}, \\ 0 & \textit{elsewhere.} \end{cases} \qquad (67)$$

Figs. 30 and 31 show the zero-Doppler and the zero-delay cuts of the AAF in Fig. 29, respectively. Recalling that the definition of the Rayleigh resolution is the peak-to-first null distance, by inspection of Figs. 30 and 31, it is apparent that the delay resolution is T and the Doppler resolution is $1/NT$. Considering that the carrier frequency of a UMTS base station if f_C =2100 MHz, we have that the range resolution of the considered waveform is of 39 m and the velocity resolution is of almost 0.71 m/s. These results are in agreement with the empirical results showed in [Pet09], [Gri03] and [Gri05], where the authors measured and analyzed the AAF of a UMTS signal.

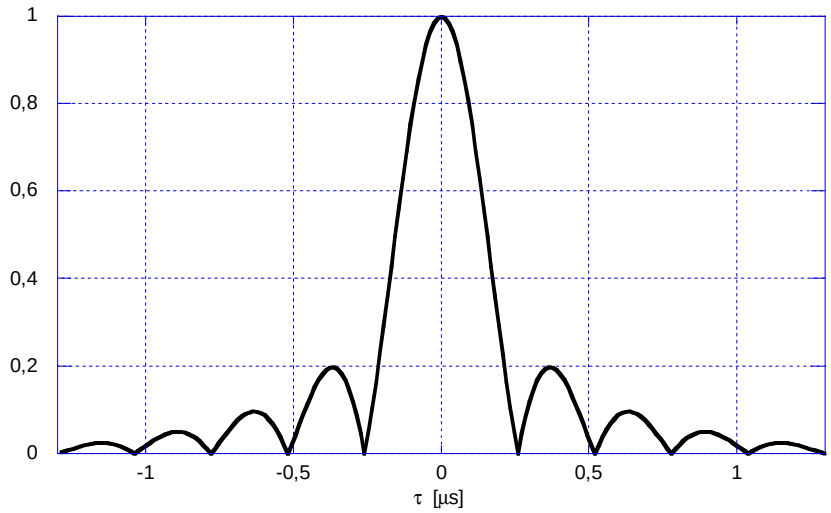

Figure 30 - Zero-Doppler cut of the AAF a QPSK signal with *NT*=0.1s, *T*=0.26μs, *α*=0.22.

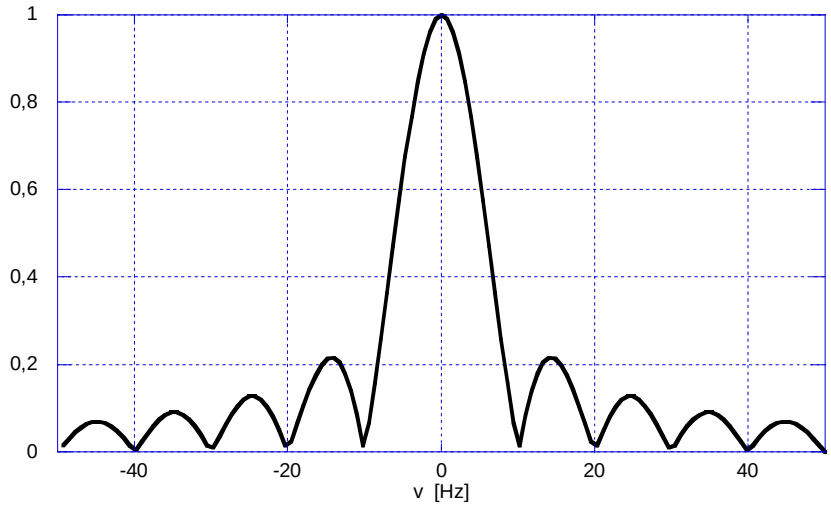

Figure 31 - Zero-delay cut of the AAF of a QPSK signal with *NT*=0.1s, *T*=0.26μs, *α*=0.22.

In monostatic configuration, estimation of the time-delay and Doppler shift directly provides information on target range and velocity. As discussed in previous sections, this information can be retrieved also in a bistatic radar configuration, even if the relations between measured delay and Doppler frequency and target distance and velocity, respectively, are not linear and depend on the geometry. As previously shown, referring to the bistatic geometry of Figure 10, the delay and the Doppler shift should be obtained using the following geometry dependent non-linear equations:

$$\tau_H = \frac{R_R + \sqrt{R_R^2 + L^2 + 2R_R L \sin\theta_R}}{c} \tag{68}$$

$$\nu_H = 2\frac{f_C}{c} V_B \sqrt{\frac{1}{2} + \frac{R_R + L\sin\theta_R}{2\sqrt{R_R^2 + L^2 + 2R_R L \sin\theta_R}}} \tag{69}$$

Similar relations hold for the actual delay τ_a and the actual Doppler shift ν_a. To obtain the Bistatic Average Ambiguity Function (BAAF) in the range-velocity plane we must calculate $\tau=\tau_H-\tau_a$ and $\nu=\nu_H-\nu_a$ and substitute them in (61). Therefore, it is apparent that in the bistatic configuration, the BAAF depends on the transmitted waveform and on the bistatic geometry parameters, i.e. the target Direction Of Arrival (DOA), the bistatic baseline length, and the distance between the target and the receiver.

Figs. 32 and 33 show the cuts of the BAAF along the range and the bistatic velocity, respectively. These figures have been obtained assuming V_a=5 m/s, R_a=3 Km and L=5 Km for three different values of the receiver look angle θ_R. It is evident that in all the cases, the BAAF reaches its maximum when the hypothesized range and velocity equal the actual range and velocity of the target. Anyway, the shape of the BAAF strongly depends on the target angle θ_R. The worst case is $\theta_R = -\pi/2$, that is, when the target is on the baseline. If the target is between the transmitter and the receiver, the BAAF is flat and the range and velocity resolutions are completely lost. This can be appreciated by realising that in this case the echo arrives at the receiver at the same instant as the direct signal, independent of the target location, and the Doppler shift of a target crossing the bistatic baseline must be zero, because the transmitter-to-target range changes in an equal and opposite way to the target-to-receiver range, independent of the magnitude and direction of the target velocity. Note also that for values of θ_R far from $-\pi/2$ the shapes of the BAAF are basically the same and their behaviour is similar to that obtained for a monostatic system.

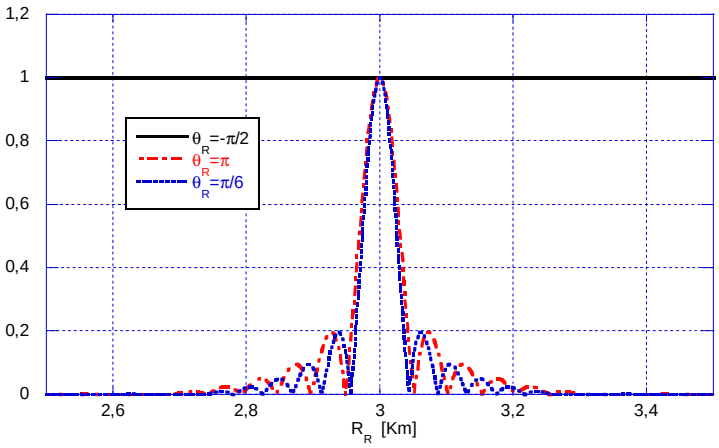

Figure 32 - BAAF as a function of range, V_a=5 m/s, R_a=3 Km and L=5 Km.

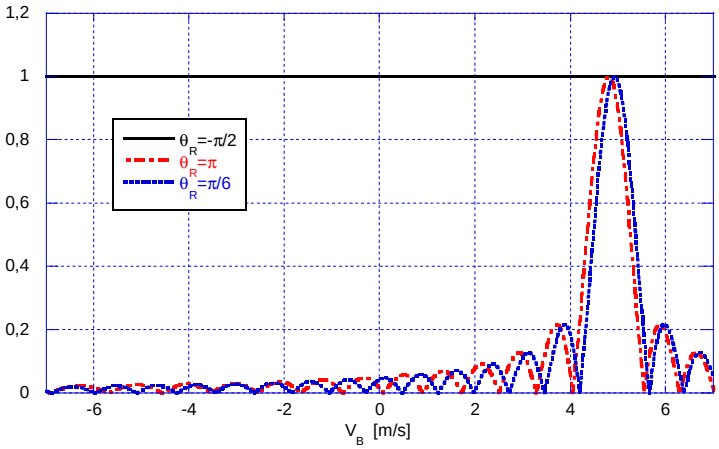

Figure 33 - BAAF as a function of the bistatic velocity, V_a=5 m/s, R_a=3 Km, L=5 Km.

8.3 Monostatic and Bistatic CRLB of the UMTS signal

Similarly to previous Section, here we calculate the CRLB exploiting the relationship between the AF and the Fisher Information Matrix (FIM) of the delay and Doppler parameters derived in [Van71]:

$$\mathbf{J}_c(\tau,\nu) = -2SNR \cdot \left[\begin{array}{cc} \dfrac{\partial^2 \left|\chi_c(\tau,\nu)\right|^2}{\partial \tau^2} & \dfrac{\partial^2 \left|\chi_c(\tau,\nu)\right|^2}{\partial \tau \partial \nu} \\ \dfrac{\partial^2 \left|\chi_c(\tau,\nu)\right|^2}{\partial \nu \partial \tau} & \dfrac{\partial^2 \left|\chi_c(\tau,\nu)\right|^2}{\partial \nu^2} \end{array} \right]_{\tau=0,\nu=0} . \qquad (70)$$

In (70) we use the subindex *c* to highlight that this relation holds for deterministic signals and hence it involves the AF for a fixed sequence of symbols $\boldsymbol{c}$. Therefore, in our case, the FIM in (70) is actually a conditional FIM (conditioned to a given sequence of symbols $\boldsymbol{c}$). The modified CRLB (MCRLB) immediately follows from the conditional FIM, since the MCRLB is given by the inverse of the modified FIM (MFIM), which is obtained by averaging the conditional FIM of (70) with respect to the symbols $\boldsymbol{c}$ [Gin98], [Gin00]. Hence, by averaging w.r.t. $\boldsymbol{c}$ the conditional FIM in (70) and then taking its inverse, we get the MCRLBs on the estimation of target time-delay and the Doppler shift (i.e. the monostatic MCRLBs). It is worth remembering that to calculate the classical CRLB on time-delay and the Doppler shift we should average out the dependence of the random symbols $\boldsymbol{c}$ in the joint probability density function (pdf) of received data and symbols. This is infeasible in our case. Hence we resort to calculation of the MCRLB, which is much easier to obtain. In fact, it is derived from the conditional FIM of (70) as previously outlined. The MCRLB was derived in [Gin98] and its relation to the CRLB investigated e.g. in [Gin98], [Gin00] and [Noa09], and it was found that the MCRLB is looser than the CRLB. The MCRLB was applied in radar e.g. in [Gin98b], [Gin00b], and [For11].

To evaluate the MFIM and hence the MCRLBs, first note that the elements of the MFIM can be expressed as [Van71]:

$$\mathbf{J}(\tau,\nu) = E\left\{\mathbf{J}_c(\tau,\nu)\right\} = 2SNR\begin{bmatrix} 4\pi^2 E\left\{\overline{f^2} - \overline{f}^2\right\} & 2\pi E\left\{\overline{ft} - \overline{f}\,\overline{t}\right\} \\ 2\pi E\left\{\overline{ft} - \overline{f}\,\overline{t}\right\} & E\left\{\overline{t^2} - \overline{t}^2\right\} \end{bmatrix} \tag{71}$$

where:

$$E\left\{\overline{f^2}\right\} = E\left\{\int_{-\infty}^{+\infty} f^2 \left|U_c(f)\right|^2 df\right\}, \tag{72}$$

$$E\left\{\overline{f}^2\right\} = E\left\{\left[\int_{-\infty}^{+\infty} f \left|U_c(f)\right|^2 df\right]^2\right\}, \tag{73}$$

$$E\left\{\overline{t^2}\right\} = E\left\{\int_{-\infty}^{+\infty} t^2 \left|u_c(t)\right|^2 dt\right\}, \tag{74}$$

$$E\left\{\overline{t}^2\right\} = E\left\{\left[\int_{-\infty}^{+\infty} t \left|u_c(t)\right|^2 dt\right]^2\right\}, \tag{75}$$

$$E\left\{\overline{ft}\right\} = E\left\{ Im\left\{ \int_{-\infty}^{+\infty} t \frac{\partial u_c(t)}{\partial t} u_c^*(t) dt \right\} \right\}, \tag{76}$$

$$E\left\{\overline{f}\,\overline{t}\right\} = E\left\{ \int_{-\infty}^{+\infty} f \left|U_c(f)\right|^2 df \int_{-\infty}^{+\infty} t \left|u_c(t)\right|^2 dt \right\}. \tag{77}$$

The expectation $E\{\bullet\}$ is with respect to the symbols $\boldsymbol{c}$, $Im\{\bullet\}$ is the imaginary part operator while $U_c(f)$ is the Fourier Transform of $u_c(t)$ of eq. (50); again we stress that we used the subindex c to highlight that the transmitted signal is considered for a fixed sequence of symbols $\boldsymbol{c}$. Note that also the elements of the MFIM matrix defined in (71) directly measure the curvature of the transmitted signal in the time-frequency domain. In [TR5] we calculated the elements of the MFIM in (71) using the definition of the QPSK signal in (71), the obtained results show that:

$$\mathbf{J}(\tau,\nu) = 2SNR \cdot \begin{bmatrix} \frac{1}{3T^2}\left(\pi^2 + 3\alpha^2\pi^2 - 24\alpha^2\right) & 0 \\ 0 & \frac{T^2}{4}\left(\frac{1}{4\alpha} + \frac{N^2-1}{3}\right) \end{bmatrix}. \tag{78}$$

The MCRLBs are given by the inverse of the MFIM of (78), being $\mathbf{J}(\tau,\nu)$ diagonal, we have:

$$\mathrm{MCRLB}(\tau) = \frac{1}{\left[\mathbf{J}(\tau,\nu)\right]_{1,1}}, \tag{79}$$

$$\mathrm{MCRLB}(\nu) = \frac{1}{\left[\mathbf{J}(\tau,\nu)\right]_{2,2}}. \tag{80}$$

In the monostatic configuration, we have $\tau = 2R/c$ and $\nu = 2Vf_C/c$, therefore it is easy to verify that the MCRLBs of the estimated parameters are:

$$\mathrm{MCRLB}(R) = \frac{3T^2c^2}{8SNR\left(\pi^2 + 3\alpha^2\pi^2 - 24\alpha^2\right)}, \tag{81}$$

$$\mathrm{MCRLB}(V) = \frac{c^2}{8f_C^2 SNR}\left[\frac{T^2}{4}\left(\frac{1}{4\alpha} + \frac{N^2-1}{3}\right)\right]^{-1}. \tag{82}$$

When SNR=0dB, NT=0.1 s, T=0.26 μs, α=0.22 and f_C=2100MHz, the values of the root MCRLB (RMCRLB) are given by: RMCRLB(R)≈15 m and RMCRLB(V) ≈1.75 m/s. Note from (79) and (81), that the MCRLB of the range is inversely proportional to $[\mathbf{J}(\tau,\nu)]_{1,1}$, that indicates the effect of the signal shape. As apparent from (71),

this term is a direct measure of the effective bandwidth. This is logical because increasing the signal bandwidth, that is, the value of α, the signal has a faster rise time giving a lower MCRLB of the target range. On the other hand, from (80) and (82) we have that the bound on the velocity estimation accuracy is determined by $[\mathbf{J}(\tau,\nu)]_{2,2}$ that, as apparent from (71), measures the effective pulse length. As a matter of fact, the larger is the number of integrated pulses N, the lower is the MCRLB on the target velocity estimation.

As done in previous sections, for the calculation of the bistatic MCRLBs we can use the result on the monostatic conditional FIM in (70) using the "chain rule" of the derivative. In particular, the bistatic conditional FIM is given by:

$$\mathbf{J}_{Bc}\left(R_R,V_B\right)=\mathbf{P}\mathbf{J}_c\left(\tau,\nu\right)\mathbf{P}^T, \tag{83}$$

where, as in the previous sections,

$$\mathbf{P}=\begin{bmatrix}\dfrac{\partial\tau}{\partial R_R} & \dfrac{\partial\nu}{\partial R_R}\\ \dfrac{\partial\tau}{\partial V_B} & \dfrac{\partial\nu}{\partial V_B}\end{bmatrix} \tag{84}$$

Finally, by averaging with respect to $\boldsymbol{c}$ we get the bistatic MFIM as:

$$\mathbf{J}_B\left(R_R,V_B\right)=E\left\{\mathbf{J}_{Bc}\left(R_R,V_B\right)\right\}=\mathbf{P}E\left\{\mathbf{J}_c\left(\tau,\nu\right)\right\}\mathbf{P}^T=\mathbf{P}\mathbf{J}\left(\tau,\nu\right)\mathbf{P}^T \tag{85}$$

The relationship in eq. (85) shows that matrix $\mathbf{P}$ takes into account only the effect of the bistatic geometry while matrix $\mathbf{J}(\tau,\nu)$ takes into account the effect of the transmitted waveform and the *SNR*. Note that also the *SNR* depends on the geometry, in fact it is inversely proportional to the energy path loss factor $(R_R\cdot R_T)^2$ due to propagation. From eq. (85), the bistatic MCRLBs of the receiver-to-target range and the bistatic velocity are given by:

$$\mathrm{MCRLB}(R_R)=\frac{\left[\mathbf{J}_B\right]_{2,2}}{\left[\mathbf{J}_B\right]_{1,1}\left[\mathbf{J}_B\right]_{2,2}-\left[\mathbf{J}_B\right]_{1,2}^2} \tag{86}$$

$$\mathrm{MCRLB}(V_B)=\frac{\left[\mathbf{J}_B\right]_{1,1}}{\left[\mathbf{J}_B\right]_{1,1}\left[\mathbf{J}_B\right]_{2,2}-\left[\mathbf{J}_B\right]_{1,2}^2} \tag{87}$$

Note that the monostatic configuration is a particular case of the bistatic case, and it is obtained for baseline L=0. In this case $\mathbf{P}$ is a diagonal matrix whose elements are $[\mathbf{P}]_{1,1}=2/c$ and $[\mathbf{P}]_{2,2}=2\cdot f_C/c$, and the MCRLBs of range and velocity are the same as in eqs. (81)-(82), respectively.

Figures 34-37 show the root MCRLBs (RMCRLBs) of range and velocity, both in the monostatic and bistatic case. These bounds have been obtained by considering the QPSK signal emitted by a UMTS base station, that is setting T=0.26 μs, α=0.22, f_C=2100MHz and NT=0.1 s. All these Figs. have been obtained for V_B=5 m/s and maintaining the SNR at 0dB, to highlight only the effects of the geometry. In particular, Fig. 34 shows the RMCRLBs as a function of the receiver-to-target range R_R, for two values of the receiver look angle, θ_R=-0.49π and θ_R=π. For the bistatic system the baseline has been set to 5 km. It is evident that, for all the parameter values we investigated, the bistatic RMCRLBs are always higher than the monostatic ones. When the distance from receiver to the target increases, the bistatic system behaves more and more as the monostatic one.

As evident, the effects of geometry are prominent where the target approaches the baseline, that is in the case of θ_R =-0.49π when $R_R \leq L$. In this case the RMCRLBs tend to be very high. Similar considerations can be drawn from Fig. 35, where the RMCRLBs are plotted as a function of the baseline L. The effects of the geometry are more apparent in Fig. 36, that shows the RMCRLBs as a function of the receiver look angle θ_R , both in the case of $R_R<L$ and $R_R>L$. In the case of $R_R<L$, when the target approaches the baseline (i.e. $\theta_R \rightarrow$-π/2), the RMCRLBs tend to infinity because the resulting delay is always L/c independent of the target position along the baseline, and the radial velocity is always zero independent of the target speed and direction. This behaviour is in agreement with the shape of the BAF plotted in Figs. 32-33.

Fig. 37 shows the RMCRLBs as a function of the observation time NT. As expected only the RMCRLB of the target velocity depends on this parameter and decreases as the observation time increases. Note that when the target is close to the baseline, the RMCRLB of the velocity is very high also for increasing values of the observation time. On the other hand, when the target is far from the baseline the performance of the monostatic system is almost the same of the monostatic one.

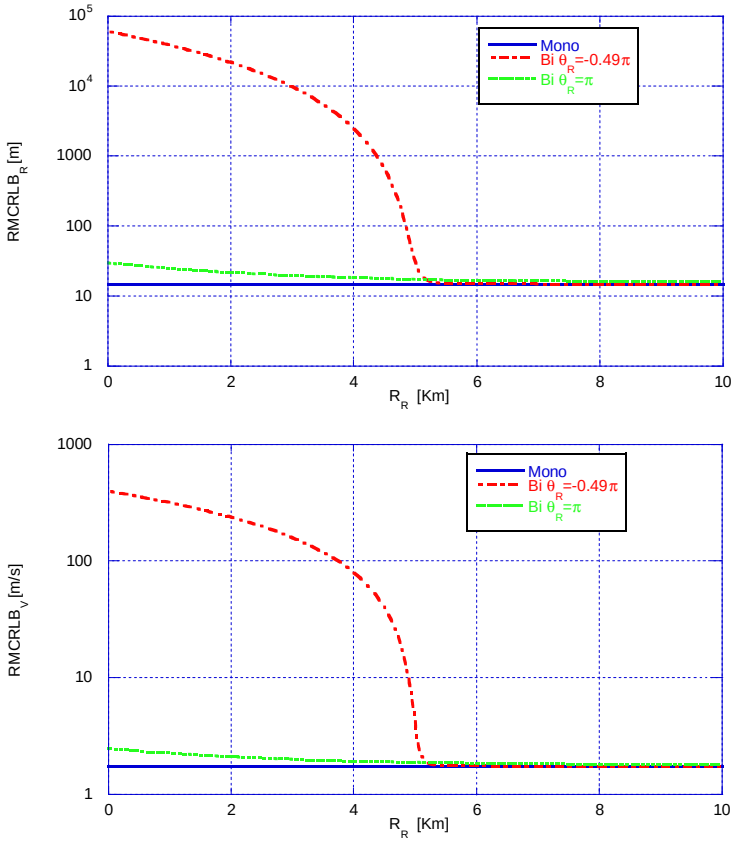

Figure 34 – Root MCRLBs as a function of range R_R, NT=0.1 s, T=0.26 μs, α=0.22, f_C=2100MHz, V_a=5 m/s, L=5Km, SNR=0dB. Monostatic and Bistatic case.

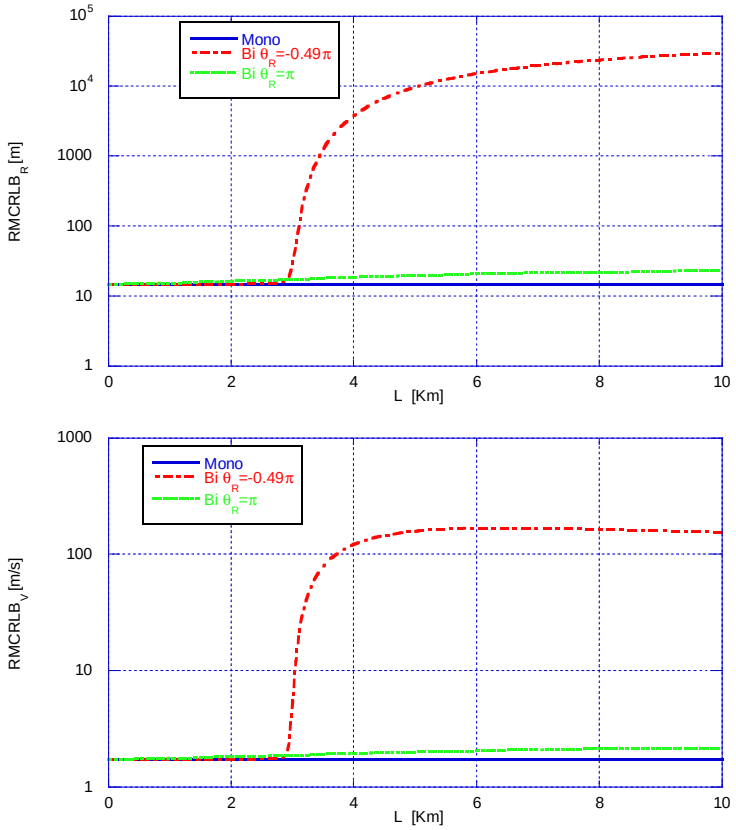

Figure 35 - Root MCRLBs as a function of the baseline *L*, *NT*=0.1 s, *T*=0.26 μs, *α*=0.22, f_C=2100MHz, V_a=5 m/s, R_R=3Km, *SNR*=0dB. Monostatic and Bistatic case.

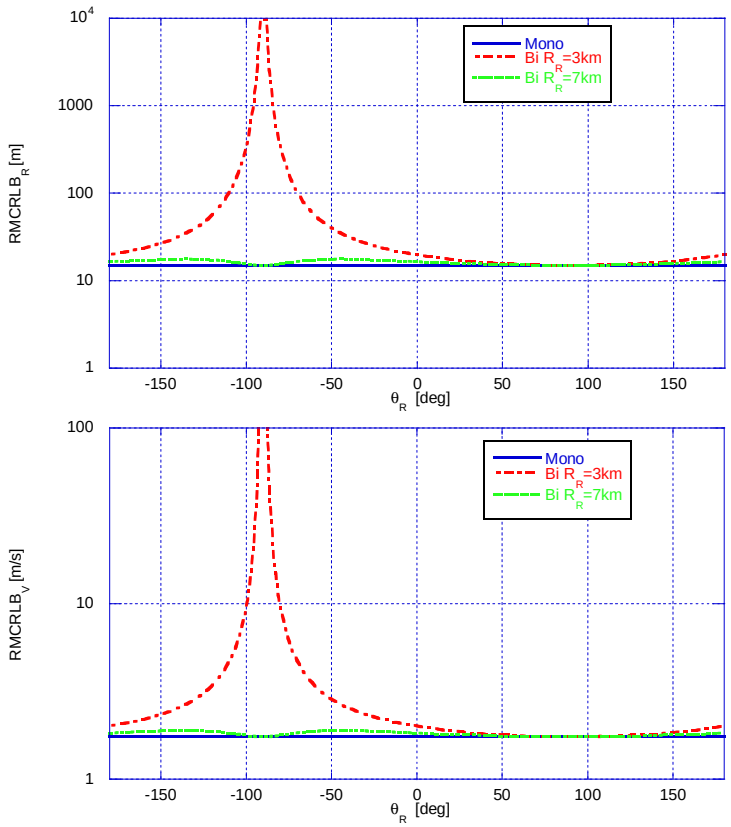

Figure 36 - Root MCRLBs as a function of receiver look angle θ_R, NT=0.1 s, T=0.26 µs, α=0.22, f_C=2100MHz, V_a=5 m/s, L=5Km, SNR=0dB. Monostatic and Bistatic case.

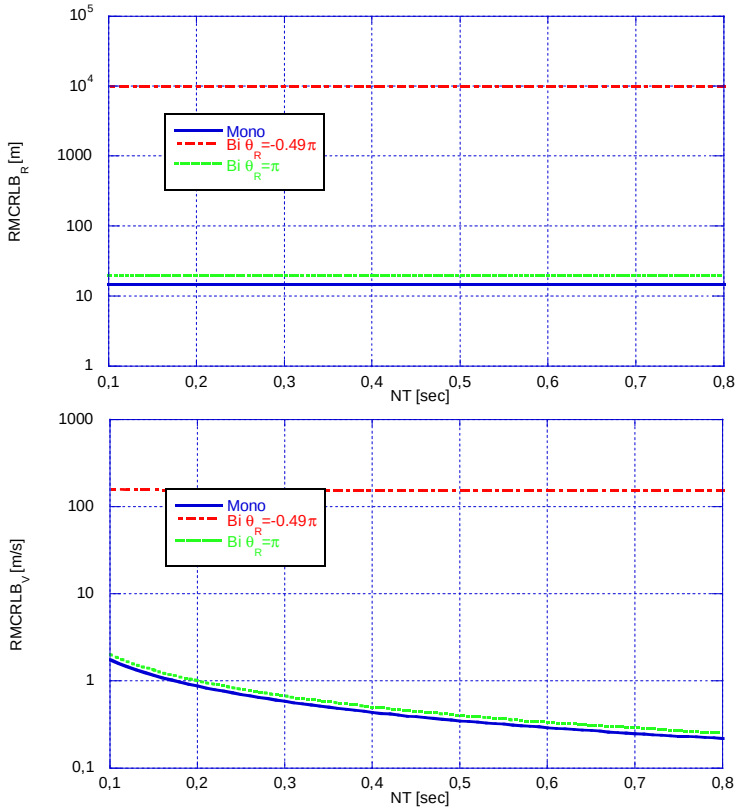

Figure 37 - Root MCRLBs as a function of the observation time *NT*, *T*=0.26 μs, *α*=0.22, f_C=2100MHz, V_a=5 m/s, R_R=3Km, *L*=5Km, *SNR*=0dB. Monostatic and Bistatic case.

9 Sensor selection for target tracking

This Section deals with the problem of sensor selection of the optimum channel in a multistatic radar system along the trajectory of the tracked target.

To this end we will calculate the Posterior Cramér-Rao Lower Bound (PCRLB) for a bistatic[2] radar system. The PCRLB is a useful tool which bounds the error variance of the sequential target state estimates produced from the radar measurements.

The Section is organized as follows. Section 9.1 presents the mathematical formulation of the problem and introduces the mathematical model of the target state and measurements equations for bistatic radar systems. Section 9.2 derives the theoretical PCRLB for bistatic target tracking both in the additive process noise case and in the zero process case. While Section 9.3 describes how to exploit the PCRLB for sensor selection in a multistatic radar system.

9.1 Target state and measurements signal model

The objective of target tracking is to estimate the target trajectories of a moving target. A point-like target motion model describes the evolution of the target state with respect to time. Let assume that the target motion equation is described by the following dynamic target state corrupted by additive noise model [Tay79]:

$$\mathbf{x}_{k+1} = \mathbf{f}_k\left(\mathbf{x}_k, \mathbf{a}_k\right) + \mathbf{n}_k \tag{88}$$

where $\mathbf{x}_k$, $\mathbf{a}_k$ and $\mathbf{n}_k$ are the target state, the target acceleration and the process noise sequences respectively while $\mathbf{f}_k$ is a known function of the state vector. The state vector at time index k is defined as $\mathbf{x}_k=[x_k,\ \dot{x}_k,\ y_k,\ \dot{y}_k\ ]^T$ where (x_k, y_k) indicate the position of the target while $(\dot{x}_k,\ \dot{y}_k)$ are the target velocity component along x and y axes of the Cartesian coordinate system. The acceleration sequence is defined as $\mathbf{a}_k=[\ \ddot{x}_k,\ \ddot{y}_k\ ]^T$, where $\ddot{x}_k$ and $\ddot{y}_k$ are the component of the target acceleration. Here this sequence is assumed known and is used as a control input parameter to describe a particular target trajectory.

The sequence $\mathbf{n}_k$ models the process noise that caters for any mismodeling effects or unforeseen disturbance in the target motion model. In this work we analyzed the linear case,

[2] This bound is also valid for monostatic configuration and can be obtained fixing the baseline length to zero.

that is the case in which $\mathbf{f}_k$ is a linear function of the state vector. In particular, we assumed that

$$\mathbf{f}_k\left(\mathbf{x}_k, \mathbf{a}_k\right) = \mathbf{F}\mathbf{x}_k + \mathbf{G}\mathbf{a}_k \tag{89}$$

where

$$\mathbf{F} = \begin{bmatrix} 1 & T & 0 & 0 \\ 0 & 1 & 0 & 0 \\ 0 & 0 & 1 & T \\ 0 & 0 & 0 & 1 \end{bmatrix}, \tag{90}$$

$$\mathbf{G}^T = \begin{bmatrix} T^2/2 & T & 0 & 0 \\ 0 & 0 & T^2/2 & T \end{bmatrix} \tag{91}$$

and T is the radar sampling interval.

Note that $\mathbf{f}_k$ is linear and its Jacobian is equal to $\mathbf{F}$.

We also assume that the random noise sequence $\mathbf{n}_k$ is zero-mean white Gaussian with covariance matrix:

$$\mathbf{Q} = q\begin{bmatrix} T^3/3 & T^2/2 & 0 & 0 \\ T^2/2 & T & 0 & 0 \\ 0 & 0 & T^3/3 & T^2/2 \\ 0 & 0 & T^2/2 & T \end{bmatrix}, \tag{92}$$

where q is a control parameter which takes into account the power of the process noise.

The objective of target tracking is to recursively estimate the target state from a set of measurement $\mathbf{z}_k$:

$$\mathbf{z}_k = \mathbf{h}_k\left(\mathbf{x}_k\right) + \mathbf{w}_k \tag{93}$$

where $\mathbf{h}_k$ is a known function of the state vector and $\mathbf{w}_k$ is a measurement noise sequence.

For the bistatic tracking problem analyzed in this work, the available measurements at time k are the range from receiver to target and the bistatic velocity[3]. In particular, the function $\mathbf{h}_k$ does not depend on k and is given by $\mathbf{h}(\mathbf{x}_k)=[r_k, v_k]^T=[h_r(\mathbf{x}_k), h_v(\mathbf{x}_k)]^T$.

To give explicit expression of $\mathbf{h}(\mathbf{x}_k)$, it is easy to verify that:

$$h_r\left(\mathbf{x}_k\right) = \sqrt{x_k^2 + y_k^2}\,, \tag{94}$$

[3] Whit respect to previous sections and for easy of notation, here the symbol r denotes the range from receiver to target, rt the range from transmitter to target while v denotes the bistatic velocity.

$$h_v(\mathbf{x}_k) = v_k = \frac{\tilde{x}_k \dot{x}_k + \tilde{y}_k \dot{y}_k}{\sqrt{\tilde{x}_k^2 + \tilde{y}_k^2}} \tag{95}$$

where

$$\tilde{x}_k = \frac{L}{L + r_k + rt_k} x_k - x_k, \tag{96}$$

$$\tilde{y}_k = \frac{L}{L + r_k + rt_k} (y_k + r_k) - y_k \tag{97}$$

$$rt_k = \sqrt{x_k^2 + (y_k - L)^2} \tag{98}$$

As apparent from eq. (93), the bistatic measurements are affected by additive noise $\mathbf{w}_k$, independent of the process noise $\mathbf{n}_k$. The additive noise $\mathbf{w}_k$ is assumed to be Gaussian distributed with zero mean vector and covariance matrix $\mathbf{R}_k$.

As previously shown, in bistatic radar systems the accuracy of the estimate of range and the bistatic velocity heavily depends on the transmitted waveform and on the geometry of the scenario. In previous sections it was shown that the Fisher Information Matrix (FIM) of the radar measurements can be expressed as $\mathbf{J}_k^B = \mathbf{P}_k \mathbf{J}_M \mathbf{P}_k^T$, where $\mathbf{J}_M$ is the monostatic FIM of time-delay and Doppler shift and depends only on the Ambiguity Function (AF) of the transmitted waveform. On the other hand, $\mathbf{P}_k$ depends on the geometry, which changes with time *k* while the target is moving along its trajectory.

9.2 PCRLB for bistatic radar systems

Let indicate with $\mathbf{J}_k$ the filtering information matrix at time *k*. Its inverse is the PCRLB that bounds the error variance of the target state estimate at time *k*, that is

$$\mathbf{J}_k^{-1} \leq \mathrm{E}\left\{ \left(\hat{\mathbf{x}}_{k|k} - \mathbf{x}_k \right) \left(\hat{\mathbf{x}}_{k|k} - \mathbf{x}_k \right)^T \right\} \tag{99}$$

where $\hat{\mathbf{x}}_{k|k}$ is an unbiased estimator of the state vector based on all the available measurements up to time *k*.

In [Tic98] the authors provided an elegant method of recursively computing the filtering information matrix $\mathbf{J}_k$. In particular, when the additive noise sequences $\mathbf{n}_k$ and $\mathbf{w}_k$ in eqs. (89) and (93) are Gaussian and mutually independent and their covariance matrix are invertible,

the information matrix can be computed recursively using the following equation [Tic98],[Tay79]:

$$\mathbf{J}_{k+1} = \left(\mathbf{Q} + \mathbf{F}\mathbf{J}_k^{-1}\mathbf{F}^T\right)^{-1} + \mathrm{E}\left\{\mathbf{H}_{k+1}^T \mathbf{R}_{k+1}^{-1} \mathbf{H}_{k+1}\right\} \tag{100}$$

where $\mathbf{H}_{k+1}$ is the Jacobian of $\mathbf{h}(\mathbf{x}_{k+1})$ evaluated at the true state $\mathbf{x}_{k+1}$; that is:

$$\mathbf{H}_{k+1} = \begin{bmatrix} \dfrac{\partial h_r}{\partial x_{k+1}} & \dfrac{\partial h_r}{\partial \dot{x}_{k+1}} & \dfrac{\partial h_r}{\partial y_{k+1}} & \dfrac{\partial h_r}{\partial \dot{y}_{k+1}} \\ \dfrac{\partial h_v}{\partial x_{k+1}} & \dfrac{\partial h_v}{\partial \dot{x}_{k+1}} & \dfrac{\partial h_v}{\partial y_{k+1}} & \dfrac{\partial h_v}{\partial \dot{y}_{k+1}} \end{bmatrix} \tag{101}$$

The recursive equation in (100) can be viewed as the sum of two terms, the first one $(\mathbf{Q}+\mathbf{F}\mathbf{J}_k^{-1}\mathbf{F}^T)^{-1}$ represents the a priori information given by the previous target state, while the second term $\mathrm{E}\{\mathbf{H}_{k+1}^T \mathbf{R}_{k+1}^{-1} \mathbf{H}_{k+1}\}$ represents the information gained by the radar measurements. The expressions of the elements of $\mathbf{H}_{k+1}$ are given by

$$\frac{\partial h_r}{\partial x_{k+1}} = \frac{x_{k+1}}{r_{k+1}}, \quad \frac{\partial h_r}{\partial \dot{x}_{k+1}} = 0, \tag{102}$$

$$\frac{\partial h_r}{\partial y_{k+1}} = \frac{y_{k+1}}{r_{k+1}}, \quad \frac{\partial h_r}{\partial \dot{y}_{k+1}} = 0, \tag{103}$$

$$\frac{\partial h_v}{\partial x_{k+1}} = \frac{1}{d_{k+1}^2}\begin{bmatrix} \left(\dot{x}_{k+1}\dfrac{\partial \tilde{x}_{k+1}}{\partial x_{k+1}} + \dot{y}_{k+1}\dfrac{\partial \tilde{y}_{k+1}}{\partial x_{k+1}}\right) d_{k+1} + \ldots \\ \ldots - \left(\tilde{x}_{k+1}\dot{x}_{k+1} + \tilde{y}_{k+1}\dot{y}_{k+1}\right)\dfrac{\partial d_{k+1}}{\partial x_{k+1}} \end{bmatrix} \tag{104}$$

$$\frac{\partial h_v}{\partial y_{k+1}} = \frac{1}{d_{k+1}^2}\begin{bmatrix} \left(\dot{x}_{k+1}\dfrac{\partial \tilde{x}_{k+1}}{\partial y_{k+1}} + \dot{y}_{k+1}\dfrac{\partial \tilde{y}_{k+1}}{\partial y_{k+1}}\right) d_{k+1} + \ldots \\ \ldots - \left(\tilde{x}_{k+1}\dot{x}_{k+1} + \tilde{y}_{k+1}\dot{y}_{k+1}\right)\dfrac{\partial d_{k+1}}{\partial y_{k+1}} \end{bmatrix} \tag{105}$$

$$\frac{\partial h_v}{\partial \dot{x}_{k+1}} = \frac{\tilde{x}_{k+1}}{d_{k+1}}, \quad \frac{\partial h_v}{\partial \dot{y}_{k+1}} = \frac{\tilde{y}_{k+1}}{d_{k+1}}, \tag{106}$$

where $d_{k+1} = \sqrt{\tilde{x}_{k+1}^2 + \tilde{y}_{k+1}^2}$. The derivatives that appear in (104) and (105) can be straightforwardly calculated and are not reported here for lack of space. From these equations it is clear that along the target trajectory, the FIM $\mathbf{J}_k$ depends on sensor accuracy (through $\mathbf{R}_k$, which is itself dependent on the target trajectory and on the transmitted waveform), the

sampling interval T and the baseline length L. In particular, as shown in the previous section, when the target is crossing the baseline, resolution is totally lost and therefore the errors of the measurements tends to infinity. Matrix $\mathbf{R}_k^{-1}$ tends to zero and hence also the second term in (100). In this case there is no information gain collected by the target measurements. Regarding eq. (100), the most critical problem in calculation appear to be the expectation operator which is taken with respect to the state vector $\mathbf{x}_k$. This calculation can be approximated through Monte Carlo simulation by generating a set of state vector realizations and then computing the average over this set. However, depending on the analyzed problem, this is rarely done in practice. Instead, often purely deterministic trajectories are considered. When the target motion equation is considered in absence of process noise, the PCRLB refers to the zero process noise case. Clearly, in this case the obtained PCRLB is a more optimistic lower bound. In absence of process noise, the evolution of the target state is purely deterministic and hence the expectation operator in eq. (100) can be dropped out. Moreover, the covariance matrix $\mathbf{Q}$ becomes zero and therefore it follows that [Tay79]:

$$\mathbf{J}_{k+1} = \left[\mathbf{F}^{-1}\right]^T \mathbf{J}_k \mathbf{F}^{-1} + \mathbf{H}_{k+1}^T \mathbf{R}_{k+1}^{-1} \mathbf{H}_{k+1} \tag{107}$$

Clearly, also in the zero process noise case, the filtering information matrix is the sum of two terms, one takes into account the a priori information while the other the measurement information. For L=0 the bistatic PCRLBs coincide with the monostatic PCRLBs.

9.3 Application of PCRLBs to sensor selection

In this Section we show how the PCRLBs can be used to sensor selection in a multistatic radar system. In particular we consider a system in the context of maritime border control scenario, composed by a Passive Coherent Location (PCL) receiver that exploits the signal emitted by two non co-operative transmitters of opportunity: a UMTS base station and a FM radio station. These kind of systems have some significant attractions because it allows the use of parts of the RF spectrum (VHF/UHF) and, since broadcast transmissions at these frequencies can have substantial transmit powers, they can have excellent coverage. Furthermore, advantage should be drawn utilising the UMTS sources of illumination. In fact, the FM system could detect targets at relatively far range and use its fine Doppler resolution to build a crude track. Once the target appears within the coverage area of the UMTS system, this can be exploited for its superior range resolution properties. The aim of this section is to

evaluate the performance of each bistatic channel in estimating the target trajectory of a target approaching Leghorn harbour and also to propose an algorithm for optimally selecting the transmitter of opportunity. This algorithm can provide a significant aid to harbour protection and can reduce the computational load of surveillance operations.

The analyzed multistatic scenario is shown in Figure 38. The receiver is placed in "via Michelangelo", between "darsena Petroli" and "darsena Pisa" of Leghorn harbour. Its antenna has a gain G=10dB and an Half Power Beam Width (HPBW) of 3°. It exploits the signals emitted by two non co-operative transmitters. The first one is a UMTS Base Station located in "Piazzale Marmi", 453m away the receiver in the South-East direction. The second transmitter is an FM commercial radio station located in "Monte Serra", 36Km away the receiver in the North-East direction.

Figure 38 - Analyzed multistatic radar System.

Figure 39 shows the Root CRLB (RCRLBs) of target range and bistatic velocity, that is the root of the diagonal elements of $\mathbf{R}_k$. The RCRLBs of the UMTS channel are shown at the top of the figure, while the RCRLBs of the FM channel are shown at the bottom. To calculate these maps we supposed that the target was moving horizontally from left to right with a constant velocity of 3m/sec. From the results it is clear that the performance in measuring the target range and the bistatic velocity strongly depends both on the geometry and the transmitted waveform. It is also interesting to note that the performance in estimating the target velocity is better in the FM channel than in the UMTS one, due to the longer time of observation. On the other hand, the range resolution is better in the UMTS channel than in the FM one. Note also that the FM channel operates with very high transmitted power giving a better coverage and appreciable resolution also in the far range. Using the information provided in Figure 39 combined with the results obtained in previous sections, it is possible to select, for each point of the analyzed area, the channel having the best performance. For each location of the surveillance area it is possible to calculate the measurement information matrix $\mathbf{J}_{k+1}^{Z} = \mathbf{H}_{k+1}^{T}\mathbf{R}_{k+1}^{-1}\mathbf{H}_{k+1}$ and then to provide a function of this matrix that evaluates the channel that gives the higher measurement information. As an example, let consider the case of a naval target approaching the harbour with constant velocity equal to 3 m/sec (see the route Palermo-Livorno (Leghorn) of Fig. 38). When the target trajectory is deterministic the bistatic PCRLBs of each channel are obtained by inverting matrix $\mathbf{J}_{k+1}$ of eq. (107). Note from (107) that the target dependent quantity det($\mathbf{R}_k^{-1}$) can be considered as an index of the measurement information and hence can be used to select the channel with the best performance.

We investigated also the performance that can be obtained using different indices of the measurement information, such as the trace, the determinant and the norm of the matrix $\mathbf{H}_{k+1}^{T}\mathbf{R}_{k+1}^{-1}\mathbf{H}_{k+1}$. The obtained performance are similar, anyway the best performance are achieved using the index det($\mathbf{R}_k^{-1}$). This is justified considering that for the particular case we analyzed, the parameters that describe the uncertainty on the state and the measurement vectors are only the probability of detection and measurement error covariance matrix and hence the index of the measurement information must be a function of these parameters.

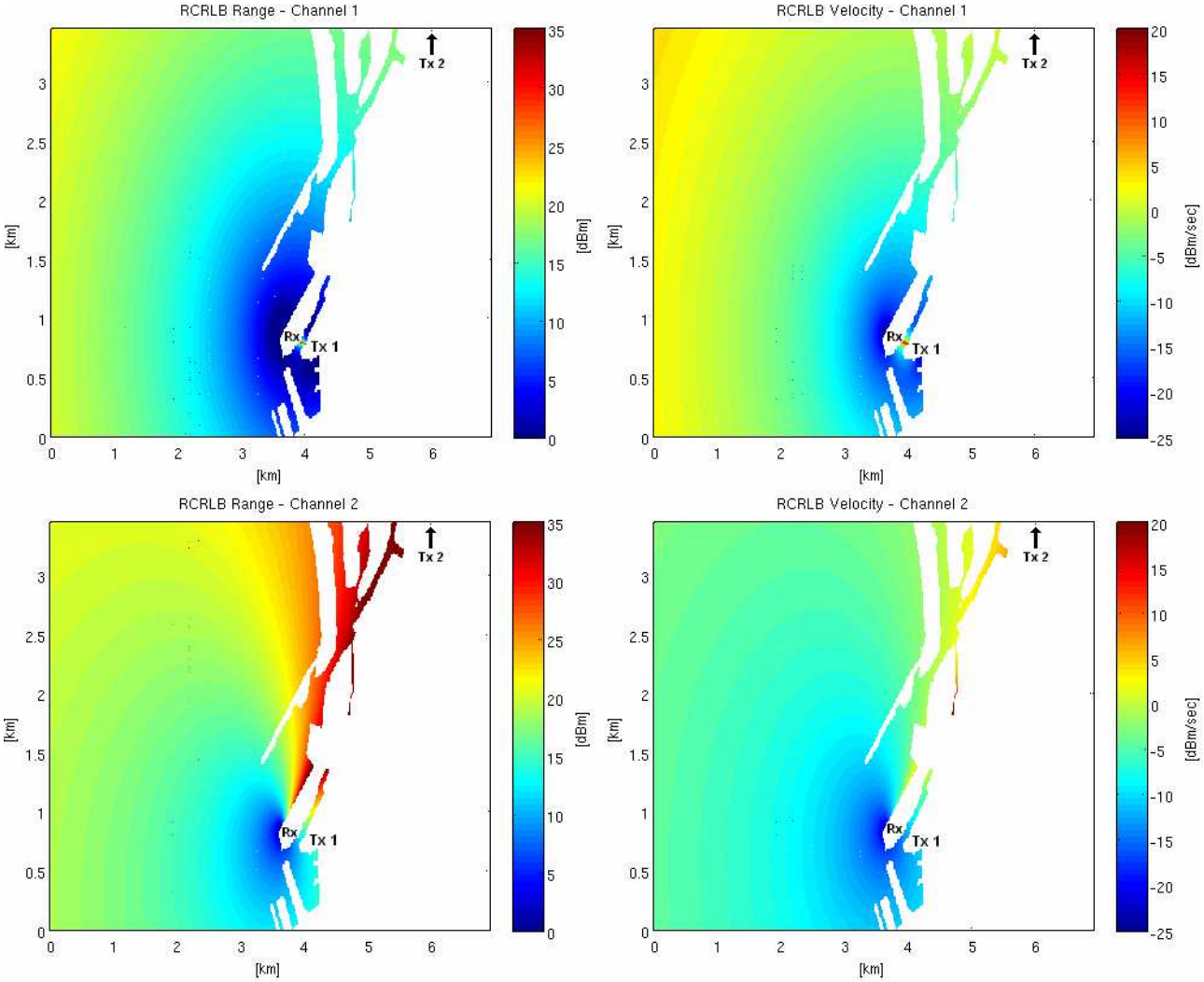

Figure 39 - Root-CRLB of range (left hand side) and bistatic velocity (right hand side) for the UMTS channel (top) and FM channel (bottom).

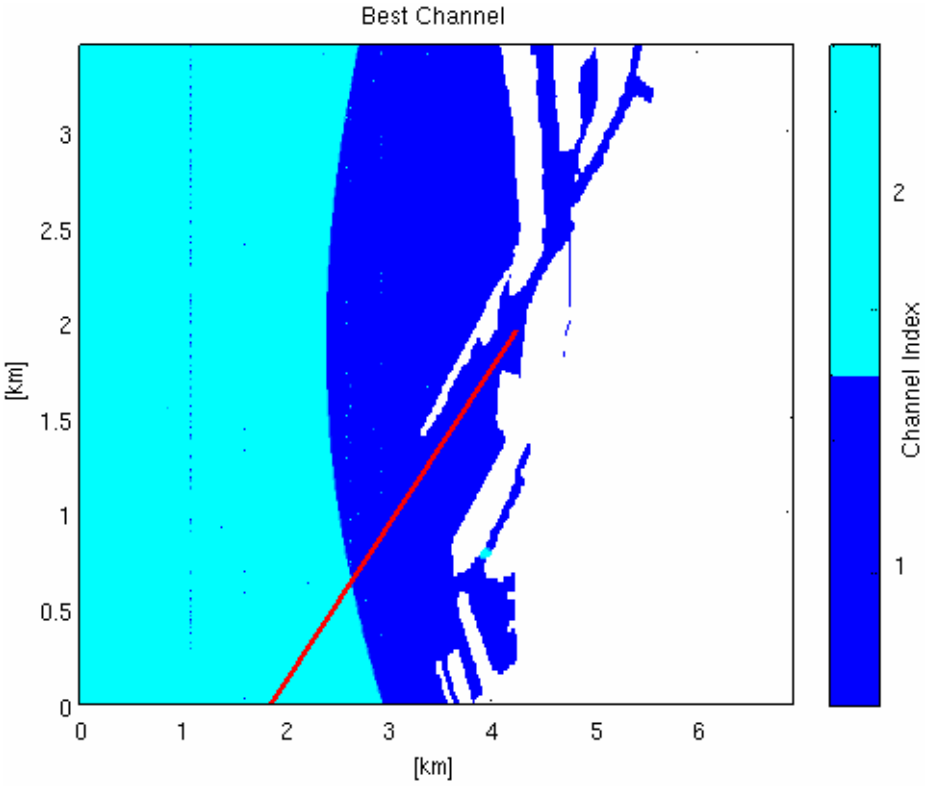

Figure 40 - Channel with the higher measurement information and target trajectory.

Figure 40 shows the channel which has the higher information for each point of the analyzed area. The scale of this figure is quantized into 2 levels: level 1 refers to the UMTS channel while level 2 to the FM channel. In Figure 40 we also plotted a red line that represents the trajectory of the ship approaching the harbour. Being the target trajectory deterministic, the PCRLBs of the receiver that dynamically select the best channel are given by:

$$\mathbf{J}_{k+1} = \left[\mathbf{F}^{-1}\right]^T \mathbf{J}_k \mathbf{F}^{-1} + \mathbf{J}_{k+1}^{CH} \tag{108}$$

where:

$$\mathbf{J}_{k+1}^{CH} = \begin{cases} \left[\mathbf{H}_{k+1}^{(1)}\right]^T \left[\mathbf{R}_{k+1}^{(1)}\right]^{-1} \mathbf{H}_{k+1}^{(1)}, & \text{if } \det\left(\left[\mathbf{R}_{k+1}^{(1)}\right]^{-1}\right) > \det\left(\left[\mathbf{R}_{k+1}^{(2)}\right]^{-1}\right) \\ \left[\mathbf{H}_{k+1}^{(2)}\right]^T \left[\mathbf{R}_{k+1}^{(2)}\right]^{-1} \mathbf{H}_{k+1}^{(2)} & \text{if } \det\left(\left[\mathbf{R}_{k+1}^{(1)}\right]^{-1}\right) < \det\left(\left[\mathbf{R}_{k+1}^{(2)}\right]^{-1}\right) \end{cases} \tag{109}$$

that is, at each step k+1 the measurement information term $\mathbf{J}_{k+1}^{CH}$ is given by selecting the channel with the higher measurement information. In (109) the upper index (1) refers to the UMTS channel while the index (2) to the FM channel. The PCRLBs of the receiver that select the best transmitter are a shown in Figure 41, where we also plotted the PCRLBs of each single channel. From the results it is evident that there is a substantial gain with respect to

each bistatic channel and the obtained performance is equal or one order of magnitude better than the performance of the channel with the lowest PCRLB. As apparent, initially the performances are the same as the FM channel. This is due to the fact that in the far range the FM channel has the best performance thanks to the higher *SNR*. When the target approaches the harbour, the UMTS channel has a better resolution and, exploiting this channel, the proposed receiver is able to increase the performance in estimating the target trajectory.

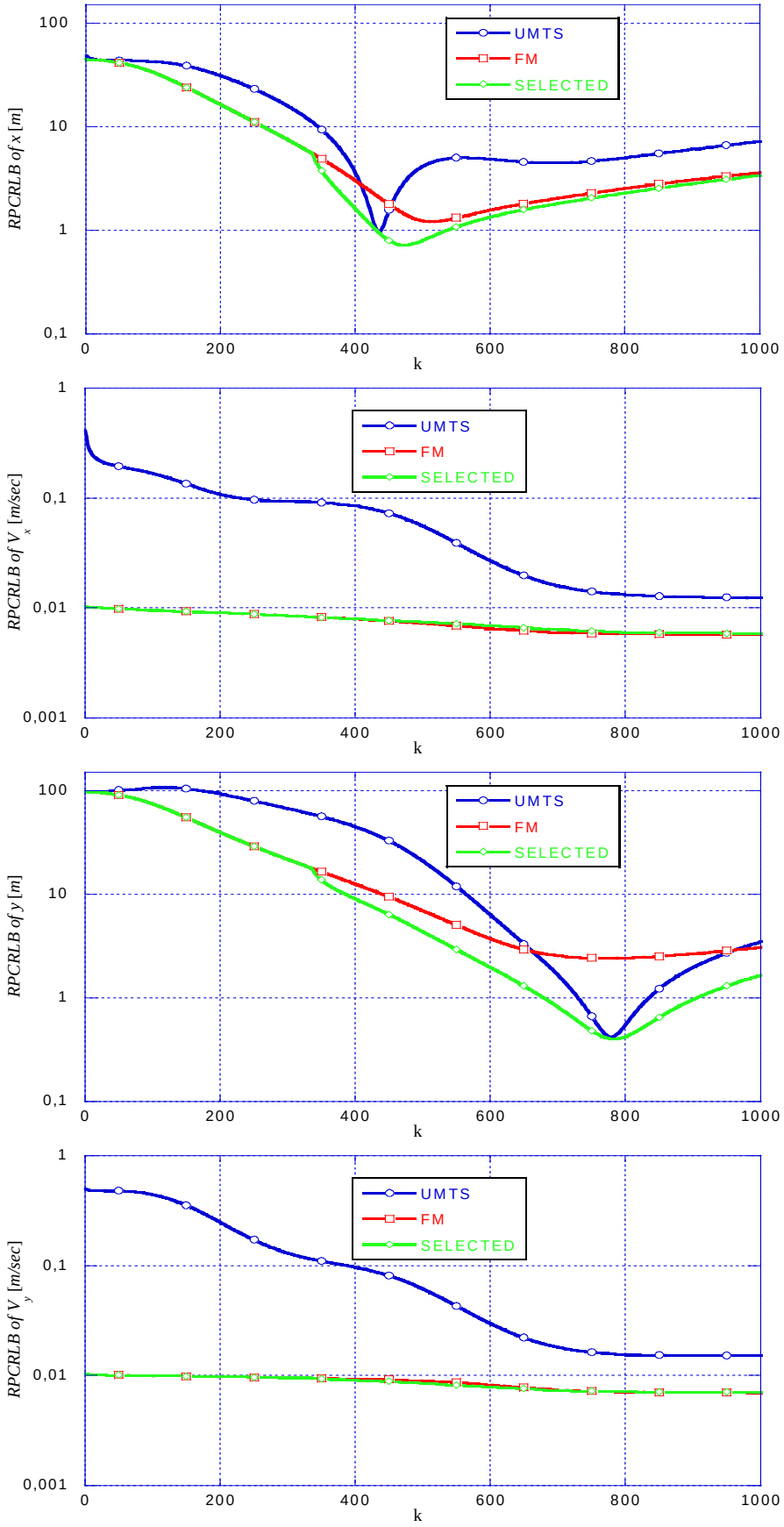

Figure 41 - Root-PCRLBs. UMTS channel, FM channel and dynamic selection channel.

Conclusions

The considerable flexibility of modern radar systems calls for new methods of designing and scheduling the waveforms to optimize the radar performance and to compensate for the environment and multi-radar interference. To this end the first part of our research activity focused on the design and analysis of a set of waveforms in the contest of netted radar systems that guarantee good target detection and parameter estimation in different scenarios and allow an optimal access to the same transmit channel. In particular we focused on the analysis of the Frequency Coded Waveforms where the frequency hop patterns were constructed upon an extension of the theory of quadratic congruences.

These signals are characterized by an auto-ambiguity function that exhibits a narrow thumb tack shape with low sidelobes and, in contrast, with small cross-ambiguity functions. In our work we also investigated the impact of an interfering signal emitted by a non cooperative radar on the performance of the reference radar in the estimation of the target direction of arrival (DOA). Our research also focused on the design and the analysis of adaptive waveform diversity technique to mitigate the impact of the interfering radar on the performance of the reference radar. To this end, we presented four DOA estimators, the Modified Pseudo-Monopulse (MPM), the Modified Maximum Likelihood (MML), the Sub-sequent Pseudo-Monopulse (SPM) and the Sub-sequent Maximum Likelihood (SML).

Our research activity on waveform diversity and design also concerned on Multistatic active radar systems, that is systems that exploit multiple transmitter and receiver. Such systems differ from typical modern active radar through consisting of several different monostatic and bistatic channels of observation. Due to this spatial diversity, these systems present challenges in managing their operation as well as in usefully combining the multiple sources of information on a particular area of surveillance.

The information gain obtained through this spatial diversity combined with some level of Knowledge-based data processing can give rise to a number of advantages over both the individual monostatic and bistatic cases in typical radar functions, such as detection, parameter estimation, tracking and identification. As known, the performance of each bistatic channel heavily depends upon the geometry of the scenario, that is the position of the target with respect to each receiver and transmitter, and the transmitted waveform. Therefore, the main goal of our research was the develop of mathematical tool that can be used to evaluate the best achievable performance of monostatic and bistatic systems. To this end we calculated

the Ambiguity Function (AF) and the Cramér-Rao Lower Bounds (CRLB) of several transmitted waveforms for both the monostatic and bistatic configurations.

Our research also focused on the analysis of passive systems, in particular we analyzed the performance of PCL (Passive Coherent Location) systems, that is passive bistatic radar systems where the transmitter of opportunity is from a non-radar transmission, such as broadcast, communications or radionavigation signal. These systems have the advantage that the receivers do not need any transmitter hardware of their own, and are completely passive, and hence undetectable. PCL multistatic systems have some significant attractions because they can allow the use of parts of the RF spectrum (VHF and UHF) that are not usually available for radar operation, and which may offer a counterstealth advantage, since stealth treatments designed for microwave radar frequencies may be less effective at VHF and UHF. Moreover, broadcast transmissions at these frequencies can have substantial transmit powers and the transmitters are usually sited to give excellent coverage. In particular, in our research we derived the AF and the CRLBs on the estimation accuracy of the target range and velocity for a QPSK signal where the pulses are shaped with a Root Raised Cosine filter. These results provide a mathematical tool to evaluate the performance of a Passive Coherent Location (PCL) system where the receiver exploits the downlink signal emitted by non co-operative UMTS base station. The actual growing coverage of UMTS signals on the international territory makes a multistatic radar configuration feasible. All the obtained results can be extended in a straightforward manner to any Pulse Amplitude Modulation (PAM) signal, in order to analyze the performance of a PCL system that exploits the signal emitted by another digital non co-operative transmitter of opportunity.

Our research activity also concerned on the design of an algorithm for optimally selecting the best channel (tranmitter-receiver pair) for the tracking and the parameter estimation of a radar target moving along a certain trajectory in a multistatic scenario. To this end we exploited the information gained through the calculation of the CRLB. The idea was to select the base station that gives the lowest CRLB for the target velocity or range. We analyzed as well the problem of the optimum sensor selection along the trajectory of a tracked target in a multistatic radar systems. To this end we evaluated the Posterior Cramér-Rao Lower Bound (PCRLB) of the sequential target state estimation and we defined an algorithm that exploits this mathematical tool to select the best channels for the tracking of the target. Our research also focused on exploiting the CRLB to compute the rules for selecting the best weighting

coefficients for fusing the signals from the receivers in a multistatic system, in order to improve the detection of the target and the estimation accuracy of its kinematic parameters.

It is important to consider that a system that exploits the CRLB to compute the rules for improving its own performance, is a system that has “cognition” and changes its mode of operation according to the way in which it perceives its operating environments.

Future research activity on waveform diversity and design can be focus on the design of Cognitive radar system. The increasing needs for frequency allocations to radiolocation services is in contrast with the growth of activities in the area of civil communications, the emergence of new technologies and new services that involve a strong demand for spectrum allocation inducing a very strong pressure upon the frequency channels currently allocated to radars. For this reason, the availability of frequency spectrum for multifunction radar system has been severely compromised, available frequency bands have been diminished and increasingly dispersed.

This unique issue of spectrum crowding and steadily increasing radar requirements cannot be addressed by traditional modes of operation. Multifunction radar systems require the ability to anticipate the behavior of radiators in the operational environment. This in turn leads to the need for critical and new found methodologies based upon cognition as an enabling technology.

There is a need to generate situational awareness and directly support the delivery of effects - then intelligent aggregation of sensor data, information sources, and knowledge in real-time is required. Achieving the effects of cognition is essential to this goal. In light of this spectrum encroachment, intelligent spectrum utilization coupled with agile waveform selection and signal processing in multifunction radars has become a necessity.

The concept of Cognitive Radar represents a way forward to address these issues from a sensor and information perspective. The Cognitive Radar will achieve the effects of cognition in the context of radar operation using perception, memory and judgment. The Cognitive Radar will have the equivalent effect of cognition, i.e., ability to “reason,” without developing “consciousness” through the effective use of radar signal/data/image/track processing; waveform generation, timing and control; platform placement; and feedback for further adaptation and enhanced control.

References

[TR1] M. Greco, F. Gini, P. Stinco, M. Rangaswamy, "DOA Estimation and Multi-User Interference in a Two-Radar System", EOARD Grant FA8655-07-1-3096, University of Pisa, Italy, June 2008.

[TR2] M. Greco, F. Gini, P. Stinco, M. Rangaswamy, "DOA Estimation and Multi-Use Interference", EOARD Grant FA8655-07-1-3096, University of Pisa, Italy, Dec. 2008.

[TR3] M. Greco, F. Gini, P. Stinco, M. Rangaswamy, "Ambiguity Function and Cramer-Rao Bounds for Multistatic Radar Networks", ", EOARD Grant FA8655-07-1-3096, University of Pisa, Italy, October 2009.

[TR4] P. Stinco, M. Greco, F. Gini, M. Rangaswamy, "Data Fusion and Optimizzation in a Multistatic Radar System", EOARD Grant FA8655-07-1-3096, University of Pisa, Italy, September 2010.

[TR5] P. Stinco, M. Greco, F. Gini, M. Rangaswamy, " Performance Analysis of Passive Radar System Exploiting the Downlink Signal Of a UMTS Base Station ", EOARD Grant FA8655-07-1-3096, University of Pisa, Italy, November 2011.

[And05] A. Andrews, “HDTV-based passive radar”, AOC 4th Multinational PCR Conference, Syracuse, New York, 5–7 October 2005.

[Azi07] Aziz, A., M., “Fuzzy track-to-track association and track fusion approach in distributed multisensor-multitarget multiple-attribute environment”, Signal Processing 87, pp. 1474-1492, 2007.

[Bel88] J.R. Bellegarda and E.L. Titlebaum, “Time-Frequency Hop Codes Based Upon Extended Quadratic Congruences,” IEEE Trans. on Aerospace and Electronic System, Vol. 24, pp. 726-742, November 1988.

[Bel90] J.R. Bellegarda, "Congruential frequency hop signals for multi-user environments: a comparative analysis", International Conference on Acoustics, Speech, and Signal Processing. ICASSP-90, 3-6 April 1990, pp. 2903-2906, vol. 5.

[Bel91a] J. R. Bellegarda, and E. L. Titlebaum, , "The Hit Array: An Analysis Formalism for Multiple Access Frequency Hop Coding," IEEE Trans. on Aerospace and Electronic Systems, Vol. 27, No.1, pp.30-39, January 1991.

[Bel91b] J.R. Bellegarda and E.L. Titlebaum, Amendment to “Time-Frequency Hop Codes Based Upon Extended Quadratic Congruences,” IEEE Trans. on Aerospace and Electronic System, Vol. 27, No. 1, pp. 166-172, 1991.

[Con83] E. Conte; E. D'Addio; A. Farina; M. Longo , "Multistatic radar detection: synthesis and comparison of optimum and suboptimum receivers," Communications, IEE Proc F,, vol.130, no.6, pp.484-494, October 1983

[Dad86] D'Addio, E.; Farina, A.; , "Overview of detection theory in multistatic radar," Communications, IEE Proc F, vol.133, no.7, pp.613-623, December 1986.

[DeM08] A. De Maio, G. Foglia, N. Pasquino, M. Vadursi, "Measurement and analysis of clutter signal from gsm/dcs-based passive radar," Radar Conference, 2008. RADAR'08. IEEE, pp. 1–6, May 2008.

[DiL08] A. Di Lallo, A. Farina, R. Fulcoli, P. Genovesi, R. Lalli, R. Mancinelli, "Design, development and test on real data of an FM based prototypical passive radar," in Proc. IEEE Radar Conference, 2008. Rome, Italy, May 2008.

[Dog01] A. Dogandzic, A. Nehorai, "Cramér-Rao Bounds for estimating Range, Velocity, and Direction with and Active Array", IEEE Trans. on Signal Processing, Vol. 49, No. 6, June 2001, pp. 1122-1137.

[Far09] A. Farina, F. Gini, M. Greco, P. Stinco and L. Verrazzani, "Optimal Selection of the TX-RX Pair in a Multistatic Radar System", COGIS'09, Paris, France, Nov. 2009.

[For11] S. Fortunati, A. Farina, F. Gini, A. Graziano, M. S. Greco, and S. Giompapa, "Least squares estimation and Cramér-Rao type lower bounds for relative sensor registration process", *IEEE Trans. on Signal Processing*, Vol. 59, No. 3, pp.1075-1087, March 2011.

[Gin98] F. Gini, R. Reggiannini, and U. Mengali, "The Modified Cramér-Rao Bound in Vector Parameter Estimation," *IEEE Trans. on Communications*, vol. 46, No. 1, pp. 52-60, January 1998.

[Gin98b] F. Gini, "A Radar Application of a Modified Cramér-Rao Bound: Parameter Estimation in Non-Gaussian Clutter," *IEEE Trans. on Signal Processing*, vol. 46, No. 7, pp. 1945-1953, July 1998.

[Gin00] F. Gini and R. Reggiannini, "On the use of Cramér-Rao-Like bounds in the presence of random nuisance parameters," *IEEE Trans. Commun.*, vol. 46, no. 7, pp. 2120-2126, December 2000.

[Gin00b] F. Gini, M. Montanari, and L. Verrazzani, "Estimation of Chirp Radar Signals in Compound-Gaussian Clutter: A Cyclostationary Approach," *IEEE Trans. on Signal Processing*, vol. 48, No. 4, pp. 1029-1039, April 2000.

[Gre08] M. Greco, F. Gini, P. Stinco, A. Farina, L. Verrazzani, "Adaptive waveform diversity for cross-channel interference mitigation, " IEEE 2008 Radar Conference, May 2008, Rome, Italy.

[Gre10] M. Greco, P. Stinco, F. Gini, M. Rangaswamy, “Cramér-Rao Bounds and TX-RX Selection in a Multistatic Radar Scenario (invited)”, IEEE Int. Radar Conf. 2010, Washington DC, USA, 10-14 May 2010.

[Gre11] M. Greco, F. Gini, P. Stinco, A. Farina "Cramér-Rao bounds and selection of bistatic channels for multistatic radar systems", Aerospace and Electronic Systems, IEEE Transactions on , vol.47, no.4, pp.2934-2948, October 2011.

[Gri03] H.D. Griffiths, C.J. Baker, H. Ghaleb, R. Ramakrishnan, E. Willman, “Measurement and analysis of ambiguity functions of off-air signals for passive coherent location”, Electronics Letters, vol.39, no.13, pp1005-1007, June 2003.

[Gri05] H.D. Griffiths, C.J. Baker, “Measurement and analysis of ambiguity functions of passive radar transmissions’, Proc. RADAR 2005 Conference, Washington DC, IEEE Publ. No. 05CH37628, pp321–325, 9–12 May 2005.

[Gri86] H.D. Griffiths, N.R.W. Long, “Television based bistatic radar”, IEE Proc. F, Commun. Radar Signal Process., 1986, 133, (7), pp. 649–657.

[Guo08]H. Guo, K. Woodbridge, C.J. Baker, “Evaluation of WiFi beacon transmissions for wireless based passive radar,” in Radar Conference, 2008. RADAR ’08. IEEE, Rome, Italy, May 26–30, 2008, pp. 1–6.

[How99] P.E. Howland, “Target tracking using television-based bistatic radar”, IEE Proc., Radar Sonar Navig., 1999, 146, (3), pp. 166–174.

[How05] P.E. Howland, D. Maksimiuk, G. Reitsma, “FM radio based bistatic radar”, IEE Proc.-Radar Sonar Navig., vol. 152, no. 3, pp. 107-115, June 2005.

[Mal07]M. Malanowski, G. Mazurek, K. Kulpa, J. Misiurewicz, “FM based PCL radar demonstrator,” in Proc. IEEE International Radar Symposium, 2007. IRS 2007, Cologne, Germany, 2007.

[Men06]U. Mendi, B. Sarkar, “Passive radar using multiple gsm transmitting stations,” Radar Symposium, 2006. IRS 2006. International, pp. 1–4, May 2006.

[Noa09] Y. Noam and H. Messer, "Notes on the tightness of the hybrid Cramér–Rao lower bound," *IEEE Transactions on Signal Processing*, vol. 57, no. 6, pp. 2074-2084, June 2009.

[Pet09] D. Petri, A. Capria, M. Martorella, F. Berizzi, “Ambiguity Function Study for UMTS Passive Radar" Proceedings of the 6th European Radar Conference, 30 September - 2 October 2009, Rome, Italy.

[Rih69] Rihaczec, A.W.: Principles of High Resolution Radar, McGraw-Hill, New York 1969.

[Sti10] P. Stinco, M. Greco, F. Gini, “Data Fusion in a Multistatic Radar System (invited)”, 2010 International Conference on Synthetic Aperture Sonar and Synthetic Aperture Radar, 13-14 September, Lerici, Italy.

[Sti12] P. Stinco, M. Greco, F. Gini, M. Rangaswamy, “Ambiguity Funtion and Cramer-Rao Bounds for Universal Mobile Telecommunications Systems-Based Passive Coherent Location Systems”, Radar, Sonar & Navigation, IET, vol.6, no.7, pp.668-678, August 2012.

[Sun08]H. Sun, D.K.P. Tan, Y. Lu, “Aircraft target measurements using a GSM-based passive radar,” in Proc. IEEE Radar Conference, 2008. RADAR ’08., Rome, Italy, May 2008, pp. 1–6.

[Tay79] J. H. Taylor, “The Cramer–Rao estimation error lower bound computation for deterministic nonlinear systems,” IEEE Trans. on Automatic Control, vol. AC-24, pp. 343–344, Apr. 1979.

[Tic98] P. Tichavsky, C.H. Muravchik, and A. Nehorai, “Posterior Cramér-Rao bounds for discrete-time nonlinear filtering”, IEEE Trans.s on SP, 46, 5 (1998), 1386-1396.

[Tit81a]E. L. Titlebaum, "Time-Frequency Hop Signals Part I: Coding Based Upon the Theory of Linear Congruences," IEEE Trans. Aerospace and Electronic Systems, Vol. 17, No. 4, pp. 490-493, July 1981.

[Tit81b]E.L. Titlebaum and L.H. Sibul, “Time-Frequency Hop Signals Part II: Coding Based Upon Quadratic Congruences,” IEEE Trans. on Aerospace and Electronic System, Vol. 17, No. 4, pp. 494-499, July 1981.

[Tit91] E.L. Titlebaum, J. R. Bellegarda, and S.V. Maric, ,"Ambiguity Properties of Quadratic Congruential Coding," IEEE Trans. on Aerospace and Electronic Systems, Vol. 27, No.1, pp. 18-29, January 1991.

[Tit93] E.L. Titlebaum "Frequency- and Time-Hop Coded Signals for use in Radar and Sonar Systems and Multiple Access Comunication Systems", 1993 Conference Record of the Twenty-Seventh Asilomar Conference on Signals, Systems and Computers, pp. 1096-1100, Vol. 2.

[TS06]Technical Specification Group Radio Access Network; Spreading and modulation (FDD), 3gpp Std. TS 25 213 V7.0.0, 2006.

[Tsa97] T. Tsao, M. Slamani, P. Varshney, D. Weiner, H. Schwarzlander, “Ambiguity Function for a Bistatic Radar”, IEEE Trans. on Aerospace and Electronic Systems, Vol. 33, No. 3, July 1997, pp. 1041-1051.

[Van71] H.L. Van Trees, Detection, Estimation and Modulation Theory. New York: Wiley, 1971, Vol. III.

[Wal98] B. Walke, Mobile Radio Networks; Networking, Protocols and Traffic Performance, John Wiley, 1998.

[Wal03] B. Walke, P. Seidenberg, M.P. Althoff, UMTS: the Fundamentals, John Wiley, 2003.

[Wod80] Woodward, P.M., Probability and Information Theory, with Applications to Radar, Pergamon Press, 1953; reprinted by Artech House, 1980.

[Xia98] Yi Xian Yang; Xin Xin Niu; "Periodic ambiguity functions of EQC-based TFHC"; IEEE Trans. on Aerospace and Electronic System, Vol. 34, No. 1, pp. 194-199, January 1998.